UNIVERSITA' DEGLI STUDI DI PARMA

Dottorato di Ricerca in Scienze Chimiche

XXIV Ciclo

Triennio accademico 2009-2011

Control of the Threading/Dethreading Process of Calix[6]arene-Based Pseudorotaxanes and Rotaxanes

Coordinatore:
Chiar.mo Prof. Predieri Giovanni

Tutor:
Chiar.mo Prof. Arduini Arturo

Dottorando: **Bussolati Rocco**

2012

Abstract

This Ph.D. thesis describes a study on the development of stimuli-responsive devices based on calix[6]arene-based rotaxanes and pseudorotaxanes.
Initially the parameters responsible for the orientation and direction of threading of asymmetric axles into the calix[6]arene wheel were investigated through kinetic and thermodynamic studies. Then the results were transferred to achieve the unidirectional transit of a viologen axle through the wheel cavity. The asymmetry of the calix[6]arene receptor has been then exploited to modify the chemical properties of a terpyridinic ligand in pseudorotaxane and rotaxane systems. As last part of this thesis the syntheses and studies of new amphiphilic calix[6]arene receptors, able to form 3D self-assembled structure in water are reported.

Keywords: molecular machines, pseudorotaxanes, rotaxanes, calix[6]arenes, viologen salts, cyclic voltammetry, metal organic rotaxane frameworks, self-assembly, supramolecular chemistry.

Riassunto

Questo lavoro di tesi di Dottorato descrive uno studio per lo sviluppo di devices in grado di rispondere a stimoli esterni basati su sistemi pseudorotaxanici e rotaxanici a base calix[6]arenica. Inizialmente sono stati investigati i parametri the guidano l'orientazione e la direzione del processo di infilamento di assi asimmetrici nella ruota calix[6]arenica attraverso studi di tipo cinetico e termodinamico. Inseguito i risultati ottenuti sono stati trasferiti per promuovere un transito unidirezionale di un asse viologeno attraverso la cavità calixarenica. L'asimmetria del recettore calix[6]arenico è stata poi sfruttata per modificare le proprietà chimiche di un legante terpiridinico in sistemi pseudorotaxanici e rotaxanici. Come ultima parte di questa tesi viene riportata la sintesi e lo studio di nuovi recettori anfifilici a base calix[6]arenica in grado di generare strutture 3D in soluzione acquosa.

Parole chiave: macchine molecolari, pseudorotaxani, rotaxani, calix[6]areni, sali di viologeno, voltammetria ciclica, metal organic rotaxane frameworks, self-assembly, chimica supramolecolare.

To my family

CONTENTS

PREFACE

General Introduction

General introduction

Every chemical species could be seen as an object endowed with an intrinsic heritage (outfit) of structural information that determine its reactivity and physical properties and are at the bases of its functions in natural processes as well as in chemistry-based sciences and technology. One of the main objective of chemists has been and still is the understanding of these properties for a deeper comprehension of natural processes as well as their exploitation for the progress of humanity.

Since the beginning of the XX Century, when Johannes Diderik van der Waals devised the theoretical bases of non-covalent interactions, [1] it emerged the idea that these weak, but very specific intermolecular attractive forces could play a fundamental role in governing the outcome of a chemical process either natural or not. It was in fact during the first decades of that century when the idea of receptor formulated by Paul Ehrlich,[2] the "lock-and-key" image by Emil Fisher[2,3] and the concepts of coordination chemistry by Alfred Werner[2] seeded the development of modern chemistry. It was however in the second part of the last century when these concepts were re-elaborated and considered as a powerful tool to organize simple components in space in order to build-up more complex aggregates able to perform programmed tasks. This gave origin to Supramolecular Chemistry, as a new and highly interdisciplinary branch of chemistry. During the following decades, thanks to the pioneering works of Cram, Pedersen and Lehn,[4] the principles and methods of this relatively new branch of chemistry were devised, and the concept of molecular machine was born, idealized by Richard Feyman[5] and transferred to the supramolecular context by J. Fraser Stoddart.[6]

This work deals with the synthesis, characterization and study of the functioning mode of calix[6]arene-based pseudorotaxane and rotaxane with dialkylviologen salts. In particular the interest of these studies is focused on:

- *Chapter 2*: identifying the parameters that guide the direction of axle threading into the calix[6]arene wheel through kinetic and thermodynamic studies.

- *Chapter 3***:** the synthesis of an oriented rotaxane in which the axial component is able to perform, under the action of an external stimulus, an unidirectional movement of threading/dethreading through the calixarene cavity.

- *Chapter 4*: the synthesis and the characterization of a metal-directed assembly of oriented calix[6]arene-based pseudorotaxanes and rotaxanes, and to the understanding the effect that the orientation of the calix[6]arene component have on a particular stopper group.

- *Chapter 5*: the synthesis and the characterization of amphiphilic calix[6]arene receptors, able to form pseudorotaxane complex with dialkylviologen salts, the study of their properties and ability to form three dimensional self-assembled systems in aqueous solution.

References

[1] a) J. N. Israelachvili: *Intramolecular and Surface Forces*, Academic Press, London, **1985**; b) M. Rigby, E. B. Smith, W. A. Wakeham, G. C. Maitland: *The Forces Between Molecules,* Claredon, Oxford, **1986**.

[2] J.-M. Lehn, in *Perspectives in Coordination Chemistry* (Eds.: A. F. Williams, C. Floriani, A. E. Merbach), VCH, Basel, **1992**, p. 447.

[3] E. Fisher, *Ber. Dtsch. Chem. Ges.*, **1894**, *27*, 2985.

[4] a) J.-M. Lehn, *Angew. Chem. Int. Ed.*, **1988**, *27*, 89-112; b) D. J. Cram, *Angew. Chem. Int. Ed.,* **1988**, *27*, 1009-1020; c) C. J. Pedersen, *Angew. Chem. Int. Ed.*, **1988**, *27*, 1021-1027.

[5] a) R. P. Feynman, *Eng. Sci.*, **1960**, *23*, 22; b) R. P. Feynman, *Saturday Rev.,* **1960**, *43*, 45.

[6] a) F. M. Raymo, J. F. Stoddart, *Supramolecular Organization and Materials Design,* (Eds.: W. Jones, C. N. R. Rao), **2002**, 332-362; b) V. Balzani, M. Gomez-Lopez, J. F. Stoddart, *Acc. Chem. Res.*, **1998**, *31*, 405-414; c) M. Gomez-Lopez, J. A. Preece, J. F. Stoddart, *Nanotechnology,* **1996**, *7*, 183-192.

CHAPTER 1

Pseudorotaxanes and rotaxanes as molecular level machines

Chapter 1
Pseudorotaxanes and rotaxanes as molecular level machines

1.1 Molecular machines: the daughters of Supramolecular Chemistry

Supramolecular chemistry refers to that area of chemistry beyond the molecules and focuses on chemical systems made up of a discrete number of molecular subunits or components that assemble through non-covalent interactions. While traditional chemistry focuses on the manipulation of covalent bonds, supramolecular chemistry examines the weaker and reversible non-covalent interactions between chemical species either charged or neutral. These forces, that include hydrogen and halogen bonding, metal coordination, hydrophobic forces, van der Waals forces, π-π, CH-π and Coulomb interactions,[1] represent the driving forces that hold the components of a supramolecular system assembled. Although they are considerably weaker than covalent bonds, which can range between 150 kJ mol^{-1} to 450 kJ mol^{-1} non-covalent interactions range from 2 kJ mol^{-1} to 300 kJ mol^{-1} passing from dispersion to electrostatic (See Table 1.1). Nonetheless when these weak interactions are used in a co-operative manner a stable supramolecular complex can exist.

Interaction	**Strenght (kJ mol^{-1})**	**Example**
Ion-ion	200-300	Tetrabutilammonium chloride
Ion-dipole	50-200	Sodium[15]crown-5
Dipole-dipole	5-50	Acetone
Hydrogen bonding	4-120	Carboxylic acids
Cation-π	5-80	K^+ in benzene
π-π	0-50	Benzene and graphite
van der Waals	< 5	Packing in molecular crystals
Hydrophobic	Related to solvent solvent interaction energy	Cyclodexstrines inclusion compounds

Table 1.1: summary of supramolecular interactions.

The idea that a molecule, thanks to its chemical and structural information, is able to interact efficiently and selectively through non-covalent interactions with others species is optimally encompassed by the concepts of *molecular recognition* and/or *host-guest chemistry*.

Molecular recognition refers to the specific interaction between two or more chemical entities through non-covalent bonding and it plays an important role in biological systems such as antigen-antibody, DNA-protein, sugar-lectin, RNA-ribosom, etc….

Host-guest chemistry describes those complexes that are composed of two or more molecules or ions, held together in a unique structural relationships by non-covalent bonds. Commonly a host is defined as a large molecule or an aggregate such as an enzyme or a synthetic macrocycle possessing a sizeable, central hole or a cavity. The guest may be a metal cation, an anion, an ion pair, a neutral species or a more sophisticated molecule. More formally, the host is defined as the molecular entity possessing convergent binding sites (*e.g.* Lewis basic donor atoms, hydrogen bond donors, etc.), while the guest possesses divergent binding site.

The binding of a guest by a host is a thermodynamically driven process. The equilibrium constant of this process is called *binding* or *association constant* and it provides a quantitative representation of the extent of supramolecular association.[2] The binding constant for a 1:1 host-guest system is calculated through equation (1) using the concentration of the species that are present at the equilibrium.

$$H + G \rightleftharpoons HG$$

$$K = \frac{[HG]}{[H][G]} \quad (1)$$

Binding constants are calculated from experimental data (titration monitored by NMR, UV-Vis, fluorescence spectroscopy, or calorimetry, for example), which supply information about the position of the equilibria. Since binding constants are thermodynamic parameters, they are related to the free energy of complexation according to the Gibbs equation: $\Delta G° = -RT \ln K$. Thus the general affinity of a host for a guest under specific conditions (solvent, temperature, *etc*.) may be given either in terms of K or $-\Delta G°$ values.

In the design of supramolecular hosts, most of the efforts have been devoted to the construction of systems able to act through multiple binding contacts with the guest. When two or more binding sites of a host (either identical or different) cooperate in the

binding process, the phenomenon is called *cooperativity*. If the overall stability of the complex is higher than the sum of the energies of the interactions of the guest with the singles binding sites, the result is *positive cooperativity*. Binding site cooperativity in a supramolecular host-guest interaction is simply a generalization of the *chelate effect* found in classical coordination chemistry.[3]

Many supramolecular host-guest complexes are even more stable than what would be expected from cooperative/chelate effects alone. In these species the hosts are usually macrocycles that include their guests. Compared with their acyclic analogues, the complexes formed by macrocyclic hosts are endowed with an additional stability by what is traditionally defined *macrocyclic effect.* This effect relates not only to the chelation of the guest by multiple binding sites, but also to their *preorganization.*[4] Macrocyclic effect makes the complexes formed by macrocycle such as *corands* (*e.g.* crow ethers) about 10^4 times more stable than the closely related acyclic *podands* towards the same guest. Bicyclic hosts such as *cryptands* are found to be even more effective than monocyclic *corands* for the same reasons (Figure 1.1). This further additional stability derives from the more rigid, preorganized nature of the macrobicycle. Host preorganization is thus a key concept since it represents a major gain to the overall free energy complexation.

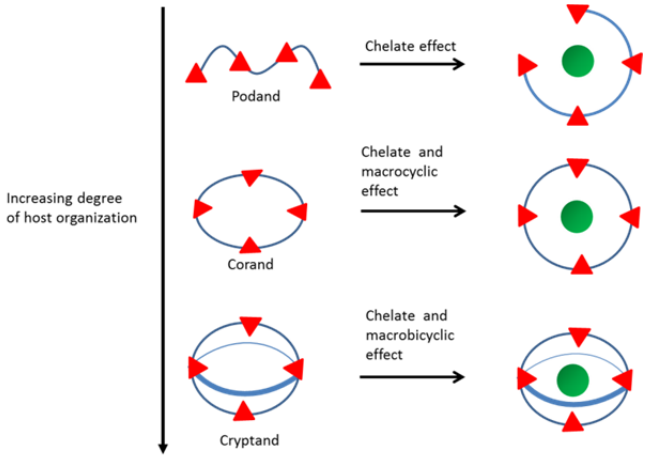

Figure 1.1: the chelate, macrocyclic and macrobicyclic effect.

In addition to the host preorganization, another key parameter in determining the affinity between the host and its guest is *complementarity*.[4] In order to be efficient a host must have binding sites suitably organized in space and possessing legating features so as to complement those of the guest. All the changes in the energetics and in the geometry of

the interacting species, which accompany host-guest complexation, such as the formation of new non-covalent bonds between host and guest molecules and the breaking of previously existing bonds with solvent molecules in the first and second solvation shells, derive from either *enthalpic* ($\Delta H°$) and *entropic* ($\Delta S°$) contributions. In designing an host both preorganization and complementarity are thus of crucial importance in determining the favourable enthalpic interaction between species. Entropic effects are also of fundamental importance and can be divided into two principal components: *solvation effects* (ΔS_{solv}) and *intrinsic effects* (ΔS_{intr}). The former are independent from molecular design and are related to the release of solvent molecules previously interacting with the host and the guest before association, which usually favourably contribute to the binding process. The latter refer to: *i)* the changes in translational and rotational entropy of the host and guest upon association; *ii)* the generation of vibrational entropy on association; *iii)* to the different possible geometrical arrangement of the binding partners. The overall free energy of complexation represents the difference between the unfavourable reorganization energy and the favourable binding energy. If the reorganization energy is large, then the overall free energy is reduced, destabilizing the complex. If the host is preorganized, this rearrangement energy is small.[5]

Concepts like *macrocyclic effect, preorganization* and *complementarity*, are the basis on which supramolecular chemistry has developed and grown. From the second half of the XX century the possibility to associate molecular species in a reversible manner to form larger, more complex supramolecular architectures according to the intrinsic information stored in their components, opened the way to explore and study a huge number of different supramolecular self-assembled systems and their functions.[6]

Since the beginning of the Industrial Era the progress of technology was strictly connected to the construction of new devices and machines. During the last fifty years this progress has been devoted to collecting, processing, displaying and storing information. The development of this technology parallels the progressive miniaturization of the components employed for the construction of such devices and machines.

The classical way followed to reach the miniaturization of components and the realization of new nanodevices is pursued through the “top-down approach”. This approach consists in the manipulation of progressively smaller pieces of matter by modern techniques and has operated in an outstanding way until now. [7] However it is becoming evident that this approach is subject to strong limitations for objects which are smaller than 100 nm. For

example the modern computer technology, which relies on silicon-based chips, is rapidly approaching the limits of its physical capabilities.[8] Nevertheless, as Richard P. Feynman stated in a famous talk to the American Physical Society in 1959, "there is plenty of room at the bottom" [9] to proceed towards further miniaturization, science and technology will have to find new ways. An alternative and more promising strategy to exploit devices at the nanometre scale is provided by the "bottom-up approach", which starts from nano or subnanoscale objects (namely, atoms or molecules) to build up nanostructures endowed with specific functions. Thus, following the "bottom-up" approach that takes advantage from the principles and methods of Supramolecular Chemistry, it is now possible to assemble large aggregates that are able to perform a programmed task and work as a machine starting from simpler molecular components, none of which, isolated, does.[10]

In the macroscopic world, devices and machines are among the main tools on which the technologic progress of humanity is based. A machine is the combination of a defined number of components assembled in a specific order. As consequence of an appropriate external energy input, some components carry out a cyclic movement that transforms the energy in a useful work. A machine is characterized by 1) the kind of energy input supplied to make it work, 2) the type of movement performed by its components, 3) the manner in which its functioning can be monitored, 4) the possibility to repeat the operation and establish a cyclic process, 5) the timescale needed to complete the cycle, and 6) the function performed by the machine. By expanding the concept of machine at the molecular level, it is possible to talk about molecular level machine as a supramolecular structure, constituted by a defined number of molecular components, designed to achieve a specific function as a result of an appropriate external stimulus.[11]

During the last 20 years the scientific interest in molecular level machines has grown up and several reviews and books covering the main aspect of this field have become available. [10,12] Among the large number of examples of supramolecular systems generated through molecular recognition processes, those belonging to the class of pseudorotaxanes and rotaxanes have been the most extensively exploited and play a key role in the construction of molecular machines.[13]

1.2 Pseudorotaxanes and rotaxanes

In the simplest istance a pseudorotaxane is a complex composed by a molecular species having an axial symmetry that, through noncovalent interactions, threads a macrocycle. The thermodynamic stability of this complex is determined by the nature and the magnitude of the intermolecular interactions between the two components. If, at the termini of the axial compound two groups having dimensions larger than the inner diameter of the macrocycle are present, a new chemical compound is obtained, called rotaxane. In this molecule the macrocycle is mechanically confined within the axial component (Figure 1.2).[13]

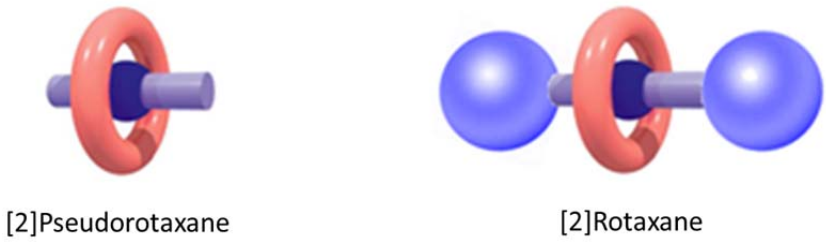

Figure 1.2: a pseudorotaxane complex and a rotaxane.

For pseudorotaxanes and rotaxanes the number of components of the species is indicated between square-brackets before the name. In current and accepted jargon, the term wheel refers to the cyclic component, the term axle to the linear component and, for rotaxanes, the term stoppers refers to the bulky groups present at the termini of the axle. Either pseudorotaxane and rotaxane can be synthetized through four main complementary strategies (Figure 1.3): i) capping: the axial component (eventually half-dumbbell-shaped) threads the cavity of the macrocycle, being the complexation process driven by noncovalent interactions. The resulting complex is a pseudoroxane, while if one or two stoppers are covalently bonded to the axle's termini the new compound obtained is a rotaxane; ii) clipping: the macrocycle is clipped around the pre-existing axial dumbbell, again the complexation process is driven by supramolecular interactions;[14] iii) slipping: the axial dumbbell and the wheel are synthesized separately, then they are heated together in solution and the macrocycle slips over the dumbbell's stoppers;[15] iv) active template: the metal plays a dual role during the assembly of the interlocked architecture,

acting as both a template for entwining or threading the components and as a catalyst for capturing the interlocked final product by covalent bond formation.[16]

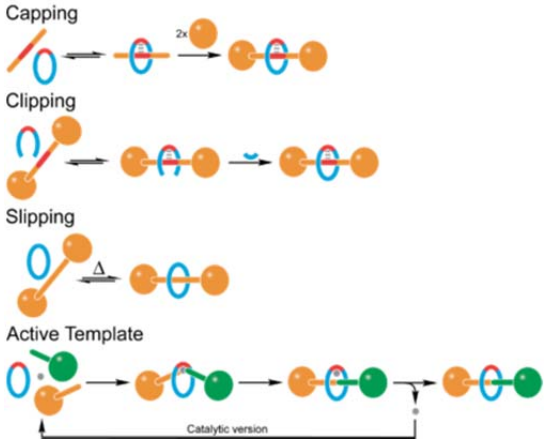

Figure 1.3: general synthetic approaches to rotaxane synthesis.

1.3 Pseudorotaxanes and rotaxanes as molecular machines

Pseudorotaxane and Rotaxane-based molecular systems are of current interest for their potential use in molecular electronics as logic molecular switching elements and as molecular motors. The ability of these systems to work as molecular machines is connected with the chemical information stored within their components.[17] If two or more identical binding sites where the macrocycle can resides are present on the axle, the rotaxane is characterized by a degenerate co-conformational equilibrium state in which the wheel can move back and forth along the dumbbell.[18] When the recognition sites differ in their chemical nature, the rotaxane can exist as two different equilibrating co-conformations whose populations reflect their thermodynamical stability; the equilibrium is determined by the strengths of the different sets of noncovalent interactions that are involved on the different binding sites (Figure1.4). It is possible to address the movement of the macrocycle along the axle using an external stimulus (chemical, electrochemical or photochemical). This stimulus has the role of changing the affinity of the wheel for a particular recognition site. As a result the wheel translates along the axle to reach a more stable conformation. Such structure represents a molecular shuttle.[19] The control of the position of the macrocycle through an external energy input allows the rotaxane to

function as molecular switch, in which each possible location of the macrocycle corresponds to a different state.

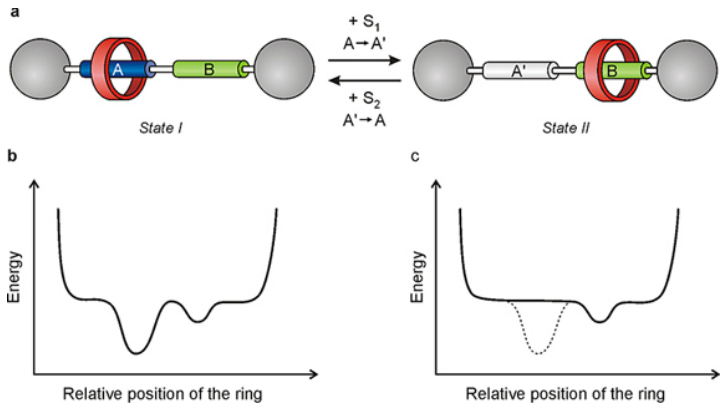

Figure 1.4: (a) Schematic representation of a two-station rotaxane and its operation as a controllable molecular shuttle. (b) A simplified representation of the potential energy of the system as a function of the position of the ring relative to the axle before (left) and after (right) switching off station A.[19]

As an arbitrary selection, some examples of rotaxane-based and pseudorotaxane-based molecular machine will be reported. One of the most remarkable example of molecular shuttle is the *Molecular Elevator* presented by the groups of J.F. Stoddart and V. Balzani in 2004.[20] This interlocked compound consists of a tripodal component where all the arms contain two different stations: a dialkyl-ammonium and a 4,4' bipyridinium unit. This compound is interlocked with a tritopic host, which plays the role of a platform that can be moved from one level to the other upon acid/based external inputs. The presence of bulky groups at the termini of the three arms prevents the dethreading of cyclic component from the tripod. Initially, because of the presence of the three ammonium stations the platform resides exclusively at the "upper level"; then, by adding a strong, non nucleophilic base, the deprotonation of the ammonium stations occurs and the platform moves down to the lower level, where it can interact with the bipyridinium sites. A subsequent addition of acid restores the ammonium centres and the platform moves back to the upper level (Figure 1.5). The movement can be monitored by NMR, adsorption or luminescent spectroscopy and by electrochemical technique. The "up and down" motion is quantitative and can be repeated several times.[21]

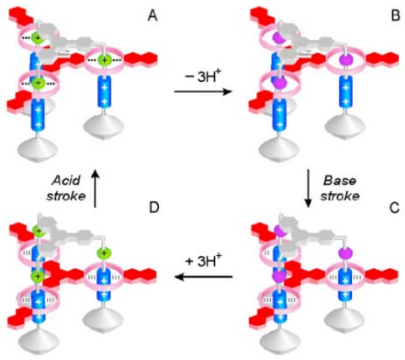

Figure 1.5: the base-acid controlled mechanical switching in the "molecular elevator".

In another example,[22] a [2]rotaxane composed by an axial compound bearing two electron-rich units, a 1,5-dioxynaphthalene (DNP) and a tetratiofulvalene (TTF), and a cyclobis(paraquat-p-phenylene) as wheel (Figure 1.6), can act as a molecular shuttle in which the movement is generated by an electrochemical stimulus. In the ground state the macrocycle exclusively encircle the TTF station, because of the strong charge transfer interactions that take place between these two units. The TTF is a redox active unit, in fact it can easily switch between the oxidized and reduced form through an electrochemical external input.[23]

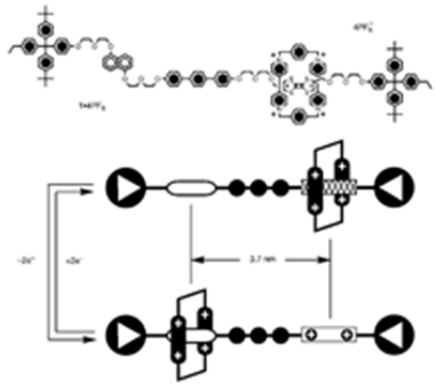

Figure 1.6: A [2]rotaxane with the TTF (hatched) and DNP (open) recognition units separated by a rigid terphenylene spacer (black circles) demonstrates a relative mechanical movement between the macrocyclic and dumbbell-shaped components.

The oxidation of the TTF to TTF^{2+} destabilizes this supramolecular interaction and induces a translation movement of the macrocyle toward the DNP station. The movement can be

monitored by NMR and UV-Vis spectroscopy. A second, opposite, electrochemical stimulus restores the original TTF and causes a shuttling of the macrocycle back to the initial state.
As in the case of rotaxanes, pseudorotaxane-based molecular machines can be divided on the basis of the energy supply to make them work that can be chemical, electrochemical or photochemical.[18] However an important difference between rotaxane and pseudorotaxane is that in the latter the action of an external energy input that reduce the affinity of the macrocycle towards the axle causes the dethreading of the axle from the wheel. For example, the 2,7-dibenzildiazapyrenium dication self-assembles (Figure 1.7) in solution with a crown ethers yielding a pseudorotaxane (step 1).[24] This dication forms adducts with aliphatic amines, probably as a result of charge-transfer interactions. Such an affinity has been exploited chemically to drive the dethreading of its pseudorotaxane with the crown ether (step 2). The dethreading process can be reversed quantitatively by addiing a stoichiometric amount of a strong acid to the solution (step 3). Each step of this process can be monitored with different techniques: NMR, absorption and luminescent spectroscopy.

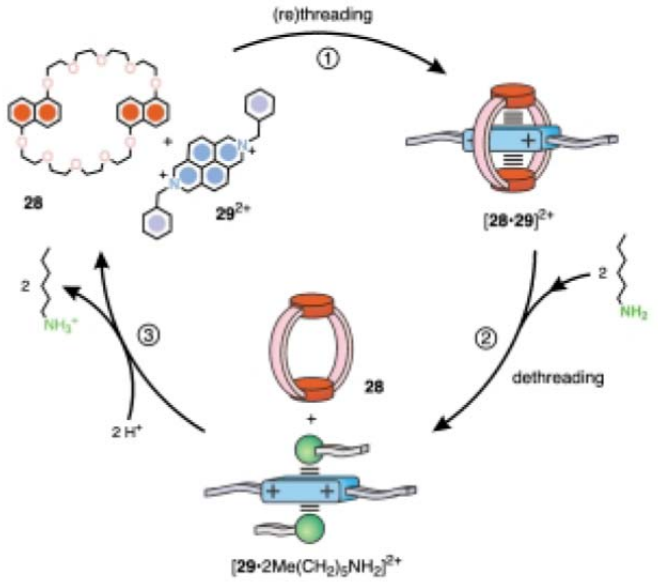

Figure 1.7: Schematic representation of the amine/acid-controlled dethreading/rethreding cycle of the pseudorotaxane.

1.4 Oriented pseudorotaxanes and rotaxanes

The ability of supramolecular structures to work as molecular devices and perform programmed tasks is strictly connected with the physicochemical properties and the spatial arrangement of the fragments or components that constitute their skeleton. One aspect that is emerging as a new challenge, and that could expand the scopes of these systems in the construction of new generation of molecular level machines, is the construction of interlocked systems in which the stimuli-promoted movement between components could be carried out in a unidirectional manner. Specifically, the development of a pseudorotaxane motif capable of performing threading and dethreading processes, under the control of external stimuli, in which the reciprocal orientation of the components can be controlled would be important for the construction of rotary motors based on catenanes and linear motors based on rotaxanes (Figure 1.8).[12b]

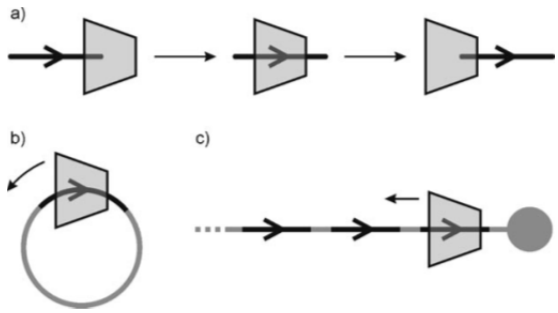

Figura 1.8: Representation of threading/dethreading of a [2]pseudorotaxane with nonsymmetric components (a), a processive linear motor based on a [2]rotaxane (b), and a rotary motor based on a [2]catenane (c).

An aspect that has been ignored so far is the possibility to gain full control on the absolute directional movement of the components in these systems. One of the aspects that is determinant to reach this goal is strictly connected with the shape of the macrocycle employed. Macrocyles can be grouped into two general categories: those having a substantially planar shape, as crown ethers, and those having a three-dimensional shape, like cucurbuturils or cyclodextrines. Because of the palindromy of their two faces in crown ether[25] cyclobis(paraquat-*p*-phenylene)[22,26] and cucurbituril [17d-27], an axle (even non-

symmetrical) can thread the wheel from both sides yielding the same pseudorotaxane, (Figure 1.9).

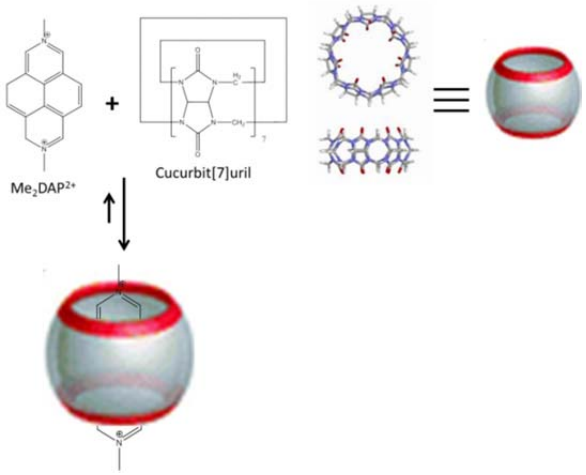

Figure 1.9: a cucurbit[7]uril-based pseudorotaxane.

On the contrary, when the three-dimensional and non-symmetrical cyclodextrins are used as the wheel, a non-symmetric axle can thread the cyclodextrin from both rims, thus leading to a mixture of orientational pseudorotaxane isomers. Functionalizing the free ends of the pseudorotaxane with bulky groups, two constitutionally isomeric rotaxanes are obtained (Figure 1.10).[28]

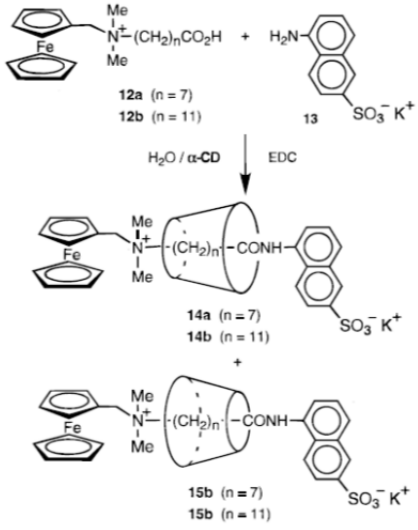

Figure 1.10: Synthesis of two pairs of orientationally isomeric cyclodexstrin-based rotaxanes.[28b]

Despite the asymmetry of the cyclodexstrines's structure, the problem to control the threading and obtain only one pseudorotaxane orientational isomer remains open, probably due to the insufficient diversity of the chemical information inserted onto the two rims, and only occasionally it has been pursued so far. Almost 20 years ago Matsuo & Co. demonstrated[29a] that cyclodexstrin can form stable oriented pseudorotaxane with appropriate asymmetrical axle. More recently this behaviour has been completely understood by Park & co-workers.[29b] They showed that an asymmetrical axle bearing a viologen group can thread the cyclodexstrin cavity from both rims with the same threading rates, although the dethreading rate of one isomer is faster than that of the other, giving mostly the thermodynamically stable isomer after a long time.

The topic of the direction of threading was studied also by Harada & Co.[30] They demonstrated that using an asymmetrical axle bearing two groups of different bulkiness at its termini threads the cyclodexstrine selectively from one of its two rims, yielding only one oriented pseudorotaxane isomer (Figure 1.11).

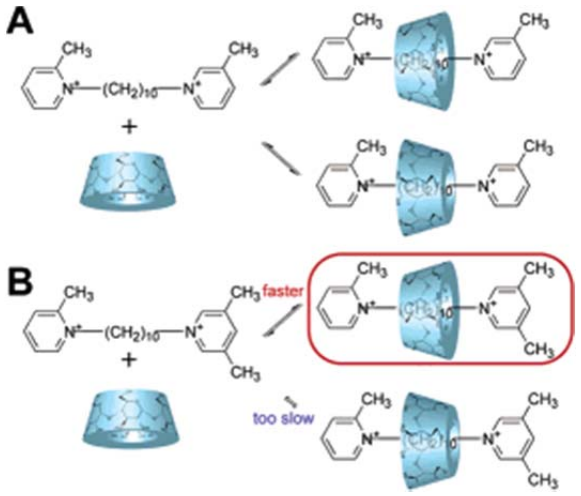

Figure 1.11: formation of cyclodexstrin-based oriented pseudorotaxanes using asymmetric axles.

1.5 Calix[6]arene-based pseudorotaxanes and rotaxanes

Another type of macrocycles belongs to the class of calix[n]arenes, and only in the last decade it has been employed for the constructions of pseudorotaxane and rotaxane. These compounds are phenolic macrocycles (Figure 1.12) extensively used in host-guest chemistry as versatile platforms for the synthesis of selective and efficient receptors for charged and neutral species. These compound have been frequently compared to cyclodextrins because of their truncated cone structure and their ability to form *endo*-cavity inclusion complexes with suitable guests. However the cavity of these two classes of hosts possesses complementary binding properties. In fact, while the cyclodextrins are water soluble and can bind neutral organic guests in their apolar cavity, the calix[n]arene-based hosts are soluble in organic solvents and can host in their electron-rich cavity organic cations as well as electron-deficient neutral guests.[31]

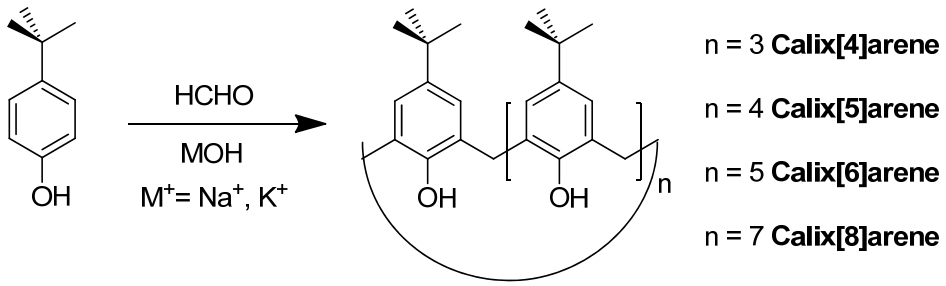

Figure 1.12: one-pot synthesis of calix[n]arene.

Within the calixarene series, the calix[4]arene has been the most extensively studied while the larger calix[6]- and the calix[8]arene have been relatively less studied, because of the difficulties to efficiently control their partial and regioselective functionalization at both rims and to control their conformational flexibility.

However, for the first time a decade ago it was discovered that in apolar solvent the tri-phenylureido calix[6]arene derivative **1** can act as wheel and form pseudorotaxanes with axles derived from dialkylviologen salts.[32] Compound **1** is able to take up crystals of **2** in CH_3Cl or toluene to afford a deep purple solution. The complex formation and its structure could be studied through ^1H NMR spectroscopy (Figure 1.13) and the data obtained were in agreement with a pseudorotaxane structure.

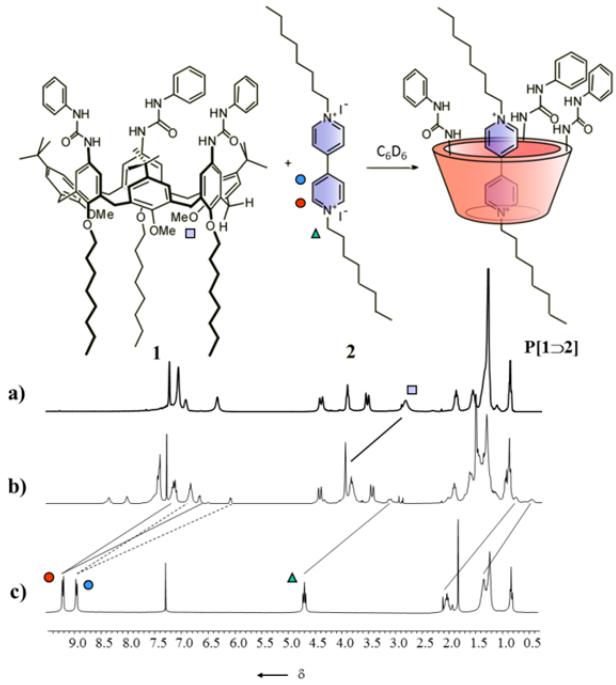

Figure 1.13: the pseudorotaxane complex formed by the three-phenylureido calix[6]arene **1** and di-octyl viologen di-iodide **2.** ^{1}H NMR spectra of: a) **1** in C_6D_6, c) **2** in CH_3CN, b) pseudorotaxane complex **P[1⊃2]** in C_6D_6.

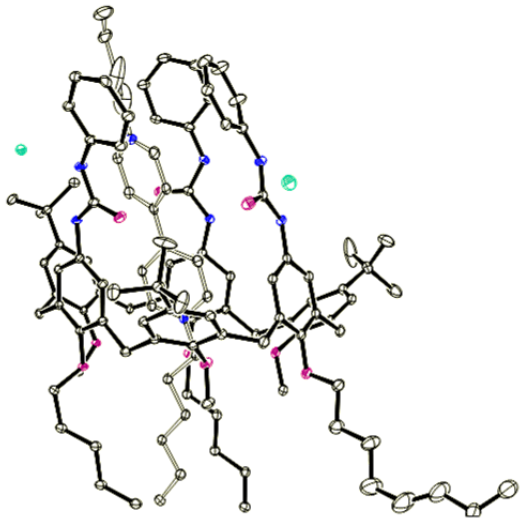

Figure 1.14: X-Ray structure of a calix[6]arene-based pseudorotaxane complex with a dioctylviologen salts (I^- as anion).

X-Ray structure (Figure 1.14) obtained from a single crystal confirmed that in the solid state the complex formed by the calix[6]arene wheel **1** with a viologen salt is stabilized by a combination of several supramolecular interactions that involve all districts of the wheel.[33] The aromatic walls of the calixarene, the oxygen atoms present at the lower rim and the phenylurea moieties are all involved in stabilizing this supramolecular complex. In addition, the two counteranions are hydrogen-bonded to the ureido NH groups present at the upper rim of the wheel. These information represented the starting point for the construction of oriented pseudorotaxanes and rotaxanes.

The contribution of the binding groups appended at both rims of the calixarene in governing the threading process was studied in order to gain a deeper understaning of the functioning mode of the calix[6]arene wheel as an asymmetrical heteroditopic three-dimensional host.[34] For this reason, to disclose the role played by the hydrogen bond donor ureido groups, compound **2** (Figure 1.15) where the nitrogen atoms have been methylated, was synthesized. Its binding ability towards dialkylviologen salts was studied in apolar solvents and all experiments gave negative results, clearly indicating that the interactions between the ureido groups and the anions are essential for the binding process. In fact the monotopic receptor **2** is not able to bind dialkylviologen guests even in presence of the potent receptor for spherical anions **3**, thus indicating that an heteroditopic receptors is more efficient with respect to the dual host system.

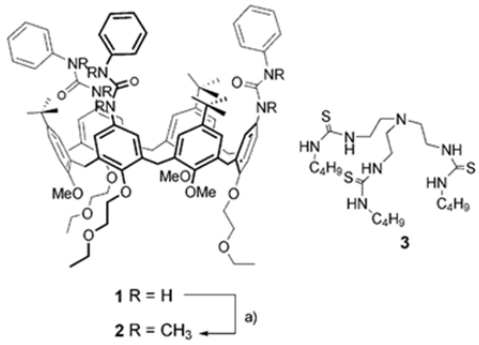

Figure 1.15: monotopic receptor **2** and receptor for spherical anions **3**.

With the purpose of evaluating whether the position of the three hydrogen bond donor groups that are at the upper rim in **1** could play also the same role when inserted at the lower rim of the calix[6]arene platform, compound **5** that bears the three phenylureido groups appended at the lower rim of the calix was synthesized (Figure 1.16). Even in this case, the macrocycle is not able to form stable complex with dialkylviologen salt in apolar

media. The lack of binding ability shows that, although receptor **5** can be considered as an heteroditopic receptor, the two binding sites are not arranged in a profitable manner.

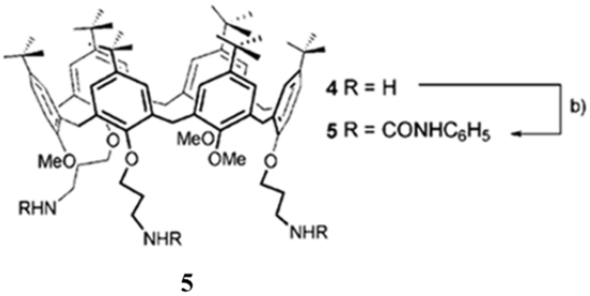

5

Figure 1.16: calix[6]arene derivative **5** that bears the three ureido groups at the lower rim.

A non-symmetrical axle that bears a diphenylacetyl stopper at one terminus was synthetized in order to verify whether the chemical and structural information stored in **1** could be exploited to guide the threading of an axle from one particular rim of the macrocycle. In principle, in the absence of control elements that drive the threading process, this axle could enter the calix[6]arene wheel either from its upper or lower rim, yielding a mixture of two oriented pseudorotxane isomers. It was verified that in apolar media this axle threads the wheel **1** exclusively from the upper rim yielding only one oriented pseudorotaxane having the stopper in proximity of the upper rim (Figure 1.17).[35]

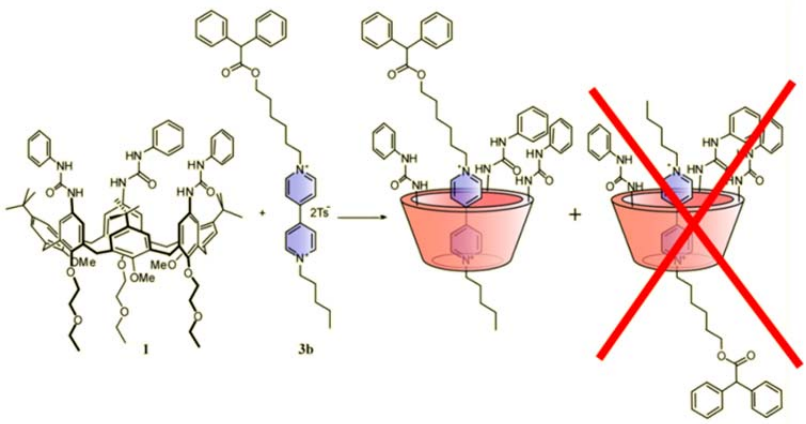

Figure 1.17: calix[6]arene-based oriented pseudorotaxane.

This behaviour was tentatively explained considering that: *i*) in apolar solvent the three OCH_3 of the calix occupy the cavity[36] and disfavour the access of the axle from the lower rim; *ii*) in apolar solvent the axle is present as a "tight" ion-pair; since the cavity of the

calixarene can host only the cationic portion of the guest, a partial separation of the cation from its counteranions should take place before axle threading; *iii*) the ureido groups that are potent hydrogen-bond donor group can interact with the anions of the axle, inducing the separation of the ion-pair and thus pivoting the threading process from the upper rim of the wheel (Figure 1.18).

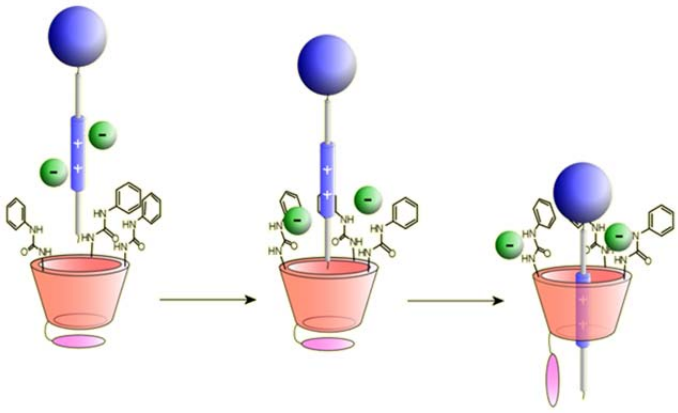

Figure 1.18: schematic representation of the threading process pivoted by the ureido groups of the wheel.

The apparent association constant of these pseudorotaxane systems, determined through UV-Vis spectroscopy, are of the order of 10^6 M^{-1}. The potential of these systems to work as molecular machines was studied through cyclic voltammetry, since the bipyridinic unit of the axle is redox active. It was shown that it is possible to reversibly dethread-thread the guest from the calix[6]arene cavity as a consequence of external electrochemical inputs (Figure 1.19).[37]

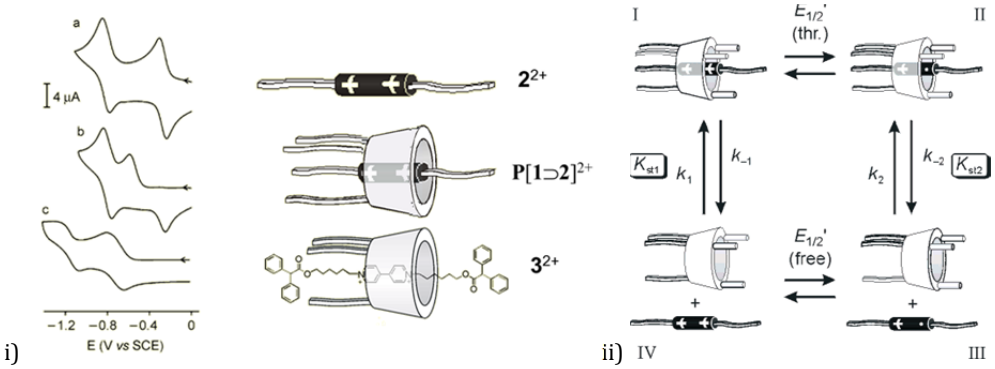

i) ii)

Figure 1.19: i) (a) Cyclic voltammetric curves (CH_2Cl_2, 0.05 M tetrabutylammonium hexafluorophosphate, 298 K; scan rate: 0.2 V s–1) for the first and second reduction of the 4,4'-bipyridinium unit in $\mathbf{2}^{2+}$ (top), in the pseudorotaxane $\mathbf{P[1\supset2]}^{2+}$ (middle), and in the rotaxane $\mathbf{3}^{2+}$ (bottom); ii) Square scheme mechanism for the one-electron reduction of $\mathbf{P[1\supset2]}^{2+}$, I and III represent the stable states, whereas II and IV are metastable intermediates. The counteranions have been omitted for clarity.

The extension of these studies has brought for the first time to the synthesis of two constitutionally isomeric oriented rotaxanes characterized by the univocal orientation of the two wheel rims with respect to the two different stoppers of the dumbbell (Figure 1.20).[38] In addition, it was observed that when the threading process between wheel **1** and a suitable axle was carried out in the more polar acetonitrile, where the three methoxy groups of the wheel reside outside the calixarene cavity and the pivoting action of the ureido NHs do not efficiently operate, a mixture of the two orientational isormeric pseudorotaxane was obtained. These data, if on the one hand support the idea that the ureido groups at the upper rim of the wheel play a central role in governing the threading process, on the other they indicate that the axle can access the wheel also from the lower rim.[38]

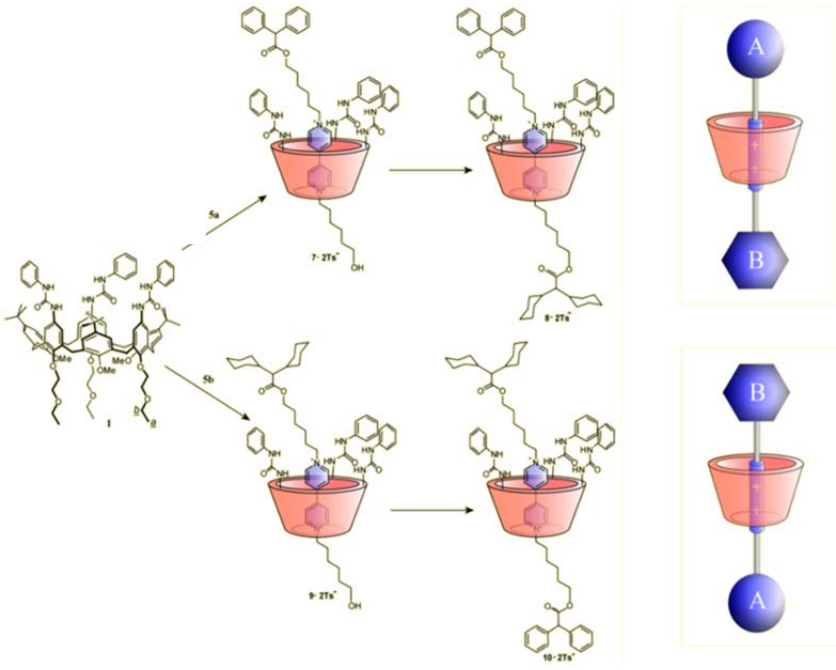

Figure 1.20: synthesis of two constitutionally isomeric oriented rotaxanes.

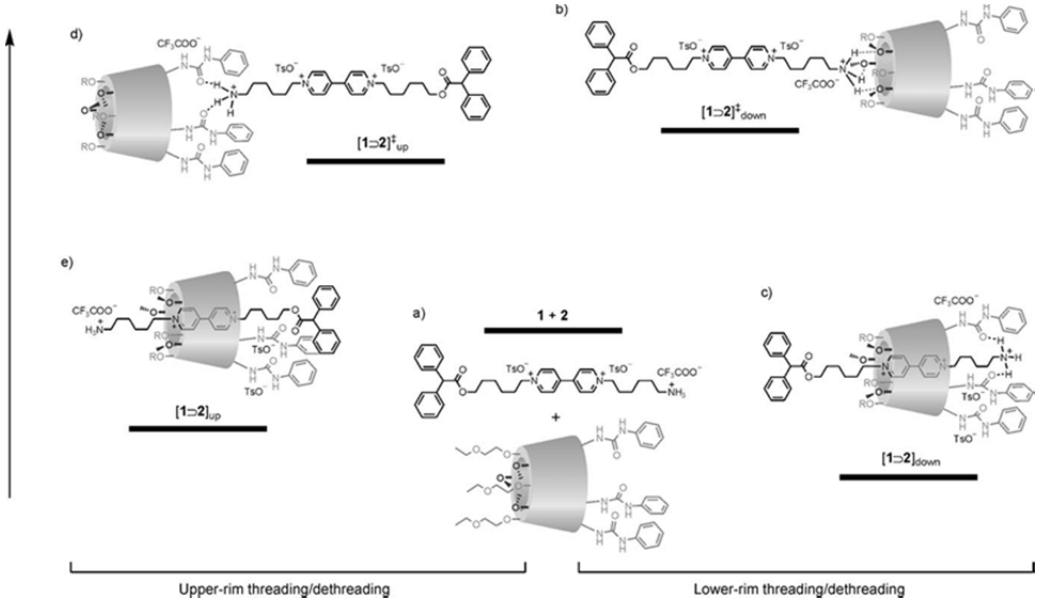

Figure 1.21: simplified potential-energy diagram for the threading/dethreading processes of axle **2** into wheel **1**, and schematic representation of the possible structures of the species involved.

More recent studies[39] showed that even the nature of the axle, in particular of the functional group appended to its terminus, can be used as control element to direct the threading process. It was demonstrated that an axle that bears a stopper at one end and a cationic ammonium group at the other can thread the wheel from both rims, depending on the condition used for the threading process. In fact while, as expected, at room temperature the axle threads the wheel from the upper rim, by increasing the temperature the oriented pseudorotaxane previously formed disassembles and reassembles yielding a pseudorotaxane isomers mixture in which the pseudorotaxane derived from the threading of the axle from the lower rim is the preferred (Figure 1.21).

References

[1] a) J. W. Steed, D. R. Turner, K. J. Wallace, *Core concepts in Supramolecular Chemistry and NanoChemistry*, John Wiley and Sons, Ltd, Chichester, UK, **2007**. b) J. W. Steed, J. L. Atwood, *Supramolecular Chemistry 2nd edition,* John Wiley and Sons, Ltd, Chichester, UK, **2009.**

[2] K. A. Connors, *Binding Costants: The Measurement of Molecular Complex Stability*, John Wiley & Sons, Ltd, Chichester, UK, **1987**.

[3] a) G. Ercolani, L. Schiaffino, *Angew. Chem. Int. Ed.*, **2011**, *50*, 1762-1768; b) R. D. Hancock, *J. Chem. Edu.,* **1992**, *69*, 615-621; c) J. D. Badjicä , A. Nelson, S. J. Cantrill, W. B. Turnbull, J. F. Stoddart, *Acc. Chem. Res.* **2005**, *38*, 723-732; d) K. Bowman-James, *Acc. Chem. Res.* **2005**, *38*, 671-678; e) J.-M. Lehn, *Acc. Chem. Res.* **1978**, *11*, 49-57; f) C. A. Hunter, H. L. Anderson, *Angew. Chem. Int. Ed.*, **2009**, *48*, 7488-7499.

[4] a) D. J. Cram, *Angew. Chem. Int. Ed.*, **1986**, 1039-1134; b) D. Fiedler, D. H. Leung, R. G. Bergman, K. N. Raymond, *Acc. Chem. Res*. **2005**, *38*, 351-360; c) P. Lhotak, *Topic in Curr. Chem.,* **2005**, *255,* 65-95; d) K. Sada, M. Takeuchi, N. Fujita, M. Numata, S. Shinkai, *Chem. Soc. Rev.*, **2007**, *36*, 415-435; e) C. D. Meyer, C. S. Joiner, J. F. Stoddart, *Chem. Soc. Rev*., **2007**, *36,* 1705–1723; f) S. F. Martin, *Pure Appl. Chem*., **2007**, *79*, 193–200; g) M. H. Filby, J. W. Steed, *Coord. Chem. Rev.*, **2006**, *250,* 3200–3218; h) M. M. G. Antonisse, D. N. Reinhoudt, *Chem. Commun*., **1998**, 443-448; i) P. Lhotak, S. Shinkai, *J. Phys. Org. Chem.*, **1997**, *10*, 273–285.

[5] a) C. Garcia, D. Humiliere, N. Riva, A. Collet, J.-P.Dutasta, *Org. & Biomol. Chem.,* **2003**, *1*, 2207-2216; b) L. Garel, B. Lozach, J.-P. Dutasta, A. Collet, *J. Am. Chem. Soc.,* **1993**, *115*, 11652-11653; c) F. P. Schmidtchen, *Coord. Chem. Rev.*, **2006**, *250*, 2918-2028.

[6] a) J. M. Lehn, *Supramolecula Chemistry: Concepts and Perspectives*, VCH, Weinheim, **1995**; b) V. Balzani, F. Scandola, *Supramolecular Photochemistry*, Horwood, Chichester, **1991**; c) F. Vögtle, *Supramolecular Chemistry An Introduction*, Wiley, Chichestrer, **1991**; d) J. S. Lindsey, *New J. Chem.*, **1991**, *15*, 153; e) G. M. Whitesides, J. P. Mathias, C. T. Seto, *Science*, **1991**, *254*, 1312; f) *Frontieres in Supramolecular Organic Chemistry and Photochemistry,* (Eds.:H.-J. Schneider, H. Dürr), VCH, Weinheim, **1991**; g) *Supramolecular Chemistry*, (Eds.: V. Balzani, L. De Cola), Kluwer, Dordrecht, **1992**; h) *Transition Metal in Supramolecular Chemistry*, (Eds.: L. Fabbrizzi, A. Poggi), Kluwer, Dordrecht, **1994**; *Comprehensive Supramolecular Chemistry,* (Eds.: J. L. Atwood, J. E. D. Davies, D. D. Macnicol, F. Vögtle), Pergamon Press, Oxford, **1996**, Vols 1-10; i) *Physical Supramolecular Chemistry*,

(Eds.: L. Echengoyen, A. E. Kaifer), Kluwer, Dordrecht, **1996**; j), *Modular Chemistry*, (Ed.:J. Michl), Kluwer, Dordrecht, **1997**; *Supramolecular Science: Where It is and Where It is Going* (Eds.: R. Ungaro, E Dalcanale), Kluwer, Dordrecht, **1999**; k) *Transition Metals in Supramolecular Chemistry* (Eds.: J.-P. Sauvage), Wiley, New York, **1999**; l) G. R. Newkome, C. N. Moorefield, F. *Dendrimers and Dendrons*, Wiley-VCH, Weinheim, **2001**; m) S. J. Rowan, S. J. Cantrill, G. R. L. Cousins, J. K. M. Sanders, J. F. Stoddart, *Angew. Chem. Int. Ed.,* **2002**, *41*, 898; n) J.-M. Lehn, *Proc. Natl. Acad. Sci. USA*, **2002**, *99*, 4763.

[7] a) G. E. Moore, *Electronics,* **1965**, *38*, 114; b) I. Amato, *Science*, **1998**, *282*, 402; c) D. Barrow. J. Cefai, S. Taylor, *Chem. Ind.,* **1999**, August 2, 591; d) J. W. Judy, *Smart Mater. Struct.,* **2001**, *10*, 1115.

[8] a) D. A. Muller, T. Sorsch, S. Moccio, F: H. Baumann, K. Evan-Lutterodt, G. Timp, *Nature*, **1999**, *399*, 758; b) G. M. Whitesides, J. C. Love, *Sci. Am.,* **2001**, *285(3)*, 32; c) R: F. Service, *Science,* **2001**, *293*, 785.

[9] a) R. P. Feynman, *Eng. Sci.*, **1960**, *23*, 22; b) R. P. Feynman, *Saturday Rev.,* **1960**, *43*, 45.

[10] a) V. Balzani, M. Venturi, A. Credi, *Molecular Devices and Machines – Concepts and Perspectives for the Nano World*, 2nd Ed., Wiley-VCH, Weinheim, **2008**; b) *Encyclopedia of Supramolecular Chemistry* (Eds.: J. L. Atwood,J. W. Steed), Dekker, New York, **2004**; c) K. Patel, S. Angelos,W. R. Dichtel, A. Coskun, Y.-W. Yang, J. I. Zink, J. F. Stoddart, *J. Am. Chem. Soc.* **2008**, *130*, 2382 – 2383; d) V. Ferri, M. Elbing, G. Pace, M. D. Dickey, M. Zharnikov, P. Samorì, M. Mayor, M. A. Rampi, *Angew. Chem. Int. Ed.* **2008**, *47*, 3407 –3409; e) D. Li, A. Wieckowska, I. Willner, *Angew. Chem. Int. Ed.* **2008**, *47*, 3927 –3931; f) A. J. Kronemeijer, H. B. Akkerman, T. Kudernac, B. J.van Wees, B. L. Feringa, P. W. M. Blom, B. de Boer, *Adv. Mater.* **2008**, *20*, 1467 –1473; g) H. Tian, Y. L. Feng, *J. Mater. Chem*. **2008**, *18*, 1617 –1622; h) S. Uchiyama, K. Iwai, A. P. de Silva, *Angew. Chem. Int. Ed*. **2008**, *47*, 4667 –4669; i) M. Kluciar, R. Ferreira, B. de Castro, U. Pischel, *J. Org. Chem*. **2008**, *73*, 6079 –6085; j) T. Gupta, M. E. van der Boom, *Angew. Chem. Int. Ed*. **2008**, *47*, 5322 – 5326; k) J. X. Yu, S. Mathew, B. S. Flavel, M. R. Johnston, J. G. Shapter, *J. Am. Chem. Soc*. **2008**, *130*, 8788 –8796; l) C. Giansante, P. Ceroni, V. Balzani, F. Vogtle, *Angew. Chem. Int. Ed.* **2008**, *47*, 5422 – 5425; m) M. Amelia, M. Baroncini, A. Credi, *Angew. Chem. Int. Ed.* **2008**, *47*, 6240 – 6243; n) J. Andrèasson, S. D. Straight, T. A. Moore, A. L. Moore, D. Gust, *J. Am. Chem. Soc.* **2008**, *130*, 11122 – 11128; o) M. Berberich, A.-M. Krause, M. Orlandi, F. Scandola, F. Wurthner, *Angew. Chem. Int. Ed.* **2008**, *47*, 6616 –6619.

[11] a) *Chem. Rev.*, **1999**, *99*, 1641-1990 (special issue on nanostructure); b) *Acc. Chem. Res.*, **1999**, *32*, 387-454 (special issue on nanoscale materials).

[12] see for example: a) D. B. Amabilino, J. F. Stoddart, *Chem. Rev.*, **1995**, *95*, 2725-2828; b) E. R. Kay, D. A. Leigh, F. Zerbetto, *Angew. Chem. Int. Ed.*, **2007**, *46*, 72-191.

[13] see for example: a) P.R. Ashton, I. Baxter, M. C. T. Fyfe, F. M. Raymo, J. F. Stoddart, A. J. White, D. J. Williams, *J. Am. Chem. Soc.*, **1998**, *120*, 2297; b) M. Asakawa, P.R. Ashton, R. Ballardini, V. Balzani, M. Belohradsky, M. T. Gandolfi, O. Kocian, L. Prodi, F. M. Raymo, J. F. Stoddart, M. Venturi, *J. Am. Chem. Soc.*, **1997**, *119*, 302; c) F. M. Raymo, J. F. Stoddart, *Chem. Rev.*, **1999**, *99,* 1643; d) *Molecular Catenanes, Rotaxanes and Knot* (Eds.: J.-P. Sauvage, C.O. Dietrich-Buchecker) Wiley-VCH, Weinheim, **1999**; e) V. Balzani, A. Credi, M. Venturi, *Proc. Natl. Acad. Sci. USA*, **2002**, *99*, 4814.

[14] D. Philp, J. F: Stoddart, *Synlett*, **1991** 445-458.

[15] F. M. Raymo, K. N. Houk, J. F. Stoddart, *J. Am. Chem. Soc.*, **1998**, *120*, 9318-9322 and references therein.

[16] a) M. J. Langton, J. D. Matichak, A. L. Thompson, H. L. Anderson, *Chem. Sci*, **2011**, *2*, 1897; b) H. M. Cheng, D. A. Leigh, F. Maffei, P. R. McGonigal, A. M. Z. Slawin, J. Wu, *J. Am. Chem. Soc.*, **2011**, *133,* 12298–12303.

[17] a) V. Balzani, G. Bergamini, P. Ceroni, *Coord. Chem. Rev.*, **2008**, *252*, 2456-2469; b) S. J. Loeb, *Chem. Soc. Rev*., **2007**, *36*, 226-235; c) F. M. Raymo,J. F. Stoddart, *Supramolecular Organization and Materials Design*, 332-363 (Eds.: W. Jones,C.N.R: Rao), **2002**; d) K. Kim, *Chem. Soc. Rev.,***2002**, *31*, 96-107; e) V. Balzani, A. Credi, F. M. Raymo, J.F. Stoddart, *Angew. Chemie, Int. Ed.*, **2000**, *39*, 3348-3391.

[18] a) P. L. Anelli, N. Spencer, J. F. Stoddart, *J. Am. Chem. Soc.*, **1991**, *113*, 5131-5133; b) P. L. Anelli, M. Asakawa, P. R. Ashton, R. A. Bissel, G. Clavier, R. Gorski, A. E: Kaifer, S. J. Langford, G. Mattersteig, S. Menzer, D. Philp, A. M. Z. Slawin, N. Spencer, J. F. Stoddart, M. S. Tolley, D. J. Williams, *Chem. Eur. J.*, **1997**, *3*, 1113-1135; c) D. A. Leigh, A. Troisi, F. Zerbetto, *Angew. Chem. Int. Ed.*, **2000**, *39*, 350-353; d) D. Sobransingh, A. E. Kaifer, *Org. Lett.*, **2006**, **8**, 3247 – 3250; e) S. J. Vella, J. Tiburcio, J.W. Gauld, S. J. Loeb, *Org. Lett.*, **2006**, *8*,3421 – 3424; f) S. Silvi, A. Arduini, A. Pochini, A. Secchi, M. Tomasulo,F. M. Raymo, M. Baroncini, A. Credi, *J. Am. Chem. Soc.*, **2007**, *129*, 13378 –13379; g) Y.-L. Huang, W.-C. Hung, C.-C. Lai, Y.-H.Liu, S.-M. Peng, S.-H. Chiu, *Angew. Chem. Int. Ed.*, **2007**, *46*, 6629 – 6633; h) D. Tuncel, M. Katterle, *Chem. Eur. J.* **2008**, *14*, 4110 – 4116; i) L. Raehm, J.-P. Sauvage, *Struct. Bonding,* **2001**, *99*, 55-78; j) M.C. Jimenez, C. O. Dietrich-Buchecker, J.-P Sauvage, *Angew. Chem. Int. Ed.,* **2000**, *39*, 3284; k) M. C. Jimenez-Molero, C. O. Dietrich-Buchecker, J.-P Sauvage, *Chem. Eur. J.*, **2002**, *8*, 1456.

[19] A. Credi, M. Semeraro, S. Silvi, *Frontiers in Bioscience*, **2008**, *13*, 1036-1049.

[20] J. D. Badjic, V. Balzani, A. Credi, S. Silvi, J. F. Stoddart, *Science*, **2004**, *303*, 1845-1849.

[21] J. D. Badjic, V. Balzani, A. Credi, S. Silvi, M. C. Ronconi, J. F. Stoddart, *J. Am. Chem. Soc.*, **2006**, *128*, 1489-1499.

[22] H.-R. Tseng, S. A. Vignon, J. F. Stoddart, *Angew. Chem. Int. Ed*. **2003**, *42*, 1491–1495.

[23] M. Bendikov, F. Wudl, *Chem. Rev.,* **2004**, *104*, 4891-4945.

[24] R. Ballardini, V. Balzani, A. Credi, M. T: Gandolfi, S: J. Langford, S. Menzer, L. Prodi, J. F: Stoddart, M. Venturi, D. J. Williams, *Angew. Chem. Int. Ed.*, **1996**, *35*, 978-981.

[25] a) P. R. Ashton, D. Philp, N. Spencer, J. F. Stoddart, *Special publication - Royal Society of Chemistry,* **1992**, *111*(*Molecular Recognition: Chemical and Biochemical Problems II*),51-63; b) M. C. T. Fyfe, J. F. Stoddart, *Advances in Supramolecular Chemistry,* **1999**, *5*, 1-53;

[26] see for examples: a) H. Li, A. C. Fahrenbach, A. Coskun, Z.-X. Zhu, G. Barin, Y.-L. Zhao, Y. Y. Botros, J.-P. Sauvage, J. F. Stoddart, *Angew. Chem., Int. Ed.* **2011**, *50*, 6782-6788 b) M. F. Hmadeh, A. C. Fahrenbach, S. Basu, A. Trabolsi, D. Benitez, H. Li, A.-M. Albrecht-Gary, M. Elhabiri, J. F. Stoddart, *Chem. Eur. J.* **2011**, *17*, 6076-6087 c) I. Yoon, D. Benitez, Y.-L. Zhao, O. S. Miljanic, S.-Y. Kim, E. Tkatchouk, K. C.-F. Leung, S. I. Khan, W. A. Goddard, J. F. Stoddart, *Chem. Eur. J.* **2009**, *15*, 1115-1122.

[27] K. M. Park, D. Whang, E. Lee, J. Heo, K. Kim, *Chem. Eur. J.*, **2002**, *8*, 498-508.

[28] a) S. A. Nepogodiev, J. F. Stoddart, *Chem. Rev.*, **1998**, *98*, 1959; b) R. Isnin, A. Kaifer, *J. Am. Chem. Soc.,* **1991**, *113*, 8188-8190; c) R. Isnin, A. Kaifer, *Pure Appl. Chem.*, **1993**, *65*, 495-498. d) A. Harada, *Acc. Chem. Res.* **2001**, *34,* 456-464;

[29] a) H. Yonemura, M. Kasahara, H. Saito, H. Nakamura, T. Matsuo, *J. Phys Chem.*, **1992**, *96*, 5765-5770; b) J. W. Park, H. J. Song, *Org. Lett.,* **2004**, *6*, 4869-4872.

[30] a) T. Oshikiri, Y. Takashima, H. Yamaguchi, A. Harada*, J. Am. Chem. Soc*. **2005**, *127*, 12186-12187; b) T. Oshikiri, H. Yamaguchi, Y. Takashima, A. Harada, *Chem. Commun*. **2009**, 5515-5517.

[31] a) C. D. Gutsche, *Calixarenes, Monographs in Supramolecular Chemistry,* Ed.: J. F. Stoddart, Royal Society of Chemistry, U.K., **1989**; b) C. D: Gutsche, *Calixarene Revisited, Monographs in Supramolecular Chemistry*, Ed.: J. F. Stoddart, Royal Society of Chemistry, U.K., **1998**; c) *Calixarene in Action*, (Eds. L.Mandolini, R. Ungaro) Imperial College Press, **2000**; d) *Calixarene 2001*, Eds.: Z: Asfari, V. Böhmer, J. Harrowfield, J. Vicens, Kluwer Academic: Dordrecht, **2001**; e) C.D. Gutsche, *Calixarene, An Introduction, Monographs in Supramolecular Chemistry*, Ed.: J. F. Stoddart, Royal Society of Chemistry: Cambridge, U.K., **2008**; f) A. Arduini, D. Demuru, A. Pochini, A. Secchi, *Chem. Commun.* **2005**, *5*, 645-647; g) A. Arduini, E. Brindani, G. Giorgi, A. Pochini, A. Secchi, *J. Org. Chem.* **2002**, *67*, 6188-6194; h) A. Arduini, G. Giorgi, A. Pochini, A. Secchi, F. Ugozzoli, *J. Org. Chem.* **2001**, *66*, 8302-8308; i) A. Arduini, W. M. McGregor, D. Paganuzzi, A. Pochini, A. Secchi, F. Ugozzoli, R. Ungaro,*J. Chem. Soc. Perkin Transactions 2*: Physical Organic Chemistry **1996**, *5*, 839-846.

[32] A. Arduini, R. Ferdani, A. Pochini, A. Secchi, F. Ugozzoli, *Angew. Chem. Int. Ed.*, **2000**, *39*, 3453-3456.

[33] F. Ugozzoli, C. Massera, A. Arduini, A. Pochini, A. Secchi, *CrystEngComm.*, **2004**, *6*, 227.

[34] Dr. Giovanni Faimani, *PhD Thesis in Chemical Sciences*, XIX cycle, University of Parma, **2007**.

[35] A. Arduini, F. Calzavacca, A. Pochini, A. Secchi, *Chem. Eur. J.*, **2003**, *9*, 793-799.

[36] a) J. P. M. van Duynhoven, R. G: Janssen, W. Verboom, S. M. Franken, A. Casnati, A. Pochini, R. Ungaro, J. de Mendoza, P. M. Nieto, P. Prados, D. N. Reinhoudt, *J.Am. Chem. Soc.,* **1994**, *116*, 5814-5822; b) W. P. van Hoom, F. C. J. M. van Veggel, D. N. Reinhoudt, *J. Phis. Chem. A*, **1998**, *102*, 6676.

[37] A. Credi, S. Dumas, S. Silvi, M. Venturi, A. Arduini, A. Pochini, A. Secchi, *J. Org. Chem.*, **2004**, *69*, 5881-5887.

[38] A. Arduini, F. Ciesa, M. Fragassi, A: Pochini, A. Secchi, *Angew. Chem. Int. Ed.*, **2005**, *44*, 278-281.

[39] A. Arduini, R. Bussolati, A. Credi, G. Faimani, S. Garaudée, A. Pochini, A. Secchi, M. Semeraro, S. Silvi, M. Venturi, *Chem. Eur. J.*, **2009**, *15*, 3230-3242.

CHAPTER 2

Threading processes under kinetic control

Chapter 2

Threading processes under kinetic control

2.1 Syntheses of the viologen axles

In the previous chapter the ability of the three-ureido calix[6]arene derivatives to act as wheel for oriented pseudorotaxanes and rotaxanes synthesis have been briefly summarized. These properties clearly indicate that the spatial arrangement and distance among its functional groups and binding sites do have a paramount importance in defining their ability to act as efficient host for 4,4'-bipyridinium-based guests.

From these data it could also be concluded that, in apolar media, regardless its nature, an axle threads the wheel from the upper rim for kinetic reasons. It remains however undisclosed whether the isomerisation observed for the tri-cationic axle (see Chapter 1 page 27) is a general property of calixarene-based oriented pseudorotaxanes or it is a property that originate from the nature of the axle.

It was thus envisaged that a deeper comprehension of the factors that govern the direction of axle threading into wheel **1** could allow the development of systems and devices endowed with a wider set of properties and possible applications. Particularly enticing was then a systematic analysis of the threading process outcome by employing wheel **1** and a series of axles composed by a common 4,4'-bipyridinium cationic core functionalized with two "simple" alkyl chains of variable (equal or different) length.

In fact in open n-alkyl chain flexible compounds, which represent the simplest series of substituents in organic compounds, the conformational space of the molecular backbone can severely intervene in defining the possible distance between the functional groups attached. This is evidenced in the case of biological membranes, many polymers, liquid crystals or functional compounds bearing n-alkyl chains, where the conformational preference of these "simple" groups plays a fundamental role in determining the properties (and reactivity) of the other functional groups that are present.[1]

It could be imagined that in these axles, the variable conformational space as function of the chain length could limit or define the possible distance between their termini and the 4,4' bipy cationic core and thus their intrinsic ability to act as axles as a function of their length. The aim was thus to study the threading process of these axles into wheel **1** from a structural, thermodynamic and kinetic point of views. For the synthesis of symmetrical and asymmetrical axles, the reaction sequence reported in Scheme 2.1 was followed.

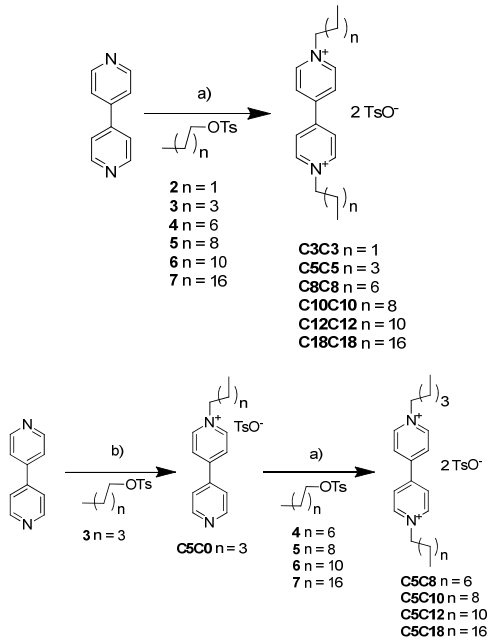

Scheme 2.1: Reagents and conditions: a) CH_3CN, 100°C in a glass autoclave, 3 days; b) CH_3CN, reflux, 2 days.

A CH_3CN solution of 4, 4' bipyridyl was reacted, in a glass autoclave at 100°C, in presence of an excess of the appropriate alkyl-tosylate (**2**–**7**) , to yield the corresponding symmetric di-alkylviologen salt (**C3C3** – **C18C18**).

To synthetize the asymmetric salts, 4, 4' bipyridyl was first reacted, in refluxing CH_3CN, with **3**. The mono alkylated **C5C0** was then reacted, in CH_3CN in a glass autoclave at 100°C, with the appropriate alkyl-tosilates (**4**–**7**) to yield the corresponding asymmetric di-alkylviologen salt **C5C8**-**C5C18**.

As an example the spectrum of the symmetric axle **C8C8** is reported in Figure 2.1.

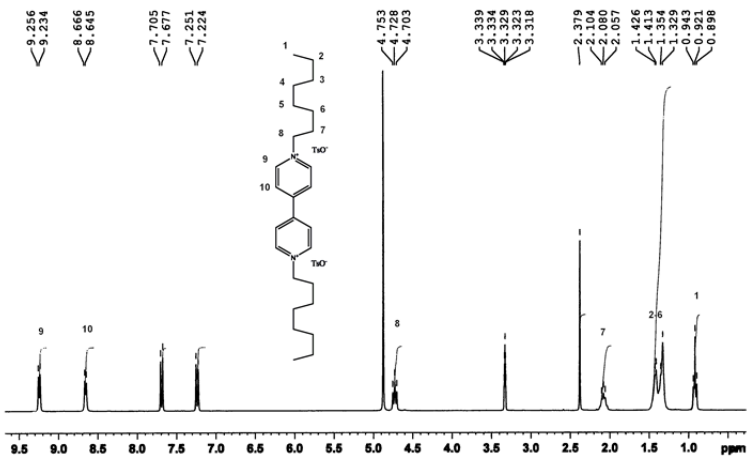

Figure 2.1: ^{1}H NMR (300 MHz) of axle **C8C8** in CD_3OD.

In axle **C8C8** protons *9* and *10* resonate as two doublets at δ =9.24 and δ = 8.65 ppm, respectively. While protons *8* and *7* resonate at δ = 4.73 and δ = 2.08 ppm respectively. Because of the symmetry, the two terminal methyl groups *1* resonate as a triplet at δ = 0.92 ppm.

2.2 NMR studies on the oriented pseudorotaxanes

In principle, in apolar media, the upper rim of wheel **1** could be threaded by axles **C5C8**-**C5C18** either through their shorter or longer chains. In separate experiments wheel **1** and a slight excess of axle **C5C8**, **C5C10**, **C5C12** and **C5C18**, were thus equilibrated in C_6D_6 at 300 K (Scheme 2.2). The deep red solution obtained in all cases, after removal of the excess of axle, was submitted to NMR analyses.

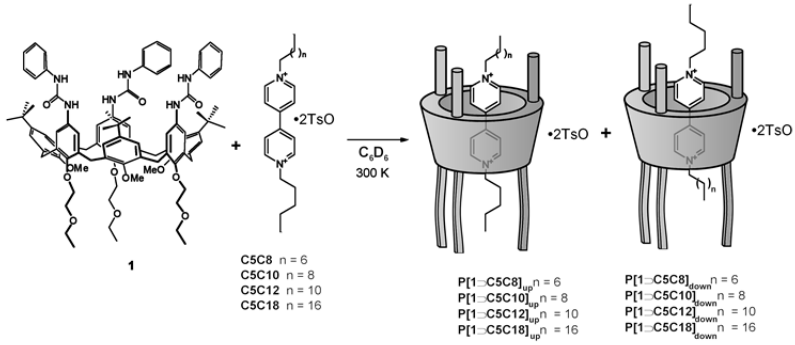

Scheme 2.2: Self-assembly of wheel **1** with asymmetric viologen axles.

The common NMR features of the spectra of the complexes formed by the different axles employed and the wheel are that the OMe groups of **1**, because of threading are expulsed from the interior of the calixarene cavity and resonate down-field shifted, at δ = 3.8-4.1 ppm. Since the presence of the axle inside the cavity renders the calixarene skeleton less conformationally flexible, the twelve bridging methylene protons resonates as an AX system. In addition, because of their involvement in the H-bonding with the two anions, the six ureido NH suffer a down shift of about 3 ppm.

When **C5C8** was used as axle, in spite of extensive overlapping of several signals observed in the 1D ^{1}H NMR spectrum (Figure 2.2), the presence of two sets of signals for the two alkyl chains linked to the 4,4′-bipyridinium core, and the presence of two distinct signal for the methoxy groups of the wheel that suggested the presence of the two orientational pseudorotaxane isomers (Figure 2.3) was evidenced through 2D TOCSY experiments.

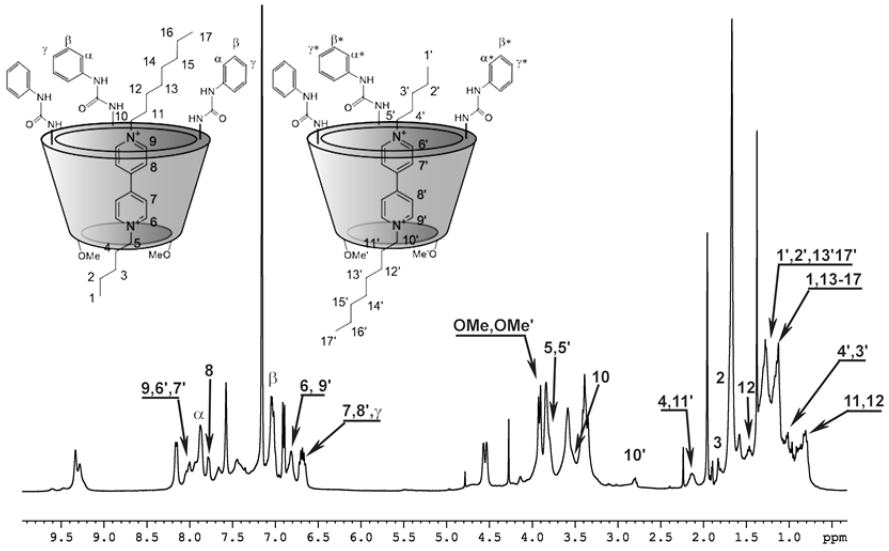

Figure 2.2: ^{1}H NMR (300 MHz) of **P[1⊃C5C8]** (up and down isomers mixture) in C_6D_6.

This hypothesis was confirmed with the 2D ROESY NMR spectra (Figure 2.4) that clearly showed spatial correlations between the methoxy groups at the lower rim of the calix[6]arene and the protons of both the octyl and the pentyl chains. It is thus possible to conclude that at room temperature axle **C5C8** can thread the upper rim of the wheel with both its alkyl chains, generating two pseudorotaxane **P[1⊃C5C8]$_{up}$** and **P[1⊃C5C8]$_{down}$** that are orientational isomers.

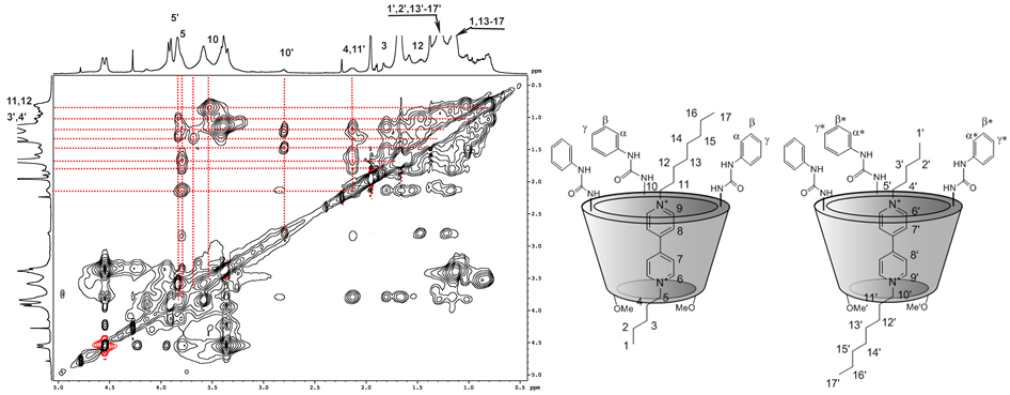

Figure 2.3: ^{1}H-^{1}H 2D TOCSY spectra in C_6D_6 (expanded region) (300 MHz, mixing time = 0.06 s) of: **P[1⊃C5C8]**.

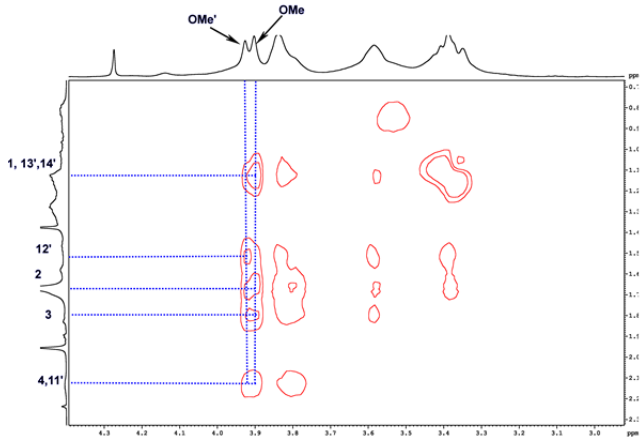

Figure 2.4: ^{1}H-^{1}H 2D ROESY (300 MHz) (expanded region) of **P[1⊃C5C8]$_{up}$** and **P[1⊃C5C8]$_{down}$** in C_6D_6 (spinlock = 200ms).

In the 1D ^{1}H NMR (Figure 2.5) and 2D NMR spectra of the pseudorotaxane formed after equilibration at 300 K of wheel **1** and axles **C5C10** in C_6D_6 a principal set of signal that was assigned to the complex where the axle threaded the wheel through the pentyl chains, yielding the pseudorotaxane **P[1⊃C5C10]$_{up}$** was visible. A second set of signals, of lower intensity, was present, and even if the assignment of all resonances was not possible, the presence of some diagnostic signals allowed to hypothesize the formation of the *down* isomer as the minor component of the mixture.

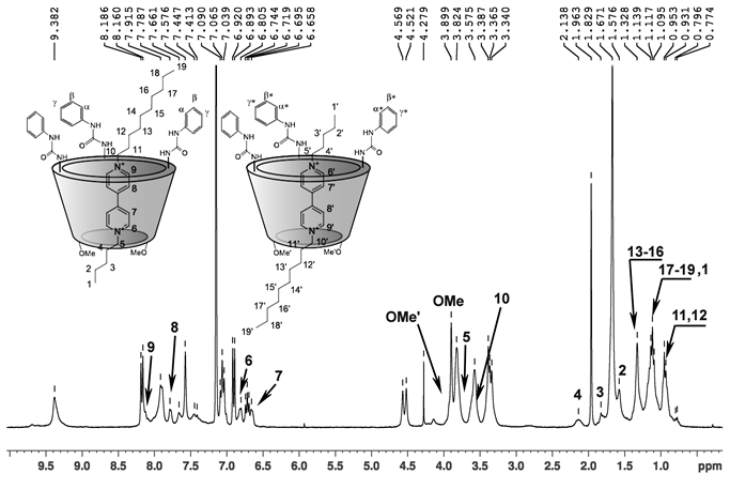

Figure 2.5: ^{1}H NMR (300 MHz) of **P[1⊃C5C10]** (up and down isomers mixture) in C_6D_6.

In the ^{1}H – ^{13}C 2D HSQC spectra (Figure 2.6) the presence of more than four correlation between the protons and carbons of the viologen unit confirmed the presence in solution of both the pseudorotaxane isomers.

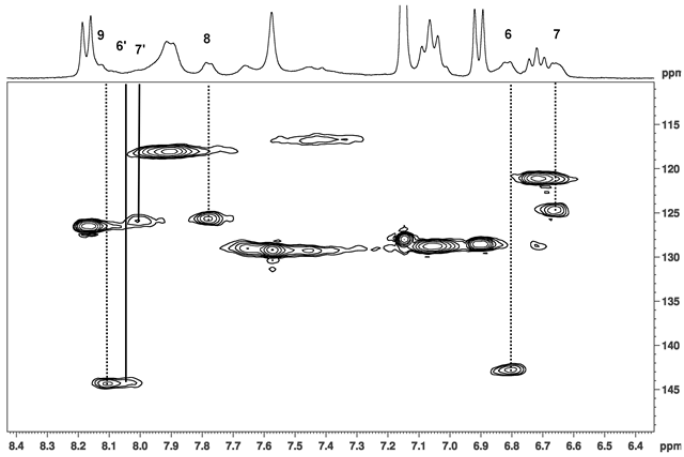

Figure 2.6: ^{1}H-^{13}C 2D HSQC (300 MHz) (expanded region) of **P[1⊃C5C10]$_{up}$** and **P[1⊃C5C10]$_{down}$** in C_6D_6.

A further proof that axle **C5C10** can thread the wheel also through its decyl chain was given by the 2D ROESY (Figure 2.7) spectra, in which spatial correlations between the methoxy groups of the wheel in the two isomers and the alkyl chains of the axle (the pentyl in one isomer and the decyl in the other) are present.

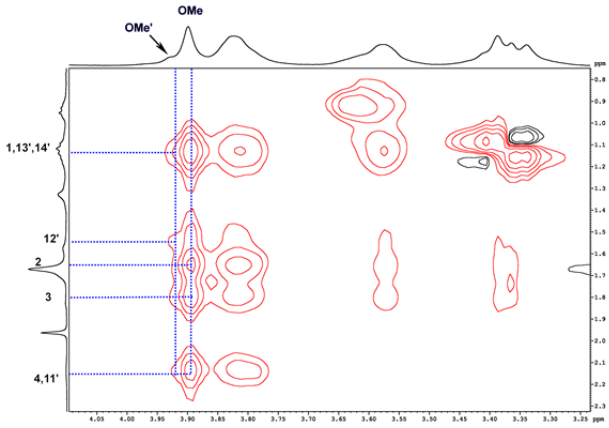

Figure 2.7: ^{1}H-^{1}H 2D ROESY (300 MHz) (expanded region) of **P[1⊃C5C10]$_{up}$** and **P[1⊃C5C10]$_{down}$** in C_6D_6 (SL = 200ms).

On the contrary, when **C5C18** or **C5C12** were employed as axles the presence of only one set of signals in the ^{1}H NMR spectra suggested the formation of only one pseudorotaxane isomer. Structure elucidation of the pseudorotaxanes was carried out through NMR techniques (COSY, TOCSY, ROESY, HSQC, HMBC).

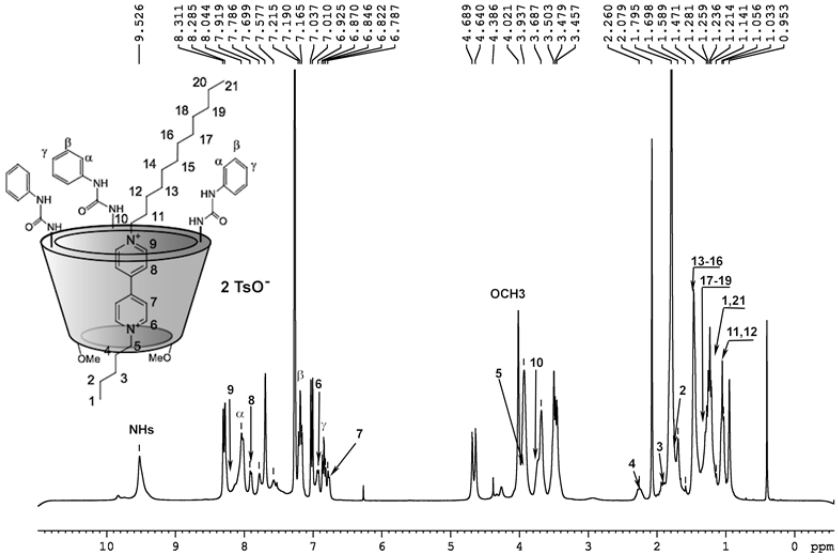

Figure 2.8: ^{1}H NMR (300 MHz) of **P[1⊃C5C12]$_{up}$** in C_6D_6.

In the ^{1}H NMR spectrum of **P[1⊃C5C12]** (Figure 2.8) protons *9, 8, 6, 7* resonate respectively at δ = 8.28 δ = 7.92, δ =6.87, and δ = 6.79 ppm because of the confinement of

the cationic portion of the axle within the shielding domain of the calix[6]arene. The presence of only one set of signal for the aromatic protons of the axle and for the two different alkyl chains, whose protons were assigned through TOCSY spectra (Figure 2.9), and the presence of only one signal for the methoxy protons of **1** suggested the presence of only one pseudorotaxane isomer.

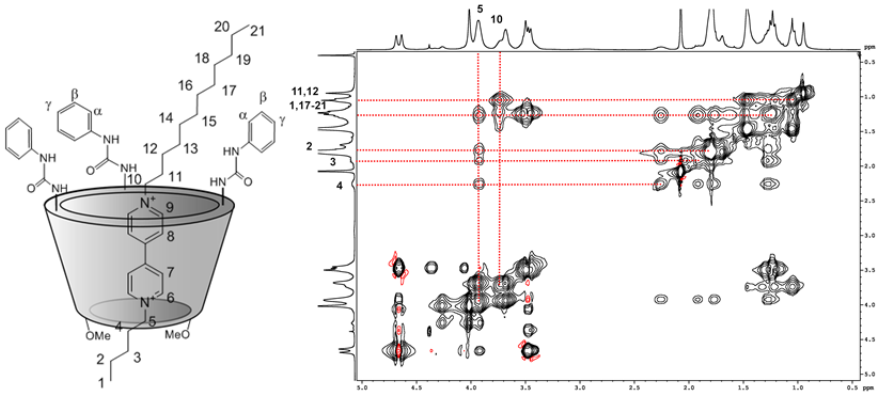

Figure 2.9: ^{1}H-^{1}H 2D TOCSY spectra in C_6D_6 (expanded regions) (300 MHz, mixing time = 0.06 s) of: **P[1⊃C5C12]$_{up}$**.

The orientation of this pseudorotaxane was established through 2D ROESY (Figure 2.10) experiments. The spatial correlations between the OCH_3 protons present at the lower rim of the calix[6]arene and protons *4, 3, 2, 1* of the axle, together with those between protons of the twelve carbon atoms chain and the aromatic protons of phenyureido groups of the wheel, confirmed that the axle had threaded the wheel from the upper rim only through the pentyl chain, and that the twelve carbon atoms chain was in proximity of the ureido groups of the wheel.

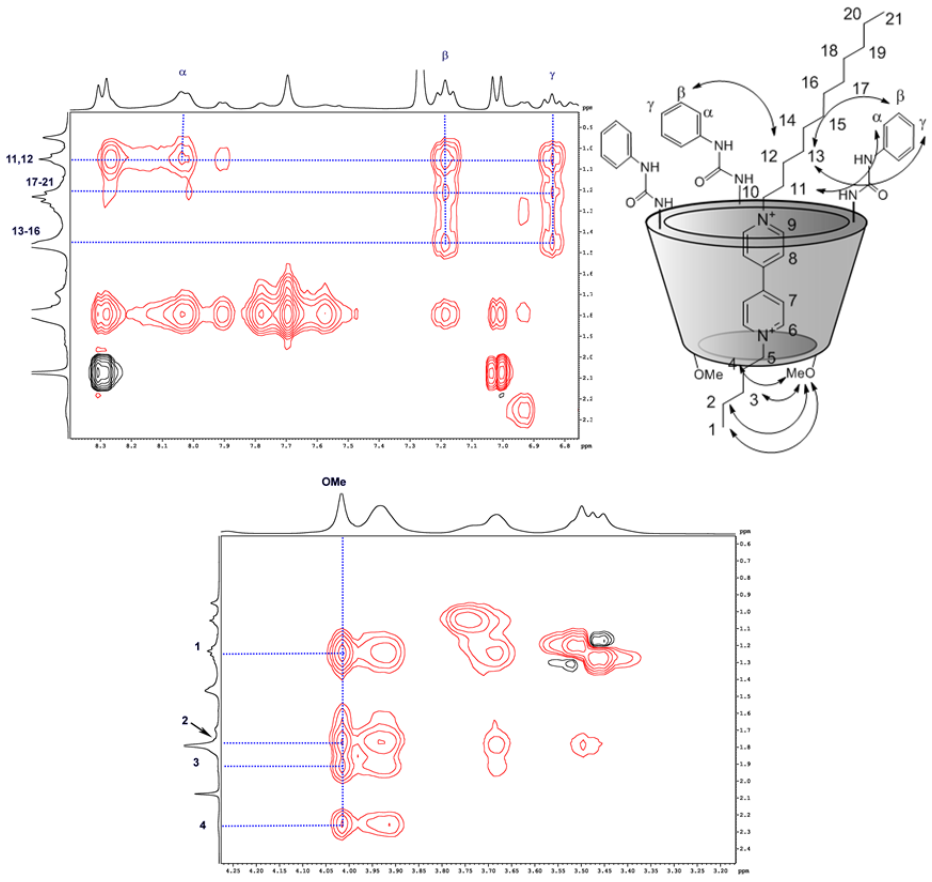

Figure 2.10: ^{1}H-^{1}H 2D ROESY (300 MHz) (enlargements) of **P[1⊃C5C12]$_{up}$** in C_6D_6 (spinlock = 200ms).

This first series of experiments clearly demonstrate that the difference in the chain length of the two alkyl groups attached at the 4,4' bipy unit has a crucial role in determining their threading orientation into **1**. From these data it emerges that when this difference is at least seven carbon atoms the complexation process yields only one pseudorotaxane isomer in which the axle had threaded the wheel through its shorter alkyl chain. On the other hand, when the chain length difference is shorter, a mixture of two orientational pseudorotaxane isomers forms. In order to quantify the percentages of the two orientational isomer in each experiment a peak's deconvolution analysis was carried out. To this extent the signals of the wheel methoxy groups, that resonate, in the pseudorotaxane isomers formed employing axles **C5C8** and **C5C10,** at different chemical shift in a spectral region relatively free from other signals were analysed (Table 2.1).

	Isomer	δ (ppm) OMe protons	%
1 + **C5C8**	**P[1⊃C5C8]$_{up}$**	3.90	53%
	P[1⊃C5C8]$_{down}$	3.93	47%
1 + **C5C10**	**P[1⊃C5C10]$_{up}$**	3.90	88%
	P[1⊃C5C10]$_{down}$	3.93	12%
1 + **C5C12**	**P[1⊃C5C12]$_{up}$**	3.90	100%
	P[1⊃C5C12]$_{down}$	/	/
1 + **C5C18**	**P[1⊃C5C18]$_{up}$**	3.90	100%
	P[1⊃C5C18]$_{down}$	/	/

Table 2.1: percentages of the orientational isomer obtained between wheel **1** with non-symmetrical di-alkyl viologen salts at room temperature.

From the data gathered in Table 2.1, it clearly emerges that the ratio among the orientational isomers approaches the 1:1 by decreasing the difference in the chain length in the different axles. To establish whether the origin of this orientational outcome derives from the different stabilities of the two orientational isomers that form with a given axle or these threading processes are kinetically controlled, the NMR samples containing the C_6D_6 solutions of the pseudorotaxane *"up"* and *"down"* isomer mixture (in the case of axles **C5C8** and **C5C10**) or only the "*up"* isomer (in the case of axles **C5C12** and **C5C18**) were heated to reflux for 24 h and the resulting solution submitted to NMR analyses.

In the cases of axles **C5C8**, **C5C10** and **C5C12** the ^{1}H NMR spectra of the pseudorotaxanes (Figure 2.11) evidenced the presence of two signals for the protons of the methoxy groups of the calix[6]arene that in all istances was *ca.* 1:1. This translates into an increase of the amount of the *"down"* isomer that forms from the dethreading of the *"up"* isomer and rethreading of the axle through its longer chain, increasing the amount of pseudorotaxane with the opposite orientation of the axle with respect to the calixarene rims. The 1:1 ratio among the two isomers suggested that, in these conditions, the thermodynamic equilibrium was reached and the two isomers possess a comparable stability.

On the contrary the behaviour of axle **C5C18** was quite different. In fact, after refluxing for 24 h the ratio between the signals of the methoxy groups in the two isomers was only 80(*up*):20(*down*).

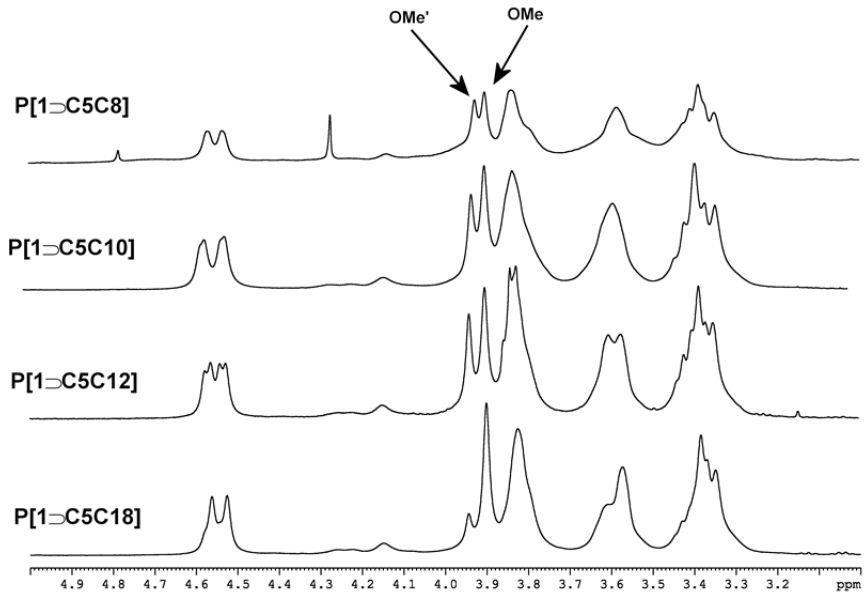

Figure 2.11: ^{1}H NMR spectra (300 MHz, C_6D_6, expanded regions) of **P[1⊃C5C18]**, **P[1⊃C5C12]**, **P[1⊃C5C10]** and **P[1⊃C5C8]**, after reflux of the samples for 24 h.

As working hypothesis, this different behavior could be explained considering that contrary to the C8, C10 or C12 chains, the C18 chain requires a higher energy barrier to thread the calix[6]arene annulus because of its larger conformational space. It could be imagined that for this chain, due to its length, the loss of conformational freedom needed to pass through the calixarene annulus before the stabilizing interactions between the viologen unit and the π rich walls of the wheel toke place, disfavors the threading of the axle through this long terminus. Refluxing of this sample up to 10 days changes the ratio between the two isomers from 80(*up*):20(*down*) to 70(*up*):30(*down*). Assuming this latter ratio as the equilibrium distribution of the two isomer, it could be hypothesized that in the *"down"* isomer possible unfavorable interactions of the octadecyl chain with the groups present at the lower rim of the calix[6]arene decrease the stability of this oriented pseudorotaxane.

These data clearly show that also in the cases of viologen salts bearing "simple" alkyl chain it is possible to govern the direction of axle threading by exploiting their different conformational space. They also suggest that the difference in chain length of the groups

appended to the cationic core of the axle can be employed to subtly tune the orientation of the axle that threads the upper rim of the wheel.

	Isomer	δ (ppm) OMe protons	% of formation
1 + C5C8	**P[1⊃C5C8]$_{up}$**	3.90	56%
	P[1⊃C5C8]$_{down}$	3.93	44%
1 + C5C10	**P[1⊃C5C10]$_{up}$**	3.90	58%
	P[1⊃C5C10]$_{down}$	3.93	42%
1 + C5C12	**P[1⊃C5C12]$_{up}$**	3.89	58%
	P[1⊃C5C12]$_{down}$	3.93	42%
1 + C5C18	**P[1⊃C5C18]$_{up}$**	3.89	79%
	P[1⊃C5C18]$_{down}$	3.94	21%
1 + C5C18 (10 days reflux)	**P[1⊃C5C18]$_{up}$**	3.89	71%
	P[1⊃C5C18]$_{down}$	3.94	29%

Table 2.2: percentages of the orientational isomers obtained refluxing the complexes yielded equilibrating **1** and the non-symmetric axles at reflux for 24 h (or 10 days).

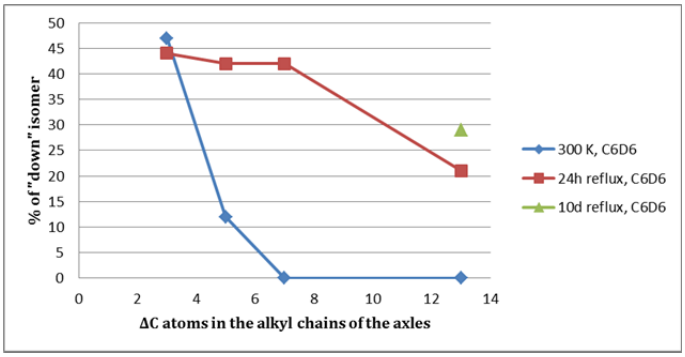

Table 2.3: % of the *"down"* isomer obtained varying the ΔC atoms of the two alkyl chains of the guest in three different experiments (room temperature ♦, 24 h reflux ■, 10 days reflux ▲).

In the attempt to better understand the peculiar behavior of the dyad **1-C5C18**, the threading process was studied also in the more polar CH_3CN. In this solvent the control elements that govern the unidirectional threading of the axle through the upper rim of the wheel, evidenced in C_6D_6, no longer operate.

Pseudorotaxane formation in CH_3CN was thus studied by ^1H NMR spectroscopy by equilibrating **1** and **C5C18** in a 1:1 molar ratio. The solvent was then evaporated at reduced pressure and the solid residue dissolved in C_6D_6 and submitted to NMR analyses. In the ^1H NMR spectrum (Figure 2.12) of the solution thus obtained, the signals of the axial methylene protons of the wheel that resonate as two doublets at $\delta = 4.57$ and $\delta = 4.55$, and the two signals assigned to the methoxy groups of the calix[6]arene that resonate at $\delta = 3.90$ and $\delta = 3.94$ ppm, suggest the presence in solution of both the *"up"* and *"down"* pseudorotaxane isomers. Deconvolution analysis, performed on these signals, indicates that the two isomers are in a 1:1 ratio. This threading outcome could be explained considering that in CH_3CN the threading process can take place from the both the rims of the wheel and the axle can thread through its shorter or longer alkyl chain. This 1:1 ratio between the *"up"* and *"down"* isomers does not change even after refluxing this C_6D_6 NMR sample for 10 days.

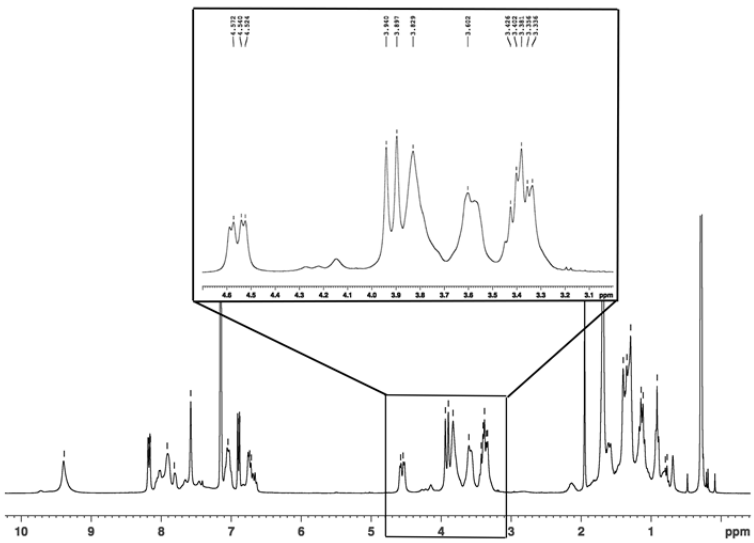

Figure 2.12: ^1H NMR spectra (300 MHz, C_6D_6) of **P[1⊃C5C18]**, after that the threading process was conducted in CH_3CN. Expanded region from 3.1 to 4.8 ppm in the inset.

Axle **C3C3** unespectedly showed a very different behaviour, compared to the other axles previously employed when equilibrated with wheel **1**. In fact the ^1H NMR of the solution obtained by equilibrating **C3C3** with **1** in C_6D_6, showed a very complex series of signals that excluded the formation of only one pseudorotaxane complex (Figure 2.13).

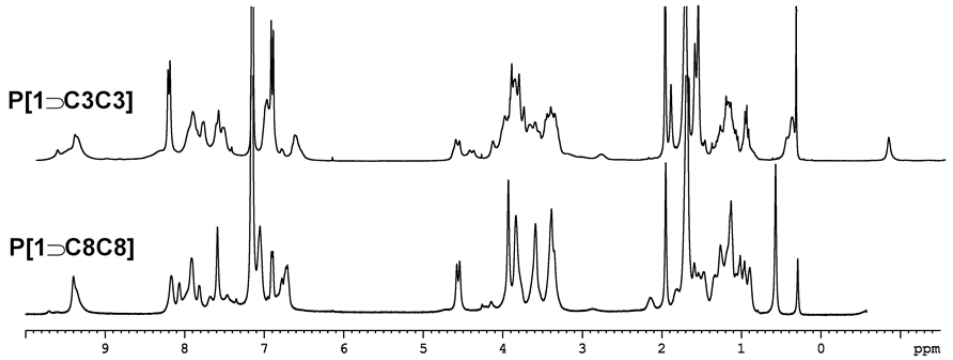

Figure 2.13: ^{1}H NMR spectra (300 MHz,C_6D_6) of **P[1⊃C3C3]** compared with the spectra of **P[1⊃C8C8]**.

2D HSQC spectrum of **P[1⊃C3C3]** (Figure 2.14) suggests the presence of at least two complexes: in one of which the wheel maintain its cone structure and another where the wheel has changed its structure to a 1, 2, 3 alternate conformation. Unfortunately variable temperature NMR experiments in the useful temperature range for C_6D_6 could not disclose wheter this different complexes could convert to one specific structure.

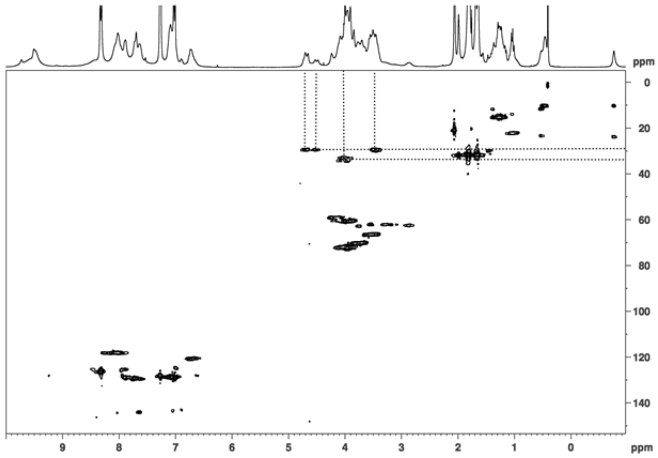

Figure 2.14: ^{1}H-^{1}H 2D HSQC (300 MHz) of **P[1⊃C3C3]** in C_6D_6.

Single crystal X-Ray analyses of **P[1⊃C3C3]** confirmed that in the solid state the complex formed by the calix[6]arene wheel **1** and axle **C3C3** possesses a pseudorotaxane structure, in which the wheel is in its trigonal prism structure. Probably different complexes coexist in solution, as the wheel has different conformations.

In the solid state the di-cation lies within the intramolecular cavity of the calix[6]arene and is shielded from strong interactions with the two counteranions.

The two tosilate anions are linked with strong hydrogen bonds with the NH groups of the calixarene host. However one tosilate forms four hydrogen bonds whereas the other forms only two hydrogen bonds as shown in figure 2.15.

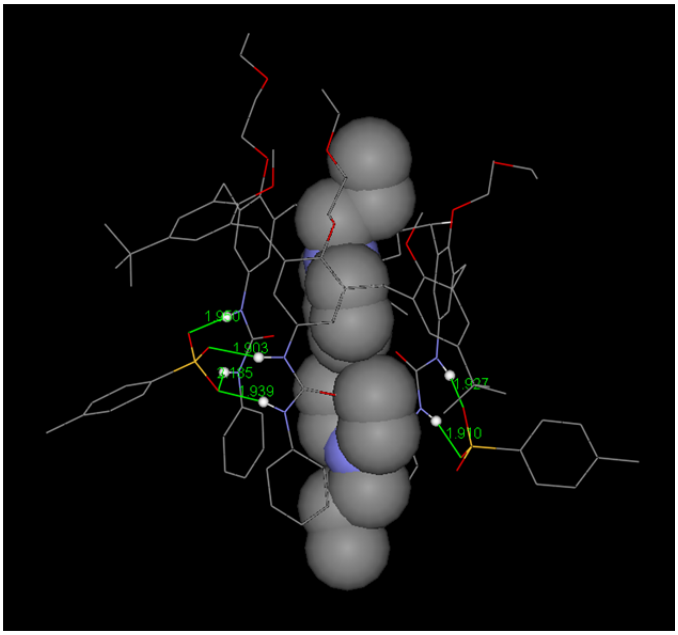

Figure 2.15: perspective view of the pseudorotaxane complex **P[1⊃C3C3]** with the cation evidenced with CPK spheres (the two toluene and the cyclohexane have been omitted for clarity). Only relevant hydrogen atoms have been reported.Hydrogen bonds have been evidenced in green. Colors: C, gray; H, white; N, violet; O, red; S, yellow.

2.3 Thermodynamic and kinetic studies on the oriented pseudorotaxanes

More quantitative data on the stability of the pseudorotaxanes between wheel **1** and symmetrical and non-symmetrical viologen salts were obtained through UV-Vis techniques by titrating the axles with **1** in CH_2Cl_2.

Upon titration of solutions of the symmetrical axles **C5C5**, **C8C8**, **C10C10**, **C12C12** and **C18C18** (concentration ranging from 1×10^{-5} to 3×10^{-5} M) with the calix[6]arene **1**, the characteristic charge transfer band centered around 460 nm was observed (Figure 2.16). In the cases of the symmetric axles **C5C5** and **C8C8** the association constants are comparable with those measured in previous studies on similar systems,[3] while for axles **C12C12** and **C18C18**, the association constants are at least one order of magnitude lower; this means that by increasing the length of the alkyl chains of the axle the supramolecular adduct becomes less stable.

Axle	$\log K_{eq}$	k_{thr} ($M^{-1}s^{-1}$)	k_{dethr} (s^{-1})
C5C5	6.7±0.3	1.6×10^{8}	32
C8C8	6.7±0.4	1.5×10^{6}	0.3
C12C12	5.6±0.2	260	6.5×10^{-4}
C18C18	5.1±0.2	150	1.2×10^{-3}
C5C8	9±1	2×10^{8}	< 20
C5C12	7.5±0.3	2×10^{8}	< 20
C5C18	7.4±0.2	2×10^{8}	< 20

Table 2.4: thermodynamic and kinetic data for the association of the axles with **1**.

However, titration experiments carried out by employing axles **C5C8**, **C5C10**, **C5C12** and **C5C18** clearly show that the association constants are independent from the length of the larger alkyl chain and, within the experimental error, they are of the same order of magnitude of that measured in the case of axle **C5C5**. These data, together with the NMR structural information characterization of the complexes formed, suggest the hypothesis that the stability of the pseudorotaxanes is not influenced by the length of the chain of the

axle that is in proximity of the upper rim of the calixarene. Moreover they suggest that the lower stability constant measured for the pseudorotaxanes **P[1⊃C18C18]** and **P[1⊃C12C12]** respect to **P[1⊃C5C5]** could be ascribed at the presence of the longer alkyl chain in the proximity of the lower rim of the calix[6]arene.

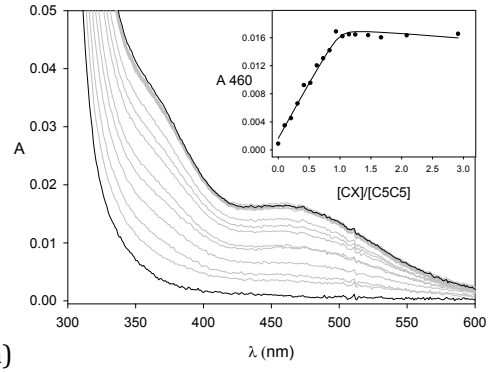

a)

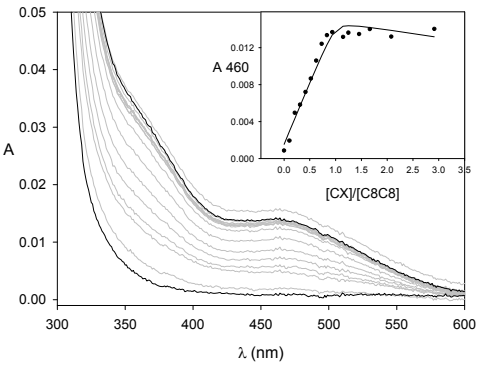

b)

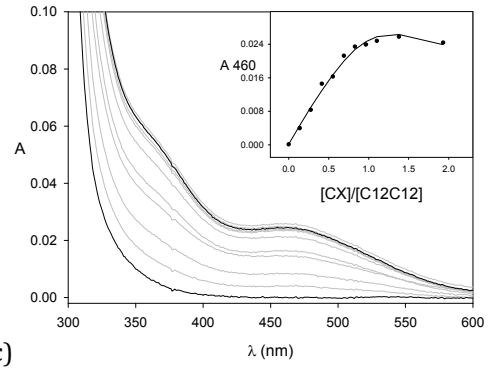

c)

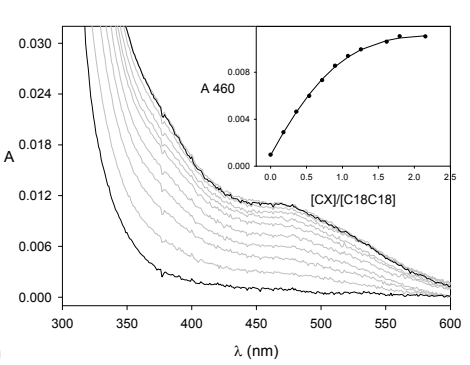

d)

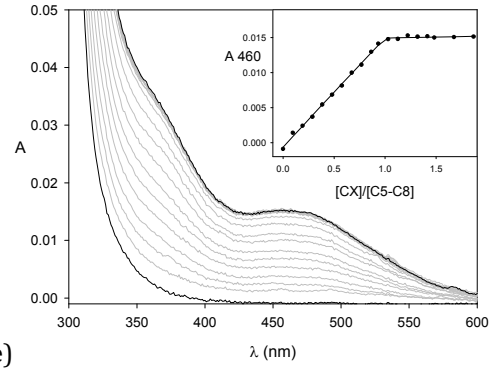

e)

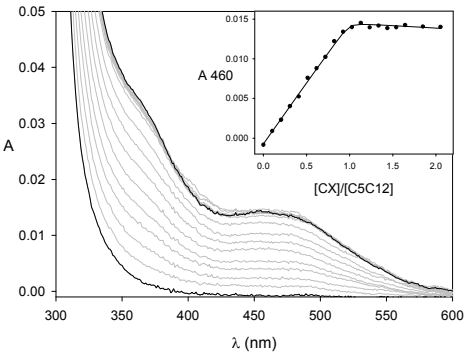

f)

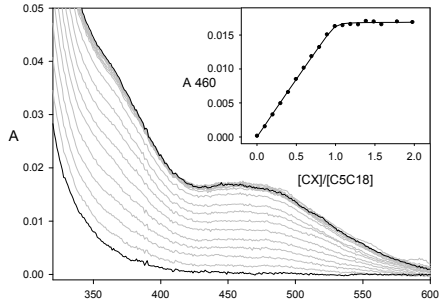

g)

Figure 2.16: absorption spectra of the axles upon titration with calix[6]arene. In the inset: plot of the absorption changes at 460 nm *vs* equivalents of calix (circles), and fitting of the data (solid line); a) [**C5C5**]=3.1×10^{-5} M; b) [**C8C8**]= 3.1×10^{-5} M; c) [**C12C12**]= 4.7×10^{-5} M; d) [**C18C18**]= 3.5×10^{-5}; e) [**C5C8**]=2.9×10^{-5} M; f) [**C5C12**]=3.4×10^{-5} M; f) [**C5C18**]=3.4×10^{-5} M. (CH_2Cl_2, RT).

In order to obtain kinetic data on the complexation processes, that is the threading and dethreading rate costants, stopped-flow experiments have been performed.

The concentration of the solutions after adding the two components ranged between 0.7 ×10^{-5} and 1×10^{-5} M. The experiments has been performed in such diluted conditions in order to slow down the fastest processes. On comparing the sum of the absorption spectra of the axles and **1** with the absorption spectra of the mixtures of the two components, besides the weak CT band centered around 460 nm, a strong increase of the absorption a 258 nm was observed. In order to optimize the signal associated with the threading process, the absorption changes at 258 nm were followed (Figure 2.17). The data were fitted with a mixed order model (equation 1), where the equilibrium constants were fixed to the values determined with the titration experiments.

$$\mathbf{A + B \leftrightharpoons C} \quad (1)$$

For the symmetric axles, the threading rate constants depend, as expected, on the length of the alkyl chain, namely the threading is slower for axles with longer chains. This effect can be rationalized considering that the increase in the number of carbon atoms of the alkyl chains goes in parallel to the increase of freedom degrees that these chains possess. Moreover, by increasing the distance between the bipyridinium station and the alkyl chains CH_3 termini, the electrostatic effect of the dicationic station decrease rapidly.

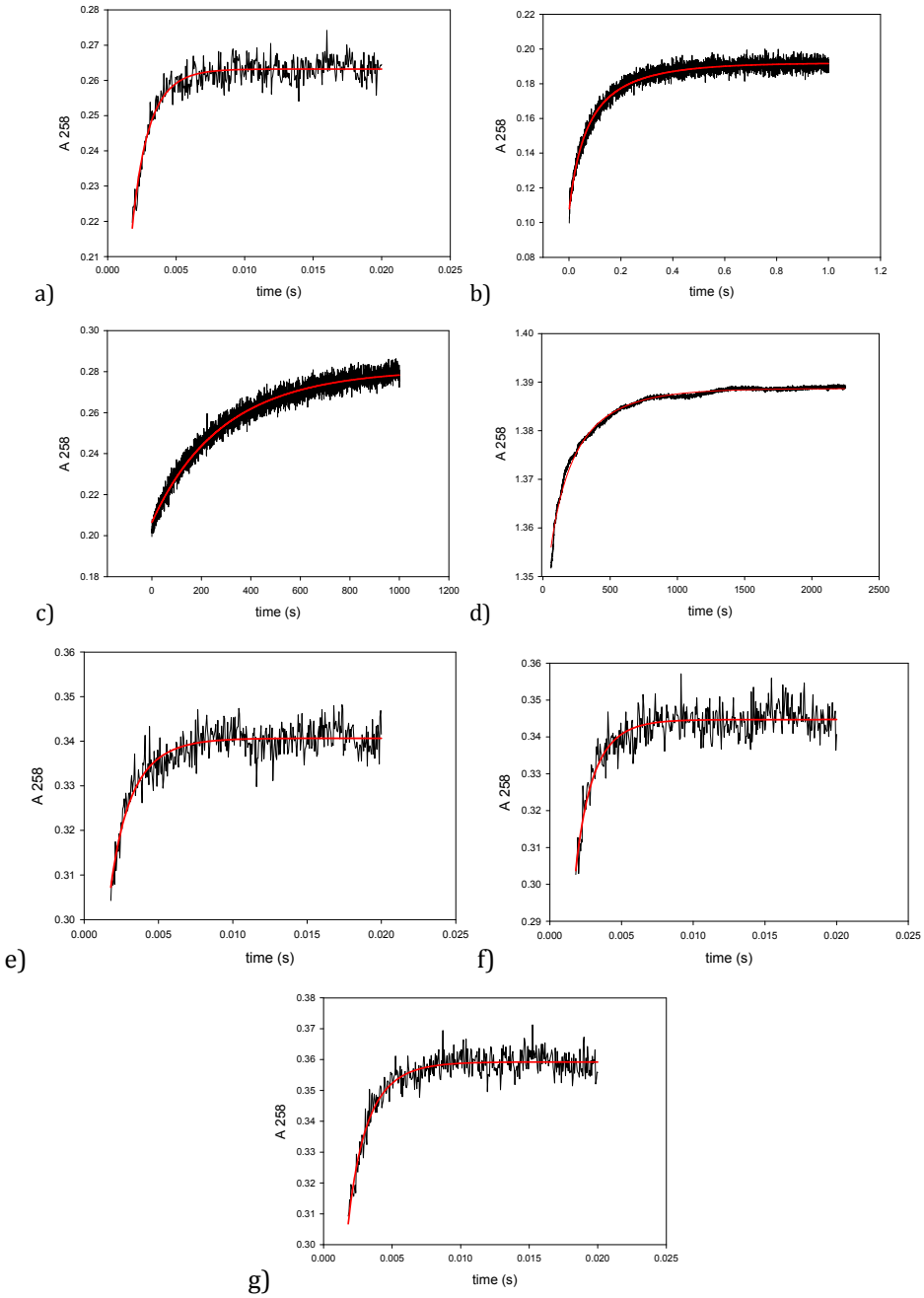

Figure 2.17: kinetic traces for the threading process of the axles into the calix: absorption changes at 258 nm (black line) and fitting of the data (red line). a) [**C5C5**]=7.7×10^{-6} M; b) [**C8C8**]= 7.7×10^{-6} M; c) [**C12C12**]= 6.3×10^{-6} M; d) [**C18C18**]= 1.2×10^{-5}; e) [**C5C8**]=7.5×10^{-6} M; f) [**C5C12**]=8.5×10^{-6} M; f) [**C5C18**]=8.5×10^{-6} M; [**1**]=1×10^{-5} M for all the experiments, except for experiment d, for which [**1**]=2×10^{-5} M (CH_2Cl_2, 293 K).

The rate constants for axles **C12C12** and **C18C18** are comparable. They are four order of magnitude lower than the rate constant for axle **C8C8**, and six order of magnitude lower respect to the rate constant of axle **C5C5** (Table 2.3).

On the other hand, non-symmetric axles thread into the wheel with the same rate, which is comparable to the threading rate constant for **C5C5**.

These results clearly suggest that the non-symmetrical axles thread into the wheel through its shorter chain, forming oriented pseudorotaxanes where the pentyl chain is in the proximity of the lower rim of the wheel. When the difference in the length of the two alkyl chains is small, as for axle **C5C8**, the rate constant for the threading through the two chains is not different enough, and this axle, at room temperature, can thread the wheel through both its side arms. From the kinetic and thermodynamic data, it is possible to calculate the rate constants for the dethreading processes. The data gathered in Table 2.3 refer to threading/dethreading processes of the axle through the upper rim of the wheel.

It is in fact reasonable to assume that the unidirectional threading/dethreading process (that is the threading of the axle from the upper rim through its shorter chain and its slippage from the lower rim) should be high energy demanding since in this dethreading mode a totally separated ion pair should form. This happens because in the pseudorotaxane the two anions are H bonded at the upper rim and the movement of the cationic component toward the lower rim should completely separate the cation from its two anions.[4]

From these data it can be inferred that the dethreading of the non-symmetric axles is fast (k_{dethr}<20 s^{-1}), and a rearrangement of the oriented pseudorotaxane can take place. Nevertheless, upon heating a solution of **P[1⊃C5C18]$_{up}$** the oriented pseudorotaxane does not rearrange in a 1:1 mixture of *"up"* and *"down"* isomers. The thermodynamic data suggests that this behavior could be due to stability reasons, i.e. the isomer with the C5 chain at the upper rim and the C18 chain at the lower rim is less stable. This destabilization can be due to: *i)* a destabilizing effect of the shorter chain on the upper rim, or *ii)* a destabilizing effect of the longer chain on the lower rim. Since the stability constants of the pseudorotaxanes are: K **P[1⊃C5C18]$_{up}$** ≥ K **P[1⊃C5C5]** >> K **P[1⊃C18C18]**, these data indicate that the position of the short C5 chain does not affect stability, whereas the position of the long C18 chain does, and the pseudorotaxane is destabilized when C18 is on the lower rim of the wheel.

Conclusions

Taken all together these data confirm that the length of the alkyl chain appended to the 4,4' bipyridinium, together with the experimental conditions at which the binding process is carried out, could be considered as control elements to govern the orientation of the axle insertion within the wheel to yield oriented pseudorotaxanes.
In particular the data show that, by increasing the length of the alkyl chains in symmetric viologen salts (passing from axle **C5C5** to axle **C18C18**) the threading rate constant decreases of four order of magnitude and the stability constant decreases of two order of magnitude. When the 4,4' bipyridinium salt bears alkyl chains of different length, it was evidenced that the axle enters the wheel selectively or exclusively through its shorter chain.

Experimental section

General: All the reagents were of reagent grade quality obtained from commercial suppliers and were used without further purification. ^{1}H and ^{13}C spectra were recorded at 300 or 400 and 75 or 100 MHz, respectively. M.p. are uncorrected. Chemical shifts are expressed in ppm (δ) using the residual solvent signals as an internal reference. Mass analyses were conducted in the ESI mode with a Micromass ZMD instrument. Compound **2**[5], **3**[6], **4**[7], **5**[8], **6**[9], **7**[10], **C5C0**[10], **C8C8**[11] were synthesized according to literature procedures.

Absorption spectra and titration experiments: measurements were carried out at room temperature (*ca.* 295 K) on air-equilibrated CH_2Cl_2 (Merck Uvasol) solutions in the concentration range of the axles from $1 \cdot 10^{-5}$ to $3 \cdot 10^{-5}$ M. All the compounds show good solubility in CH_2Cl_2, with the exception of **C18C18**, which is difficult to solubilize at concentrations above 10^{-4} M. For the titrations of axles **C12C12** and **C18C18**, after addition of each aliquot of **1** the solutions were left 15 minutes at rest in order to let the system reach the equilibrium. UV-vis absorption spectra were recorded with a Perkin-Elmer λ40 spectrophotometer. The apparent stability constants of the pseudorotaxanes (Table 2.3) were calculated by fitting the absorption titration curves according to the

equation K_{st1} = [complex]/[host][guest], using [host] = [host]^0 - [complex] and [guest] = [guest]^0 - [complex].

Stopped-flow absorption experiments: Reaction kinetic profiles were collected on air-equilibrated CH_2Cl_2 (Merck Uvasol) solutions at 293 K with an Applied Photophysics SX 18 MV stopped-flow spectrophotometer interfaced to a computer for data collection and analysis. The optical path length of the cell was 1 cm, and the driving ram for the mixing system was operated at the recommended N_2 pressure of 8.5 bar. Under these conditions, the time required to fill the 1-cm observation cell was experimentally determined to be <1.3 ms (based on a test reaction). The concentration of the reactants after mixing was in the range from 0.7 $\times 10^{-5}$ and 1×10^{-5} M. On comparing the sum of the absorption spectra of the axles and **1** with the absorption spectra of the mixtures of the two components, besides the weak CT band centered around 460 nm, a strong increase of the absorption at 258 nm was observed. In order to optimize the signal associated with the threading process, the absorption changes at 258 nm were followed (Figure 2.18). The kinetic for the threading of axle **C18C18** was measured with the spectrophotometer.
The kinetic absorbance curves were analyzed with a kinetic treatment for an equilibrium **A + B** $\leftrightharpoons$ **C** as implemented into the SPECFIT software.[12] A fitting of the data trace with a simple second-order rate equation, however, was equally satisfactory, owing to the very high value of the equilibrium constant.

X-ray crystallographic studies: data were collected on a Bruker SMART diffractometer equipped with graphite monochromated MoKa radiation source (λ = 0.71073 Å) and CCD detector. The frames data were processed to give structure factors using the program SAINT.[13] Intensity data were corrected for absorption with SADABS [14]. The crystal data and the most relevant experimental parameters used in the X-ray measurements and in the crystal structure analysis are reported in Table 2.5. The structure was solved by Direct methods using SIR2004 [15]. Two toluene and one cyclohexane molecules were found in the crystal lattice. The structure was refined on F_o^2 by full-matrix least-squares procedures, using SHELXL-97. [16] All the non-hydrogen atoms were refined with anisotropic atomic displacements. The hydrogen atoms were included in the last cicles of refinement at idealized geometry (C-H 0.96 Å) and refined "riding" on the corresponding parent atoms

with isotropic thermal parameters 1.2 times those of the attached atoms. Molecular geometry calculations were carried out using PARST97. [17]

Crystal Data	
chemical formula	$C_{90}H_{108}N_6O_{12}\cdot C_{16}H_{22}N_2\cdot 2C_7H_7SO_3\cdot 2C_7H_8\cdot C_6H_{12}$
fw	2319.062
crystal system	triclinic
space group	*P-1*
a (Å)	17.094(1)
b (Å)	19.034(1)
c (Å)	22.604(1)
α (°)	106.481(1)
β (°)	108.200(1)
γ (°)	97.672(1)
V (Å^3)	6497.4(6)
Z	2
ρ_{calc}. (g cm^{-3})	1.185
μ (mm^{-1})	0.108 (Mo-K$_\alpha$)
Data Collection and Refinement	
2θ max for data collection (°)	58.67
Temperature (K)	293
data collected (*h, k, l*)	(-23, -26, -31) to (23, 26, 31)
total reflections	98500
unique reflections	35454 (R_{int} = 0.038)
observed reflections	20805[Fo>4.0σ(Fo)]
Goodness-of-fit on F^2 [a]	1.004
Final R indices (obs. data)[b]	R_1=0.062, wR_2=0.168
R indices (all data) [b]	R_1=0.1098, wR_2=0.1992
Largest diff. peak and hole (e/Å^{-3})	0.46/ -0.40

[a]Goodness-of-fit $S = [\Sigma w(Fo^2\text{-}Fc^2)^2/ (n\text{-}p)]^{1/2}$, where *n* is the number of reflections and *p* the number of parameters. [b]$R_1 = \Sigma \,||\, Fo|\text{-}|Fc||/\Sigma|Fo|$, $wR_2 = [\Sigma\, w(Fo^2\text{-}Fc^2)^2/\, \Sigma wFo^4]^{1/2}$.

Table 2.5. Crystal Data, Data Collection and Refinement Parameters for **P[1⊃C3C3].**

Syntheses

General procedure for the synthesis of compounds C5C8, C5C10, C5C12,C5C18: In a 100 ml glass autoclave flask compound **C5C0** (0.4 g, 1.0 mmol) and the appropriate derivative **4** - **7** (1.5 mmol) were dissolved in CH_3CN (50ml) and the solution was refluxed for 3 days. Then the solvent was evaporated at reduced pressure and the residue obtained was triturated with EtOAc (3x 20 ml) until the product precipitated from the trituration solvent as a solid compound. The solid was recovered by suction filtration and purified by recrystallization from CH_3CN to afford product **C5C8, C5C10, C5C12,C5C18** as a white solid.

C5C8 (0.5 g, 75% yield), ^{1}H NMR (300MHz, CD_3OD): δ = 9.26 (d, *J* = 6.0, 4H), 8.67 (d, *J* = 6.0, 4H), 7.70 (d, *J* = 7.8, 4H), 7.24 (d, *J* = 7.8, 4H), 4.74 (t, *J* = 7.5, 4H), 2.38 (s, 6H), 2.2-2.0 (m, 4H), 1.5-1.3 (m, 14H), 1.1-0.9 (m, 6H); ^{13}C NMR (100 Mhz, CD_3OD): δ = 149.8, 145.7, 142.3, 140.3, 128.5, 126.9, 125.5, 61.9, 31.5, 31.2, 30.8, 28.8, 28.7, 27.9, 25.8, 22.3, 21.8, 19.9, 13.0, 12.7; MS (ES): *m/z* (%): 511 $[M\text{-}TsO^-]^+$ (30), 339 $[M\text{-}2TsO^-\text{-}H^+]^+$ (60); m.p. = 197.5°- 199.8° C.

C5C10 (0.5 g, 75% yield), ^{1}H NMR (300MHz, CD_3OD): δ = 9.24 (d, *J* = 6.9, 4H), 8.65 (d, *J* = 6.9, 4H), 7.69 (d, *J* = 8.1, 4H), 7.24 (d, *J* = 8.1, 4H), 4.73 (t, *J* = 7.5, 4H), 2.38 (s, 6H), 2.2-2.0 (m, 4H), 1.5-1.3 (m, 18H), 1.1-0.9 (m, 6H); ^{13}C NMR (100 Mhz, CD_3OD): δ = 149.8, 145.6, 142.3, 140.3, 128.5, 126.9, 125.5, 61.9, 31.6, 31.1, 30.8, 29.2, 29.0, 28.7, 27.9, 25.8, 22.3, 21.8, 19.9, 13.0, 12.7; MS (ES): *m/z* (%): 367 $[M\text{-}2TsO^-\text{-}H^+]^+$ (60); m.p. = 188.5°- 191.8° C.

C5C12 (0.5 g, 70% yield), ^{1}H NMR (300MHz, CD_3OD): δ = 9.25 (d, *J* = 6.9, 4H), 8.66 (d, *J* = 6.9, 4H), 7.69 (d, *J* = 8.1, 4H), 7.24 (d, *J* = 8.1, 4H), 4.73 (t, *J* = 7.5, 4H), 2.38 (s, 6H), 2.2-2.0 (m, 4H), 1.5-1.3 (m, 22H), 1.1-0.9 (m, 6H); ^{13}C NMR (100 Mhz, CD_3OD): δ = 149.8, 145.6, 142.3, 140.3, 128.5, 126.9, 125.5, 61.9, 31.7, 31.2, 30.8, 29.3, 29.2, 29.1, 29.0. 28.8, 27.9, 25.8, 22.32, 21.8, 19.9, 13.0, 12.7; MS (ES): *m/z* (%): 567 $[M\text{-}TsO^-]^+$ (30), 395 $[M\text{-}2TsO^-\text{-}H^+]^+$ (60); m.p. = 167.2°- 172.3° C.

C5C18 (0.65 g, 80% yield), ^{1}H NMR (300MHz, CD_3OD): δ = 9.26 (d, *J* = 6.6, 4H), 8.66 (d, *J* = 6.6, 4H), 7.69 (d, *J* = 8.1, 4H), 7.24 (d, *J* = 8.1, 4H), 4.73 (t, *J* = 7.5, 4H), 2.38 (s, 6H), 2.2-2.0 (m, 4H), 1.5-1.3 (m, 34H), 1.1-0.9 (m, 6H); ^{13}C NMR (100 Mhz, CD_3OD): δ = 149.8, 145.7, 140.3, 128.5, 126.8, 125.5, 61.9, 31.7, 31.2, 30.8, 29.4, 29.3, 29.1, 29.0, 28.8, 27.9, 25.9, 22.34, 21.79, 19.9, 13.1, 12.8; MS (ES): *m/z* (%): 395 $[M\text{-}2TsO^-\text{-}H^+]^+$ (60); m.p. = 169.1°- 172.3° C.

General procedure for the synthesis of compounds P[1⊃C5C18], **P[1⊃C5C12]**, **P[1⊃C5C10]**, **P[1⊃C5C8]**: compound **1** (10 mg, 0.0068 mmol) and a slight excess of the appropriate axle (**C5C8** - **C5C18**) (0.01 mmol), were equilibrated in 0.5 ml of C_6D_6 at 300 K for 1 h, until the solution assumes a deep red colour. The excess of axle was removed by filtration, and the homogeneous solution obtained was characterized through NMR techniques.

P[1⊃C5C18]: ^{1}H NMR (300MHz, C_6D_6): δ = 9.35 (m, 6H), 8.15 (d, *J* = 6.2, 4H), 8.00-8.10 (m, 2H), 7.87 (bs, 6H), 7.78 (bs, 2H), 7.66 (bs, 3H), 7.57 (s, 6H), 7.44 (bs, 3H), 6.9-7.1 (m, 6H), 6.90 (d, *J* = 6.2, 4H),6.70 (bs, 2H), 6.6-6.7 (m, 5H), 4.55 (d, *J* = 14.2, 6H), 3.93-3.90 (s, 9H), 3.84 (bs, 8H), 3.58 (bs, 8H), 3.3-3.4 (m, 12H), 2.80 (bs, 2H), 2.24 (bs, 2H), 1.96 (s, 6H), 1.67 (bs, 2H), 1.58 (s, 29H), 1.28 (bs, 2H), 1.0-1.2 (m, 25H), 0.7-0.9 (m, 8H).

P[1⊃C5C10]: ^{1}H NMR (300MHz, C_6D_6): δ = 9.36 (m, 6H), 8.0-8.2 (m, 6H), 7.90 (bs, 6H), 7.75 (bs, 2H), 7.65 (bs, 3H), 7.55 (s, 6H), 7.43 (bs, 3H), 7.05 (t, *J* = 7.5, 6H), 6.88 (d, *J* = 6.5, 4H),6.79 (d, *J* = 5.4, 2H), 6.69 (t, *J* = 7.5, 3H), 6.64 (d, *J* = 5.4, 2H), 4.52 (d, *J* = 15.0, 6H), 3.88 (s, 9H), 3.80 (bs, 8H), 3.56 (bs, 8H), 3.3-3.4 (m, 12H), 2.12 (bs, 2H), 1.94 (s, 6H), 1.80 (bs, 2H), 1.65 (s, 29H), 1.30 (bs, 16H), 1.0-1.2 (m, 19H), 0.7-0.9 (m, 4H).

P[1⊃C5C12]: ^{1}H NMR (300MHz, C_6D_6): δ = 9.52 (m, 6H), 8.2-8.3 (m, 6H), 8.05 (bs, 6H), 7.90 (bs, 2H), 7.78 (bs, 3H), 7.70 (s, 6H), 7.57 (bs, 3H), 7.20 (t, *J* = 7.5, 6H), 7.02 (d, *J* = 6.5, 4H), 6.93 (d, *J* = 5.3, 2H), 6.85 (t, *J* = 7.5, 3H), 6.78 (d, *J* = 5.3, 2H), 4.55 (d, *J* = 15.0, 6H), 3.93 (s, 9H), 3.85 (bs, 8H), 3.65 (bs, 8H), 3.3-3.5 (m, 12H), 2.26 (bs, 2H), 2.07 (s, 6H), 1.90 (bs, 2H), 1.80 (s, 29H), 1.45 (bs, 16H), 1.1-1.3 (m, 23H), 1.05 (bs, 4H).

P[1⊃C5C18]: ^{1}H NMR (300MHz, C_6D_6): δ = 9.52 (m, 6H), 8.29 (bs, 4H), 8.15 (bs, 2H), 8.05 (bs, 6H), 7.93 (bs, 2H), 7.79 (bs, 3H), 7.70 (s, 6H), 7.60 (bs, 3H), 7.20 (bs, 6H), 7.03 (d, *J* = 6.5, 4H), 6.8-6.9 (m,7H), 4.66 (d, *J* = 15.0, 6H), 3.93 (s, 9H), 3.85 (bs, 8H), 3.65 (bs, 8H), 3.3-3.5 (m, 12H), 2.26 (bs, 2H), 2.07 (s, 6H), 1.90 (bs, 2H), 1.80 (s, 29H), 1.45 (bs, 28H), 1.1-1.3 (m, 23H), 1.05 (bs, 4H).

General procedure for the synthesis of compounds C3C3, C5C5, C10C10, C12C12, C18C188: In a 100 ml glass autoclave flask 4,4'-bipyridine (0.4 g, 2.5 mmol) and the appropriate derivative **2**, **3**, **4**, **5**, **6** or **7** (3.5 mmol) were dissolved in CH_3CN (50ml) and the solution was refluxed for 3 days. Then the solvent was evaporated at reduced pressure and the obtained residue was triturated with EtOAc (3x 20 ml) until the product

precipitated from the trituration solvent as a solid compound. The solid was recovered by suction filtration and purified by recrystallization from CH_3CN to afford product **C3C3, C5C5, C10C10, C12C12** or **C18C18** as a white solid.

C3C3 (0.4 g, 70% yield), ^{1}H NMR (300MHz, CD_3OD): δ = 9.22 (d, *J* = 6.9, 4H), 8.64 (d, *J* = 6.9, 4H), 7.68 (d, *J* = 8.1, 4H), 7.24 (d, *J* = 8.1, 4H), 4.69 (t, *J* = 7.5, 4H), 2.37 (s, 6H), 2.2-2.0 (m, 4H), 1.05 (t, *J* = 7.2, 6H); ^{13}C NMR (100 Mhz, CD_3OD): δ = 149.5, 145.6, 142.3, 140.3, 128.5, 126.9, 125.5, 63.2, 24.4, 19.9, 9.3; MS (ES): *m/z* (%): 242 $[M- 2TsO^- - H^+]^+$ (100); m.p. = 140.5°- 142.5° C.

C5C5 (0.5 g, 80% yield), ^{1}H NMR (300MHz, CD_3OD): δ =9.24 (d, *J* = 6.6, 4H), 8.65 (d, *J* = 6.6, 4H), 7.69 (d, *J* = 8.4, 4H), 7.23 (d, *J* = 8.4, 4H), 4.72 (t, *J* = 7.5, 4H), 2.37 (s, 6H), 2.1-2.0 (m, 4H), 1.5-1.3 (m, 8H), 0.92 (t, *J* = 7.2, 6H); ^{13}C NMR (100 Mhz, CD_3OD): δ = 149.8, 145.6, 142.3, 140.3, 128.5, 126.9, 61.9, 30.8, 27.9, 21.8, 19.9, 12.7; MS (ES): *m/z* (%): 663 $[M+Na^+]^+$ (10), 297 $[M- 2TsO^- - H^+]^+$ (100); m.p. = 215.5°- 216.8° C.

C10C10 (0.6 g, 70 % yield), ^{1}H NMR (300MHz, CD_3OD): δ = 9.26 (d, *J* = 6.6, 4H), 8.66 (d, *J* = 6.6, 4H), 7.70 (d, *J* = 8.4, 4H), 7.24 (d, *J* = 8.4, 4H), 4.74 (t, *J* = 7.5, 4H), 2.39 (s, 6H), 2.1-2.0 (m, 4H), 1.5-1.3 (m, 20H), 0.92 (t, *J* = 7.2, 6H); ^{13}C NMR (100 Mhz, CD_3OD): δ = 148.3, 144.5, 140.7, 138.8, 126.9, 125.3, 124.0, 61.8, 30.1, 29.6, 27.7, 27.6, 27.5, 27.2, 24.3, 20.7, 18.4, 11.5; MS (ES): *m/z* (%): 440 $[M - 2TsO^- + H^+]^{2+}$ (50); m.p. = 195.5°- 196.8° C.

C12C12 (0.7 g, 80% yield), ^{1}H NMR (300MHz, CD_3OD): δ = 9.24 (d, *J* = 6.6, 4H), 8.65 (d, *J* = 6.6, 4H), 7.69 (d, *J* = 8.1, 4H), 7.23 (d, *J* = 8.1, 4H), 4.73 (t, *J* = 7.5, 4H), 2.38 (s, 6H), 2.1-2.0 (m, 4H), 1.5-1.3 (m, 36H), 0.92 (t, *J* = 7.2, 6H); ^{13}C NMR (100 Mhz, CD_3OD): δ = 149.8, 145.6, 140.3, 128.5, 126.9, 125.5, 61.9, 31.6, 31.1, 29.3, 29.2, 29.1, 29.0, 28.8, 25.8, 22.3 19.9, 13.0; MS (ES): *m/z* (%): 247 $[M- 2TsO^-]^{2+}$ (50); m.p. = 183.5°- 184.5° C.

C18C18 (0.5 g, 50% yield), ^{1}H NMR (300MHz, CD_3OD): δ = 9.25 (d, *J* = 6.7, 4H), 8.65 (d, *J* = 6.7, 4H), 7.68 (d, *J* = 8.1, 4H), 7.22 (d, *J* = 8.1, 4H), 4.72 (t, *J* = 7.6, 4H), 2.36 (s, 6H), 2.1-2.0 (m, 4H), 1.5-1.3 (m, 60H), 0.89 (t, *J* = 6.9, 6H); ^{13}C NMR (100 Mhz, CD_3OD): δ = 149.8, 145.6, 140.2, 128.4, 126.8, 125.5, 61.8, 31.6, 31.6, 31.1, 29.3, 29.2, 29.1, 29.0, 28.7, 25.8, 22.3 19.9, 13.0; MS (ES): *m/z* (%): 834 $[M- TsO^-]^+$ (100); m.p. = 172.5°- 174.5° C.

References:

[1] a) R. Berardi, F. Spinozzi, C. Zannoni *Chem. Phys. Lett.* **1996**, *260*, 633-638; b) F. Goodsaid-Zalduondo, D.M. Engelman *Biophys. J.* **1981**, *35*, 587-594; c) T. Nakaoki, H. Nagano, T. Yanagida *J. Mol. Struct.*, **2004**, *699*, 1-7; d) B. Smith, J. I. Siepmann, *Science*, **1994**, *264*, 1118-1120; e) D. Bessières, M. M. Piñeiro, G. De Ferron, F. Plantier, *J. Chem. Phys*. **2010**, *133*, 074507-1; f) R. Göttlich, B. C. Kahrs, J. Krüger and R. W. Hoffmann *Chem. Commun.*, **1997**, *3*, 247-252.

[2] a) A. Arduini, F. Calzavacca, A. Pochini, A. Secchi, *Chem. Eur. J.*, **2003**, *9*, 793-799; b) A. Arduini, F. Ciesa, M. Fragassi, A: Pochini, A. Secchi, *Angew. Chem. Int. Ed.*, **2005**, *44*, 278-281; c) A. Arduini, R. Bussolati, A. Credi, G. Faimani, S. Garaudée, A. Pochini, A. Secchi, M. Semeraro, S. Silvi, M. Venturi, *Chem. Eur. J.*, **2009**, *15*, 3230-3242.

[3] A. Credi, S. Dumas, S. Silvi, M. Venturi, A. Arduini, A. Pochini, A. Secchi, *J. Org. Chem.*, **2004**, *69*, 5881-5887.

[4] F. Ugozzoli, C. Massera, A. Arduini, A. Pochini, A. Secchi, *CrystEngComm.*, **2004**, *6*, 227.

[5] R. S. Tipson, *J. Org. Chem.* , **1944**, *9*, 235.

[6] S. Oae,H. Togo, *Bull. Chem. Soc. Jpn.*, **1983**, *56*, 3813-3817.

[7] Y. Yoshida, Y. Sakakura, N. Aso,S. Okada, Y. Tanabe, *Tetrahedron*, **1999**, *55*, 2183-2192.

[8] G. W. Kabalka, M. Varma, S. Varma, *J. Org. Chem.,* **1986**, *51*, 2387.

[9] C. V. Sekera, C. S. Marvel, *J. Am. Chem. Soc.,* **1933**, *55*, 345.

[10] A. Boccia, V. Lanzillotto, R. Zanoni, L. Pescatori, A. Arduini, A. Secchi, *Phis. Chem. Chem. Phis.*, **2011**, *13*, 4444-4451.

[11] A. Arduini, R. Ferdani, A. Pochini, A. Secchi, F. Ugozzoli, *Angew. Chem. Int. Ed.*, **2000**, *39*, 3453-3456.

[12] Binstead, R. A. *SPECFIT*; Spectrum Software Associates: Chapel Hill, NC, 1996.

[13] Siemens: Area Detector Control Integration Software. Version 4.0 in SMART and SAINT, Siemens Analytical X-ray Instruments Inc., Madison Winsconsin, 1996.

[14] R. Blessing, SADABS, Acta Crystallogr., Sect. A: Found. Crystallogr. 1995, 51, 33-38.

[15] Burla M.C., Caliandro R., Camalli M., Carrozzini, B., Cascarano G.L., De Caro L., Giacovazzo C., Polidori G.,Spagna R., **2005** *J. Appl. Cryst. 38*, 1381-388.

[16] G. M. Sheldrick, **SHELX-97**, *Program for Crystal Structure Refinement*, University of Göttingen, 1997; http://shelx.uni-ac.gwdg.de/shelx/index.html.

[17] M. Nardelli, PARST97, updated version of PARST95, *J. Appl. Crystallogr.,* **1995**, *28*, 659.

CHAPTER 3

Unidirectional transit of a nonsymmetric molecular axle into a nonsymmetric molecular wheel.

Chapter 3

Unidirectional transit of a nonsymmetric molecular axle into a nonsymmetric molecular wheel.

3.1 Introduction

The development of a pseudorotaxane motif capable of performing unidirectional threading and dethreading processes is particularly important for the construction of processive linear motors based on rotaxanes.[1]

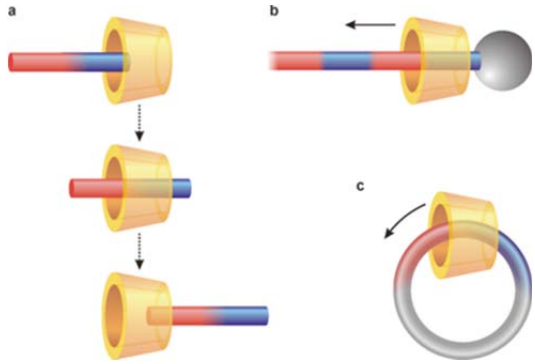

Figure 3.1 Representation of unidirectional threading/dethreading of a [2]pseudorotaxane with nonsymmetric components (a), a processive linear motor based on a [2]rotaxane (b), and a rotary motor based on a [2]catenane (c).

The essential feature of molecular motors is indeed the directional control of the motion, which is achieved by modulating not only the thermodynamics but also the kinetics of the transition between the mechanical states of the device. This result can be achieved by applying ratcheting concepts[2] to the design of the systems. While a few examples of artificial molecular rotary motors and DNA-based linear motors[3] have been described, only one prototype of a fully synthetic linear motor molecule, not based on rotaxane system, is available.[4] Therefore, the construction of linear supramolecular motors is still an open problem and an important challenge, because linear movements are essential both in Nature and technology.

The achievements gained on the kinetic and thermodynamic control on the threading direction of an axle into the non-symmetric wheel **1** suggest that this full control in the threading process from the upper rim of the calixarene could be extended so as to prove the principle that the external stimuli promoting unidirectional transit of an axle through the wheel could be achieved.

As working hypothesis, this principle could be verified by studying the threading-dethreading process by employing an axle bearing at one of its termini a group that, at room temperature, could act as a "kinetic stopper", small enough to pass through the calixarene annulus but larger than the group at the other terminus. In principle, by equilibrating this non-symmetric axle with wheel **1** only an orientational pseudorotaxane isomer could be obtained (step 1, Scheme 3.1). By inserting the bulky group B at the terminal –OH group the corresponding rotaxane could be obtained. As a consequence of an external stimulation (step 3) the dumbbell dethreads from lower rim of the calixarene cavity completing an unidirectional movement through the macrocycle.

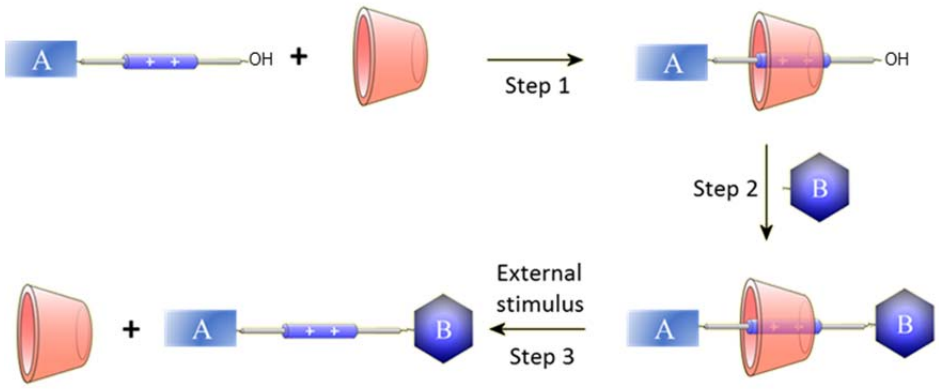

Scheme 3.1: representation of the unidirectional translation of the axle from the upper to the lower rim of the calix[6]arene wheel.

3.2 Synthesis of the axles

In order to address this issue wheel **1**, axles **2** and **3** as tosylate salts and dumbbell **4** and **5** have been synthesized. They are composed by a central electron-acceptor 4,4'-bipyridinium core, functionalized with an hexanol chain at one side, and a stilbene (**2**) or a 4-*t*-butyl-substituted stilbene (**3**) unit connected through a C6 chain at the other side (Figure 3.2).

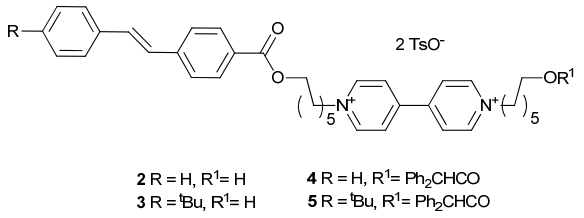

Figure 3.2: the axles **2** and **3**, and the dumbbells **4** and **5**, targets of these syntheses.

The terminal –OH group was incorporated as it is easily involved in stoppering reactions, whereas the stilbene in **2** and 4-*t*-butyl-substituted stilbene in **3** head groups were selected since: i) their dimensions are not too big to prevent their slippage[4] through the wheel **1**, but large enough to enable a kinetic control of the threading/dethreading of the axles in the wheel, as molecular mechanics calculations suggested;[6] ii) their capability of undergoing *E-Z* photoisomerization, with the consequent change in structure and hampering effect[7] that can be exploited as a further element to kinetically control the threading/dethreading movements.

For the synthesis of **2** and **3** the reaction sequence reported in Scheme 3.2 was followed. The styrene derivative **6a** or **6b** was reacted with **7** through an Heck's coupling reaction to give the stilbene acid derivative **8a** or **8b**. The carboxylic function was then activated in presence of oxalyl chloride and the acyl halide was reacted with 6-hydroxyhexyl 4-methylbenzenesulfonate **10** to yield esters **11a** or **11b**.

The reaction of these compound with an excess of 4,4' bipyridine in refluxing acetonitrile gave the mono-alkylated bipyridines **12a** or **12b**, which, after purification were reacted in refluxing CH_3CN with **10** for two weeks to give the axle **2** or **3** as white powder. Dumbbell **4** and **5** were synthetized reacting **12a** or **12b** with 6-(tosyloxy)hexyl 2,2-diphenylacetate **13**.

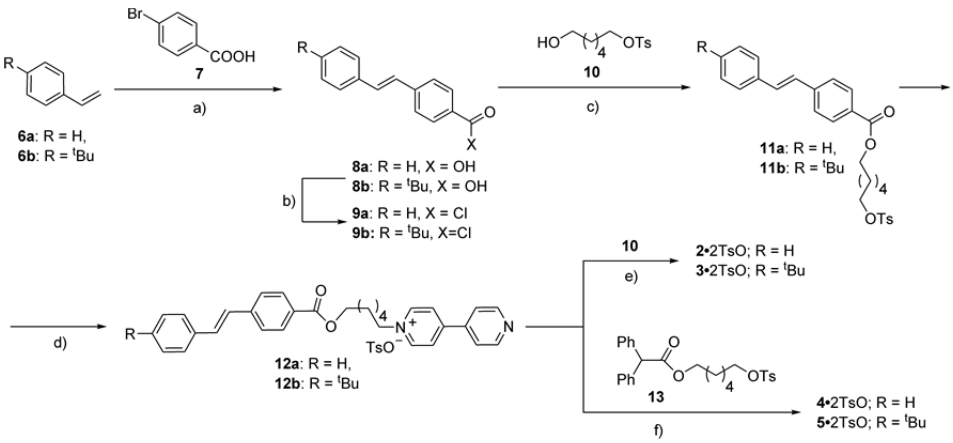

Scheme 3.2: synthetic scheme followed for axles **2** and **3,** and dumbbells **4** and **5**. Reagents and conditions: (a) $Pd(OAc)_2$, K_2CO_3, N,N dimethyl-β-alanine, DMF, reflux, 6 h; (b) oxalyl chloride, $CHCl_3$, reflux, 2h; (c) NEt_3, DMAP, CH_2Cl_2, 48h; (d) 4,4′-bipyridine, CH_3CN, reflux, 72h; (e) CH_3CN, reflux, 15 d; (f) CH_3CN, reflux, 15 d.

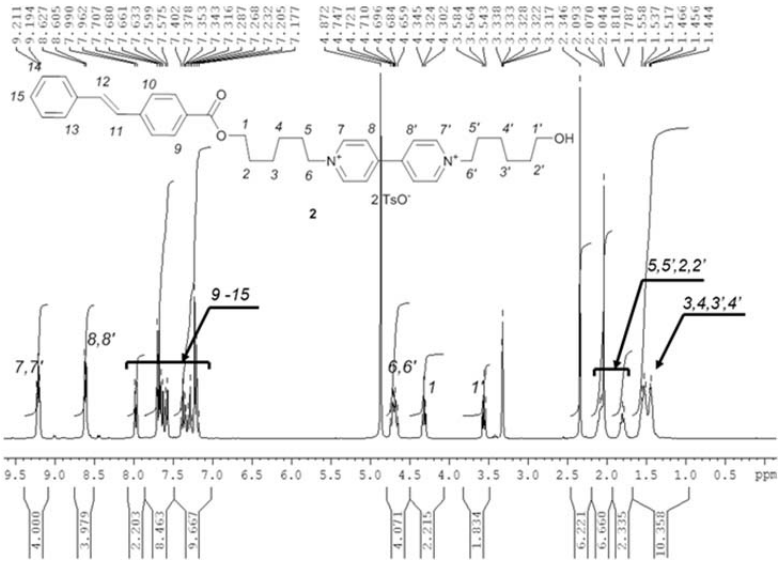

Figure 3.3: ^1H NMR (300 MHz) of axle **2**•2TsO in CD_3OD.

As an example the ^1H NMR spectra recorded in CD_3OD of **2** is reported (Figure 3.3). The pyridyl protons *7*, *7'* and *8*, *8'* resonate as two sets of signals at δ =9.20 and δ = 8.61 ppm, respectively. The signals of protons *6* and *6'* resonates, partially overlapped, at δ = 4.71 ppm while protons *1'* and *1* resonate, as triplets, at δ = 4.32 and δ = 3.56 ppm, respectively.

3.3 Oriented pseudorotaxanes and rotaxanes syntheses

With the objective of verify the hypothesis that the stilbene-type head group of axles **2** and **3** can act as a kinetic control element during the threading process, in separate experiments wheel **1** and a slight excess of axle **2** or **3** were equilibrated in C_6D_6 at room temperature (Scheme 3.3). The deep red solution obtained in both cases, after removal of the excess of axle, was characterized through NMR techniques. In the ^1H NMR spectra only one set of signals was observed for both solution indicating that only one pseudorotaxane isomer had formed.[8]

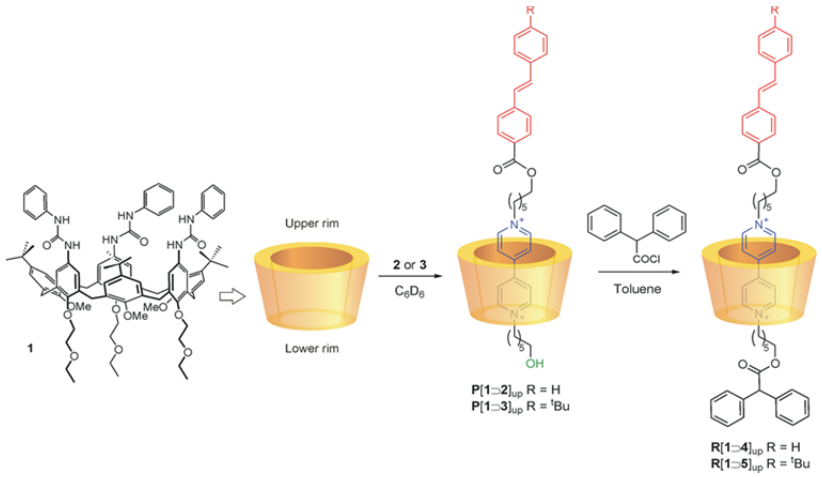

Scheme 3.3: Self-assembly of **P[1⊃2]$_{up}$** and **P[1⊃3]$_{up}$**, and synthesis of **R[1⊃4]$_{up}$** and **R[1⊃5]$_{up}$**.

As expected, the threading of axles **2** or **3** into the wheel results in a substantial rearrangement of the calix[6]arene structure (Figure 3.3). For example, a downfield shift of about 1.1 ppm of the methoxy groups and the appearance of the AX quartet, at δ = 4.65 and δ = 3.50 ppm respectively, experienced by the six pseudo axial & six pseudo equatorial protons of the methylene bridges, are clearly evidenced. In addition, the six ureido NHs are downfield shifted of about 3 ppm and resonate at δ = 9.50 ppm because of their involvement in hydrogen bonding with the two tosylate anions. The inclusion inside the wheel also affects the resonances of the protons of axles **2** and **3**. In particular, the aromatic protons of the 4,4′-bipyridinium core originate four doublets denoted as *7*, *7*′, *8* and *8*′ centered, in both pseudorotaxanes, at δ = 8.10, 6.90, 7.90 and 6.80 ppm, respectively. The presence of only four doublets indicates that the axles have effectively

threaded the wheel, since the protons of the two pyridinium moieties experience an asymmetrical magnetic environment due to their inclusion into the non-symmetric cavity of the calix[6]arene macrocycle.

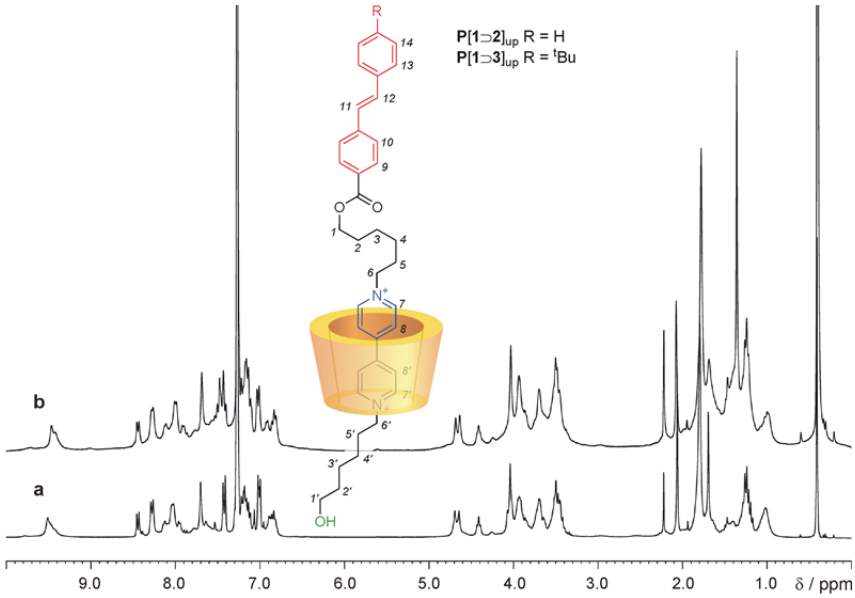

Figure 3.3: ^{1}H NMR spectra (300 MHz, C_6D_6) of the pseudorotaxanes formed by wheel **1** and (a) axle **2** or (b) axle **3**.

Further to this, 2D TOCSY experiments highlight the presence of only one set of signals for the two alkyl chains linked to the 4,4′-bipyridinium core in both pseudorotaxanes. (Figure 3.4). The presence of only two sets of cross peaks, one for the protons of the alkyl chain that links the stilbene unit to the central dicationic station (H from 1 to 6), and the other for the protons of the alkyl chain that bears at one end the hydroxyl group (H from 1' to 6'), it is clearly visible.

The 2D ROESY NMR (Figure 3.5) spectra show that in both pseudorotxanes **P[1⊃2]$_{up}$** and **P[1⊃3]$_{up}$** the stilbene-based head group of axles **2** and **3** is positioned at the upper rim of the wheel, thereby suggesting that both axles had entered the wheel through the calixarene upper rim with their less sterically demanding –OH terminus to give the oriented species **P[1⊃2]$_{up}$** and **P[1⊃3]$_{up}$** (Scheme 3.2).

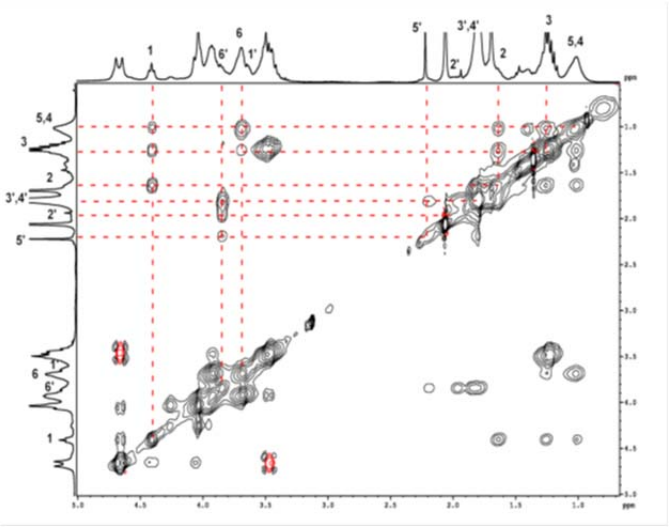

Figure 3.4: ^{1}H-^{1}H 2D TOCSY spectrum (expanded region) (300 MHz) of **P[1⊃2]**$_{up}$ in C_6D_6 (mixing time = 0.06 s).

In fact correlations between the signals of the protons of the alkyl chain (H from 1 to 6) that links the stilbene unit to the bipyridine station and the aromatic protons of the ureido moieties & the methoxy groups at the lower rim of the wheel and the protons of the alkyl chain that bears the –OH end, confirmed the orientation of the axle towards the calixarene rims. This strict orientational control during pseudorotaxane formation can be explained on the basis of the structural features of both the wheel and the axle. In fact, at least in principle, axles **2** and **3** could enter the wheel from its upper rim either through the –OH or through the stilbene terminus. The fact that under these experimental conditions only one orientational pseudorotaxane isomer is formed, clearly indicates that the wheel pivots the threading of the axles from the upper rim and that this latter components access the macrocycle through the less sterically demanding –OH terminus in a process that is kinetically controlled by the different size of the termini of the axles.

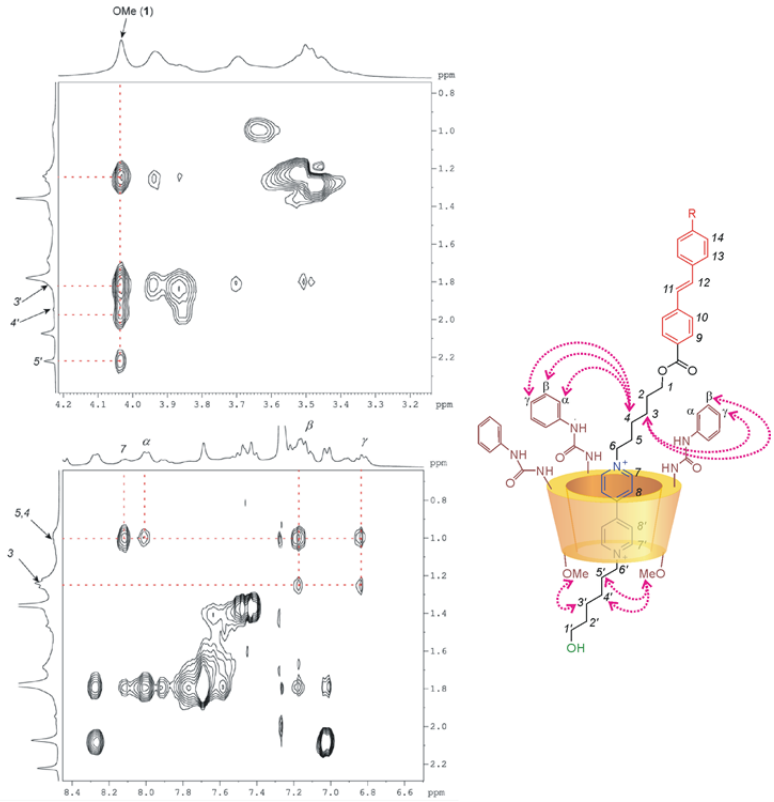

Figure 3.5: Portions of 2D ROESY NMR spectra (300 MHz, C_6D_6) of **P**[**1**⊃**3**]$_{up}$ showing the most representative axle-wheel spatial correlations.

These data demonstrate that the stilbene groups allow a kinetic control on the threading process, leading to the formation of only the "up" isomer of the oriented pseudorotaxanes. With the aim to determine the stability constants of these systems, UV-Vis titrations of axles **2** and **3** with wheel **1** have been performed in CH_2Cl_2 at room temperature by looking at the spectral region 320-600 nm (Figure 3.6). The resulting absorption band is typical of the CT interactions[9] between the cationic 4,4′-bipyridinium unit of the axles and the π-electron-rich aromatic walls of the wheel it is are responsible of the red colour of the solution. The titration curves are satisfactorily fitted with a 1:1 association model and yield apparent stability constants of the order of 10^6 M^{-1} for both the pseudorotaxanes, as per the results previously obtained for similar systems.[9a,10] Also the energy (λ_{max} ~ 460 nm) and the intensity (ε_{max} ~ 500 M^{-1} cm^{-1}) of the CT absorption band are consistent with those of similar compounds previously investigated.

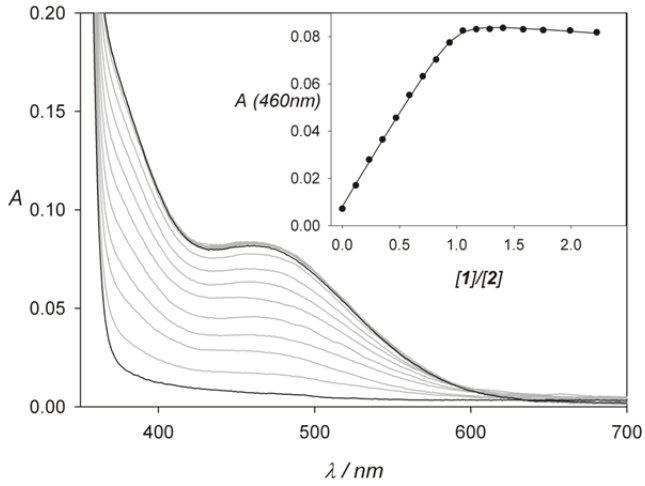

Figure 3.6: Absorption spectral changes observed upon titration of axle **2** (1.7×10^{-4} M) with increasing aliquots of a 4.0×10^{-3} M solution of **1** in CH_2Cl_2 at RT. The inset shows the fitting with a 1:1 association model (—) of the titration data obtained at 460 nm.

Subsequently the hydroxyl end group of pseudorotaxanes **P**[**1**⊃**2**]$_{up}$ and **P**[**1**⊃**3**]$_{up}$ was functionalized with the bulky diphenylacetyl moiety by submitting the pseudorotaxanes to the stoppering reaction with diphenylacetyl chloride in toluene (Scheme 3.2)

The structure of compounds **R**[**1**⊃**4**]$_{up}$ and **R**[**1**⊃**5**]$_{up}$ was inferred through NMR techniques (Figure 3.7).

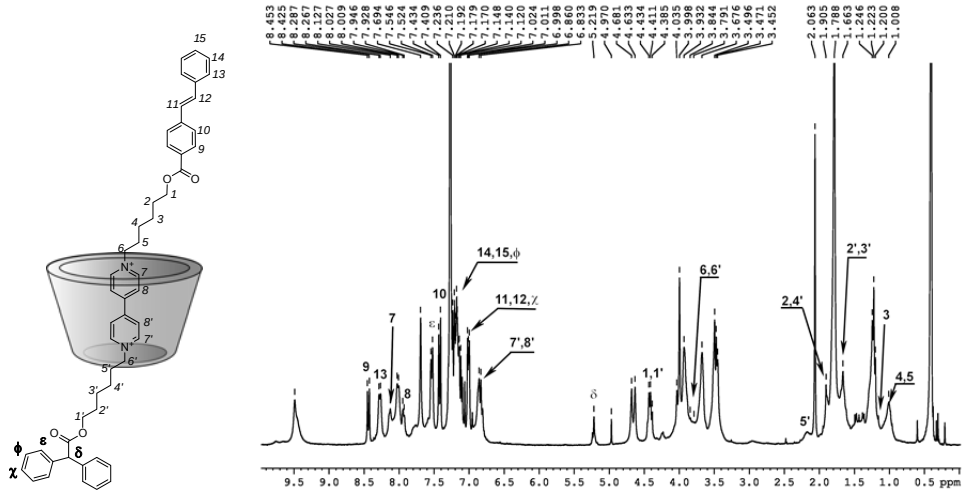

Figure 3.7: ^{1}H NMR (300 MHz) of **R[1⊃4]**$_{up}$ in C_6D_6.

In particular the 2D ROESY NMR experiments (Figure 3.8) confirm that the stilbene-based head group of dumbells **4** and **5** is still positioned at the upper rim of the wheel in both rotaxanes, confirming that during the stoppering reaction no isomerization process take place.

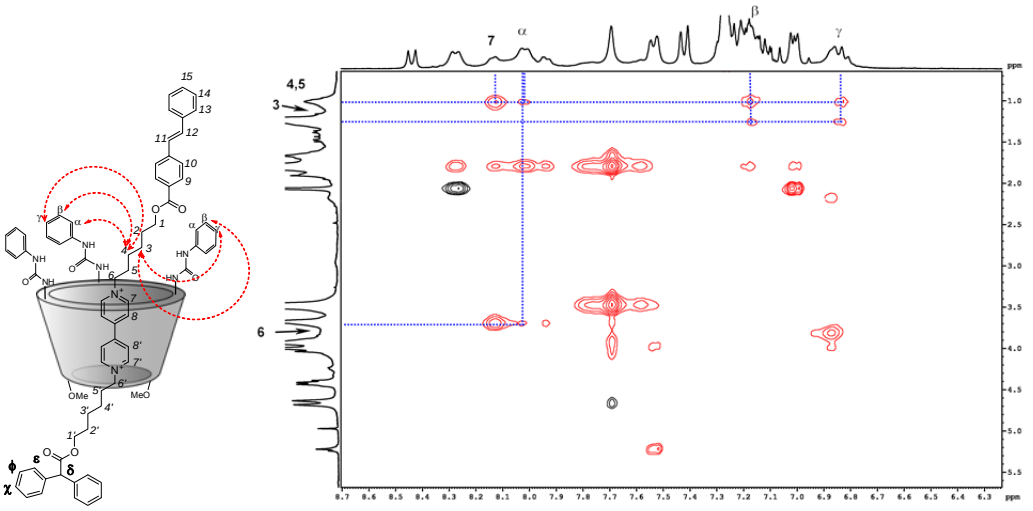

Figure 3.8: ^{1}H-^{1}H 2D ROESY spectrum (expanded region) (300 MHz) of **R[1⊃4]**$_{up}$ in C_6D_6

In order to further confirm the structure of rotaxanes **R[1⊃4]**$_{up}$ and **R[1⊃5]**$_{up}$ the synthesis of rotaxanes having the opposite orientation of the dumbbell by threading the wheel with threads **4** and **5** was tackled. In principle the axial compound can thread the calixarene only from the upper rim through the stilbene-type unit since the diphenylacetyl moiety is too large to pass the calixarene annulus. As expected at room temperature in C_6D_6 the dumbbells do not thread the wheel, probably for kinetic reasons. However by refluxing the solution that contain **1** and **4** for 12 hours, it assumes a deep purple color, characteristic of the CT interactions between the electron-rich calixarene cavity and the electron-poor bipyrididium unit (Figure 3.9). The 1D and 2D NMR experiments confirm the structure of the compound in which the stilbene unit is positioned at the lower rim of the wheel (Figure 3.10).

In the case of dumbbell **5,** no threading into the wheel takes place, even by refluxing the components for 7 days. Tentatively this behavior could be explained considering that the steric hindrance of 4-t-butyl substituted stilbene unit is larger than that of the

unsubstituted stilbene, and under this conditions the energy barrier for its threading is too high.

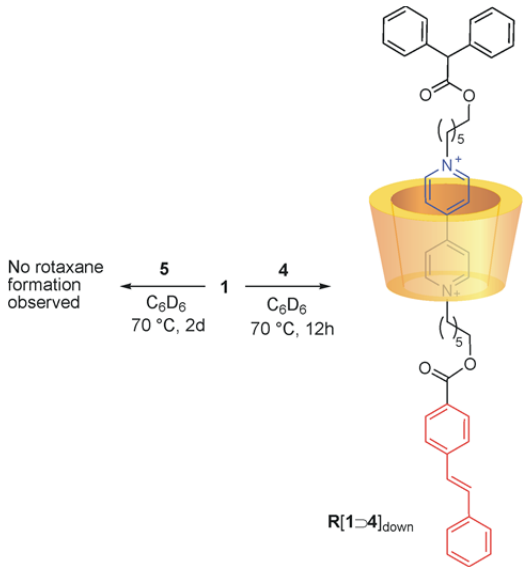

Figure 3.9: Synthesis of compound **R[1⊃4]**$_{down}$.

In figure 3.10 the ^{1}H NMR spectrum of **R[1⊃4]**$_{down}$ recorded in C_6D_6, in which all the signals of dumbell's protons are assigned, is reported.

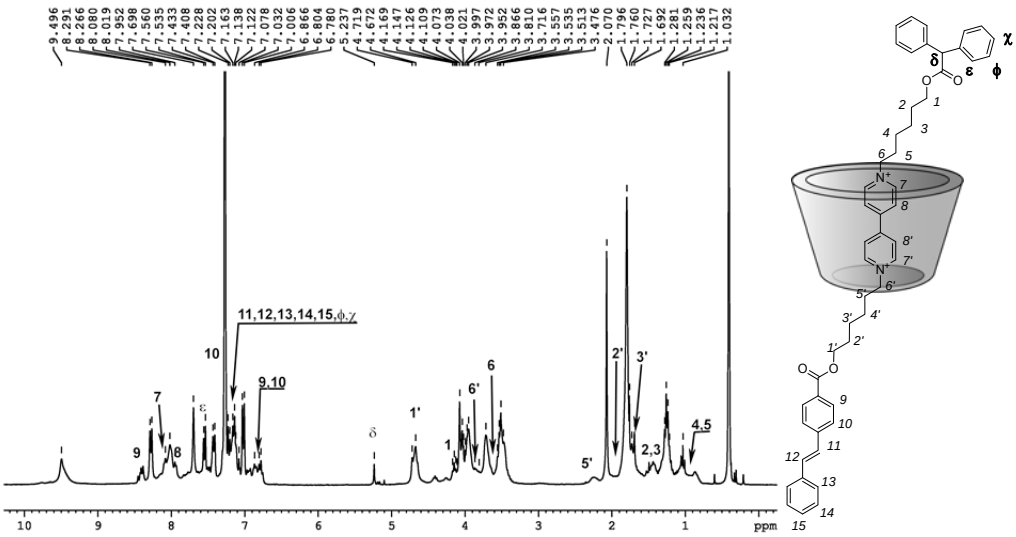

Figure 3.10: ^{1}H NMR (300 MHz) of **R[1⊃4]**$_{down}$ in C_6D_6.

The main features of **R[1⊃4]**$_{down}$ are the chemical shifts of protons *1*, *1'* that, contrary to **R[1⊃4]**$_{up}$ where they resonate, overlapped, at δ = 4.50 ppm, now experience different chemical shifts and resonate at δ = 4.10 ppm and δ = 4.70 ppm respectively. The orientation of the dumbbell termini towards the two rims of the wheel was established through 2D ROESY NMR experiments (Figure 3.11). The cross-peaks between protons *3', 4', 5'* of the dumbbell with the OCH_3 protons of the wheel, together with the spatial correlations between protons *2, 3, 4, 5* of the axle with the aromatic moieties that are present at the upper rim of the calix, unambiguously confirmed the orientation of the dumbbell threaded into the wheel.

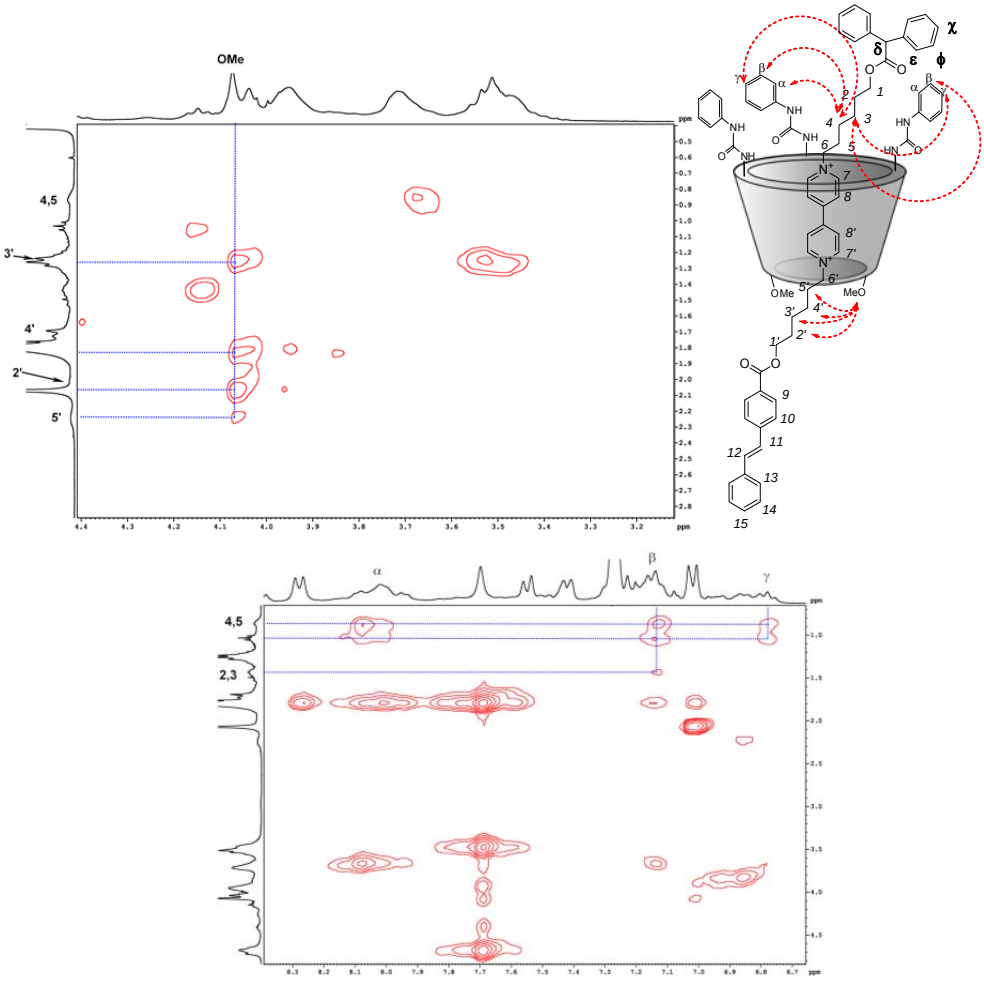

Figure 3.11: ^{1}H-^{1}H 2D ROESY spectra (expanded regions) (300 MHz) of **R[1⊃4]**$_{down}$ in C_6D_6.

R[**1**⊃**4**]$_{up}$ and **R**[**1**⊃**5**]$_{up}$ were also characterized by UV-Vis spectroscopy in air-equilibrated CH_2Cl_2 solution at room temperature. Their common spectral features are two bands at λ = 320 and λ = 260 nm ascribed to the absorption of the wheel and the 4,4' bipyridinium unit of the axle and to the stilbene-type end group of the axle, respectively. The spectra of **R**[**1**⊃**4**]$_{up}$ and **R**[**1**⊃**5**]$_{up}$ also show a weak and broad band centred at 460 nm that is not present in the spectra of the separated molecular components and that is responsible of their red color. As in the cases of **P**[**1**⊃**2**]$_{up}$ and **P**[**1**⊃**3**]$_{up}$ this visible band can be ascribed to the CT interactions between the electron-rich aromatic rings of the wheel and the electron-poor 4,4′-bipyridinium unit of the axles (Figure 3.12). Their rotaxane-like character is clearly confirmed by the fact that the molar absorption coefficients of the CT absorption band are not affected by concentration.

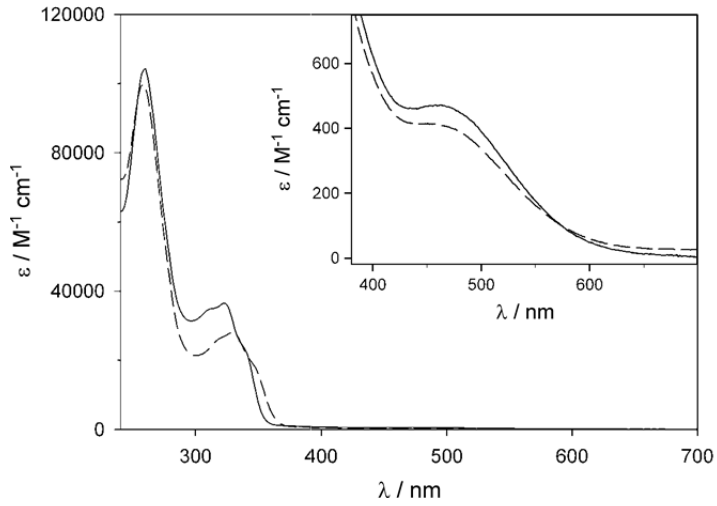

Figure 3.12: Absorption spectra (CH_2Cl_2, RT) of compounds **R**[**1**⊃**4**]$_{up}$ (full line) and **R**[**1**⊃**5**]$_{up}$ (dashed line). The inset shows an enlarged view of their charge-transfer absorption bands.

3.4 Unidirectional dethreading processes of oriented rotaxanes

In apolar solvents compounds **R**[**1**⊃**4**]$_{up}$ and **R**[**1**⊃**5**]$_{up}$ are mainly stabilized by: *i*) CT interactions between the aromatic rings of the wheel and the bipyridinium moiety of the axles; *ii*) hydrogen bonding between the counteranions of the axles and the ureido groups of the wheel; and *iii*) solvophobic effects on account of the low solubility of bipyridinium salts in non-polar solvents. These interactions are weakened, or nullyfied, in polar solvents; it was thus expected that dissolution of compounds **R**[**1**⊃**4**]$_{up}$ and **R**[**1**⊃**5**]$_{up}$ in such kind of solvents the weakening of the intercomponent interaction promoted the dethreading. Because of the presence of the diphenylacetyl stopper at one end of the axles, it could also be expected that dethreading occurred by involving the other end side, i.e. through the slippage of the sufficiently slim stilbene-type unit from the lower rim of the wheel (Scheme 3.4).

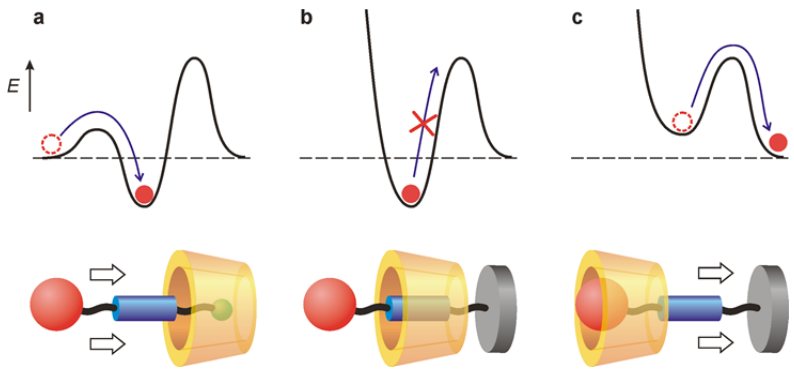

Scheme 3.4: Simplified potential energy curves representing the steps that account for the unidirectional transit of the axle through the wheel. The horizontal coordinate of the diagrams represents the axle-wheel distance. (a) Threading of the axle through the upper rim of the wheel in apolar solvents; (b) stoppering reaction to convert the pseudorotaxane in a rotaxane-like species; (c) dethreading of the axle from the lower rim of the wheel occurring in polar solvents.

DMSO was chosen as polar solvent to induce the dethreading process, since it is polar enough to weaken the interactions between wheel and dumbbell and because, thanks to the high solubility of the separated components in this solvent it could be, in principle, possible to follow the process through NMR techniques. In fact the ^{1}H NMR spectrum

taken immediately from dissolution of **R**[**1**⊃**4**]$_{up}$ showed that after five minutes after dissolution extensive dethreading of the axle from the wheel had taken place (Figure 3.13). This means that the disassembly of dumbbell **4** from the wheel in DMSO was too fast to be monitored through NMR.

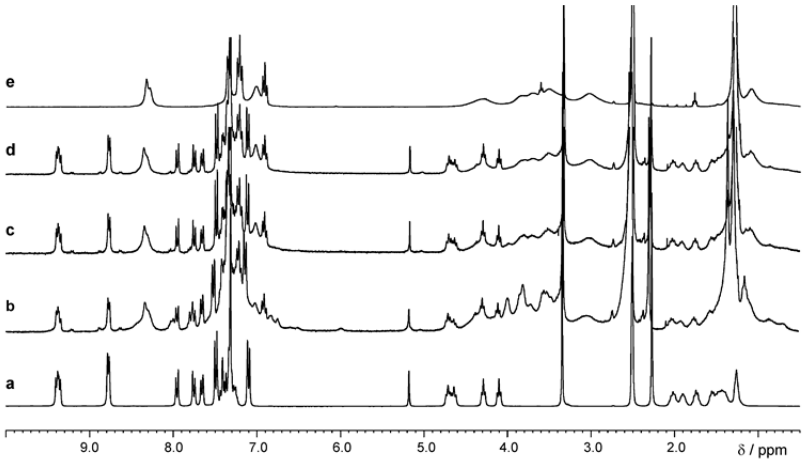

Figure 3.13: ^{1}H NMR spectra (300 MHz, DMSO-d_6) of dumbbell **4** (a), **R**[**1**⊃**4**]$_{up}$ 5 min (b), 10 min (c) and 30 min (d) after dissolution, and wheel **1** (e).

On the contrary, when **R**[**1**⊃**5**]$_{up}$ was dissolved in DMSO-d_6 the dethreading process was slower than in the previous case, in fact only after 9 hours from dissolution, the signals assigned to the rotaxane had disappeared in the NMR spectra (Figure 3.14).

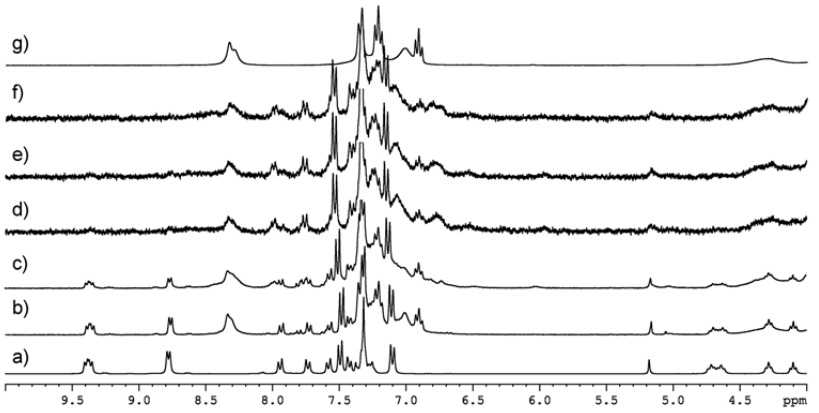

Figure 3.14: ^{1}H NMR spectra (300 MHz, DMSO-d_6) of axle **5** (a); **R**[**1**⊃**5**]$_{up}$ 80 h (b), 8.5 h min (c), 0.5 h (d); 0.25 h (e), 0.05 h (f) after dissolution; and wheel **1** (g).

A more quantitative study was carried out monitoring the dethreading process with UV-Vis spectroscopy. The CT absorption band at around 460 nm, characteristic of the assembled structure, was monitored for both systems from dissolution of rotaxane in DMSO. For both compounds the intensity of this band decreased over time and, in agreement with NMR data, this decrease was faster for $\mathbf{R}[\mathbf{1}\supset\mathbf{4}]_{up}$ than for $\mathbf{R}[\mathbf{1}\supset\mathbf{5}]_{up}$. The absorption spectra observed when the time-dependent changes were finished coincide with the sum of the spectra of the respective separated components. This outcome was in agreement with the dethreading of pseudorotaxanes promoted by the solvent-induced weakening of the supramolecular interactions.

Data fitting[13] showed that the absorbance decays at 460 nm took place with a first order kinetic law and with rate constants of 5.9×10^{-3} s^{-1} and 9.3×10^{-5} s^{-1} for $\mathbf{R}[\mathbf{1}\supset\mathbf{4}]_{up}$ and $\mathbf{R}[\mathbf{1}\supset\mathbf{5}]_{up}$, respectively (Figure 3.15). The fact that the rate constants were influenced by the stilbene structure (un-substituted and 4-*t*-butyl substituted) was a clear evidence that dethreading took place through the slippage of this group from the lower rim of the wheel. The two orders of magnitude lower rate constant of $\mathbf{R}[\mathbf{1}\supset\mathbf{5}]_{up}$ compared with $\mathbf{R}[\mathbf{1}\supset\mathbf{4}]_{up}$ could indeed be explained on the basis of the higher hampering effect of the *t*-butyl substituted stilbene in axle **5** compared with the unsubstituted one in axle **4**.

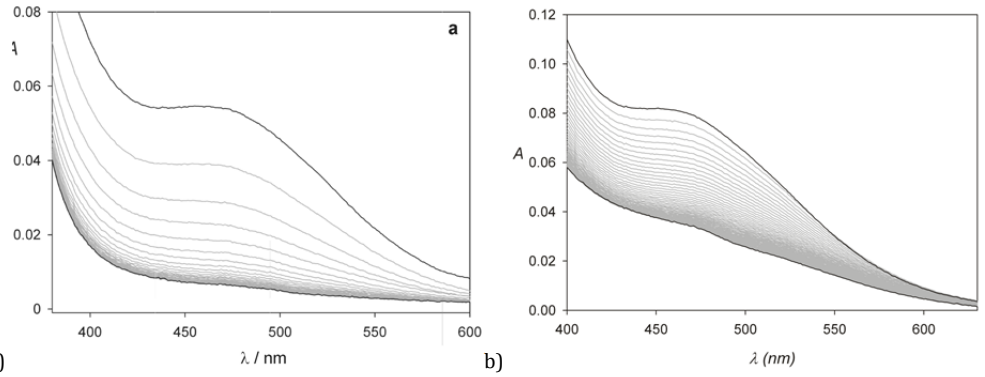

Figure 3.15: Decrease of the CT absorption band of: (a) compound $\mathbf{R}[\mathbf{1}\supset\mathbf{4}]_{up}$, (b) compound $\mathbf{R}[\mathbf{1}\supset\mathbf{5}]_{up}$ after dissolution in DMSO at RT.

With the objective of further support the involvement of the stilbene-type unit in the dethreading process, the rate dethreading constants in DMSO obtained for $\mathbf{R}[\mathbf{1}\supset\mathbf{4}]_{up}$ and $\mathbf{R}[\mathbf{1}\supset\mathbf{5}]_{up}$ were compared with those obtained in the same condition for the

pseudorotaxanes **P**[**1**⊃**2**]$_{up}$ and **P**[**1**⊃**3**]$_{up}$. In these cases, as expected, the dissolution of **P**[**1**⊃**2**]$_{up}$ and **P**[**1**⊃**3**]$_{up}$ in DMSO causes their quantitative and fast dethreading. In fact, the absorption spectra of such solutions, immediately monitored after dissolution (i.e. within 30 s), did not show CT band, indicating that disassembly occurred on a faster timescale than that required for dissolution; in other words, the dethreading rate constant was > 0.1 s^{-1}. The fact that this value was at least two order of magnitude higher than that measured for **R**[**1**⊃**4**]$_{up}$ and **R**[**1**⊃**5**]$_{up}$, indicated that for the pseudorotaxanes a different dethreading mechanism operate. In other words, axles **2** and **3** dethreaded from the upper rim of the wheel with the side carrying the –OH group, which means in a opposite direction from that of the threading.

3.5 Photocontrol in the dethreading rate

The presence of the stilbene unit, further to behaving as kinetic stopper and to allowing the formation of only one oriented pseudorotaxane isomer, could also be exploited because this unit is photoactive and can undergo *E*-*Z* photoisomerization when irradiated with UV light at 334 or 313 nm. As molecular mechanics calculations indicated[5] the steric hindrance of these moiety in the *Z* conformation was higher than in the *E* one, and this should result in a lower dethreading rate constant for the *E* isomer with respect to the *Z*. Compounds **R**[**1**⊃**4**]$_{up}$ and **R**[**1**⊃**5**]$_{up}$ were irradiated in CH_2Cl_2 solution of 334 or 313 nm to induce the *E*-*Z* isomerization of the stilbene end group of the axle. The photoreaction did not cause any change in the CT absorption band, suggesting that the configuration of the stilbene unit did not affect the inclusion of the 4,4′-bipyridinium unit inside the wheel. Only the band in the 300-350 nm region, characteristic of the stilbene unit, was affected, as evidenced by irradiation carried out on separate axles **4** and **5**. For both **R**[**1**⊃**4**]$_{up}$ and **R**[**1**⊃**5**]$_{up}$ it was found that an irradiation of 90 minutes causes about 70% conversion of the stilbene unit from the *E* to the *Z* isomer.[14] After evaporation of CH_2Cl_2 and addition of DMSO, the CT absorption band of **R**[**1**⊃**4**]$_{up}$ and **R**[**1**⊃**5**]$_{up}$ was monitored. For the photoisomerized compounds, as already observed for the non-irradiated ones, the CT band decreased over time indicating the occurrence of axle dethreading.

In the case of **R**[**1**⊃**4**]$_{up}$ the best fitting of the absorption values at 460 nm clearly evidenced that the disappearance of CT band occurs according to two superimposed first order kinetics with rate constants of 5.9×10^{-3} s^{-1} and 2.3×10^{-5} s^{-1}, respectively. The faster process, which accounts for 30% of the total decay, was attributed to the dethreading of the axle carrying the stilbene in the *E* configuration since its rate constant coincides with that measured for the non-irradiated **R**[**1**⊃**4**]$_{up}$. Consequently, the slower process could be assigned to the dethreading of the axle having the stilbene in the *Z* configuration. The low value of this rate constant was in agreement with the higher hampering effect of the *Z* isomer compared with the *E* isomer, which renders the slippage of the dumbbell from the lower rim of the wheel more difficult. It was interesting to notice that the *E*→*Z* photoisomerization affects the dethreading rate constant more than the incorporation of the *t*-butyl group on the stilbene unit. The rate constant observed upon isomerization was

indeed about one order of magnitude slower than that observed in the case of the *t*-but substituted stilbene.

In the case of **R**[**1**⊃**5**]$_{up}$ only about a 30% decrease of the CT absorption band is observed. The best fitting of the absorption values at 460 nm evidenced that this decrease occurred according to a first order kinetics with a rate constant of 4×10^{-5} s^{-1}, which was quite similar to that measured for the dethreading of the non-irradiated **R**[**1**⊃**5**]$_{up}$. It was thus possible to conclude that the observed decay of the CT absorption band relates to the portion of the compound with the axle carrying the *E* isomer of the *t*-butyl stilbene, and that the photoisomerized compound did not undergo dethreading, accounting for the 70% of the CT absorption intensity that did not disappear in DMSO (Figure 3.16). Hence, these results showed that the *Z* isomer of the *t*-butyl stilbene was too bulky to pass through the lower rim of the wheel, and that **R**[**1**⊃**5**]$_{up}$ in its *Z* configuration behaved as a real rotaxane.

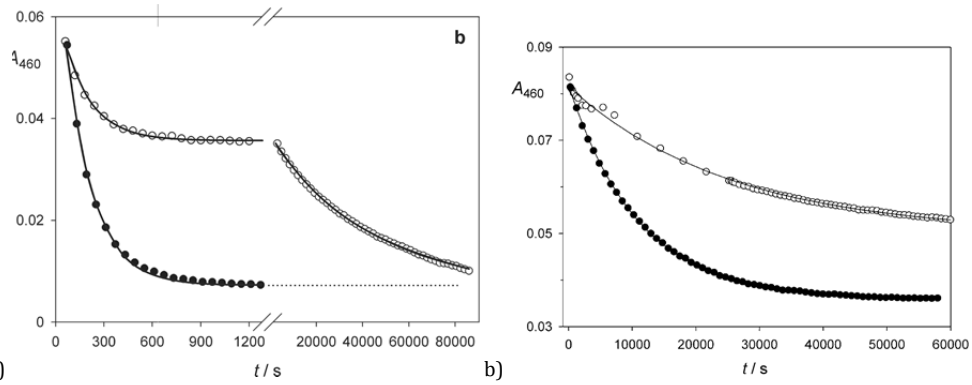

Figure 3.16: a) absorbance decrease at 460 nm upon dissolution in DMSO of **R**[**1**⊃**4**]$_{up}$ before (full circles) and after (open circles) exhaustive irradiation at 334 nm. The first-order fitting curves are also shown; b) Absorbance decrease at 460 nm upon dissolution in DMSO of **R**[**1**⊃**5**]$_{up}$ before (full circles) and after (open circles) exhaustive irradiation at 313 nm. The first-order fitting curves are also shown.

3.6 Conclusions

Taken all together these data confirm that this strategy enabled to obtain the unidirectional transit of a molecular axle through a molecular wheel. The use of an appropriately non-symmetrical molecular component had a key role for the achieving of this goal. The whole process could be divided in three steps:

1. In C_6D_6 axle **2** or **3** threaded the wheel **1** from the upper rim and with the alkyl chain bearing the hydroxyl group yielding the corresponding oriented pseudorotaxanes that bear the –OH group positioned at the lower rim of the wheel. This orientational control is kinetically driven since the energy barrier for the threading through the stilbene unit was too high.
2. The stoppering reaction of the oriented pseudorotaxanes $\mathbf{P}[\mathbf{1}\supset\mathbf{2}]_{up}$ and $\mathbf{P}[\mathbf{1}\supset\mathbf{3}]_{up}$ with the bulky diphenylacetyl moiety yields the corresponding rotaxanes $\mathbf{R}[\mathbf{1}\supset\mathbf{4}]_{up}$ and $\mathbf{R}[\mathbf{1}\supset\mathbf{5}]_{up}$.
3. In DMSO, where the supramolecular interactions that held togheter the components $\mathbf{R}[\mathbf{1}\supset\mathbf{4}]_{up}$ and $\mathbf{R}[\mathbf{1}\supset\mathbf{5}]_{up}$ no longer operate, slippage of the dumbbell from the lower rim, which is in same direction of the axle threading, takes place. The complete unidirectional transit of the axle through the wheel was, therefore, accomplished.

Experimental section

Materials and synthetic methods. Toluene and dichloromethane were dried using standard procedure, all other reagents were of reagent grade quality obtained from commercial suppliers and were used without further purification. NMR spectra were recorded at 400 and 300 MHz for ^{1}H and 100 and 75 MHz for ^{13}C. Melting points are uncorrected. Chemical shifts are expressed in ppm (δ) using the residual solvent signal as internal reference. Mass spectra were recorded in ESI mode. Calix[6]arene (**1**),[8a] (*E*)-4-styrylbenzoic acid (**8a**),[11] 6-hydroxyhexyl tosylate (**10**),[12] and 6-(tosyloxy)hexyl 2,2-diphenylacetate (**13**),[9b] were synthesized according to literature procedures.

Syntheses

(*E*)-4-(4-tert-butylstyryl)benzoic acid (8b): 4-bromo benzoic acid **7** (1 g, 4.97 mmol), $Pd(OAc)_2$ (cat.), 1-tert-butyl-4-vinylbenzene **6b** (1.2 g, 7.5 mmol), K_2CO_3 (1.4 g, 10 mmol), N,N dimetyl-β-alanine (cat.) were added to a stirred solution of DMF (250 ml) kept under argon atmosphere. The resulting heterogeneous mixture was refluxed for 6 h. After this period, the reaction mixture was cooled to room temperature, diluted with water (100 ml) and extracted twice with diethyl ether (2 × 100 ml). The organic phase was separated, dried with Na_2SO_4 and evaporated under reduced pressure. The orange oily residue was taken up with ethyl acetate and the desired product **8b** was precipitated as a white solid (1 g, 71%) by addition of n-hexane. M.p. = 296.0 - 297.1 °C. ^{1}H NMR (300 MHz, $CDCl_3/CD_3OD$ 1:1): δ = 7.96 (d, *J* = 8 Hz, 2H), 7.49 (d, *J* = 8 Hz, 2H), 7.42 (d, *J* = 8 Hz, 2H), 7.33 (d, *J* = 8 Hz, 2H), 7.15 (d, *J* = 16 Hz, 1H), 7.03 (d, *J* = 16 Hz, 1H), 1.27 (s, 9H); ^{13}C NMR (75 MHz, $CDCl_3/CD_3OD$ 1:1): δ = 151.4, 146.1, 142.0, 133.8, 130.9, 130.2, 128.7, 126.7, 126.4, 126.0, 125.6, 77.2, 31.1; MS (ESI): *m/z* (%): 279 (100) $[M–H^+]^-$.

General procedure for the synthesis of 11a,b: in a 100ml round-bottomed flask, the appropriate stilbene derivate **8a,b** (4.5 mmol) and oxalyl chloride (13.4 mmol) were dissolved in 40 ml of dry $CHCl_3$. The resulting solution was refluxed for two hours under

nitrogen atmosphere, then the solvent was evaporated under reduced pressure. The yellow solid residue of the acylic chloride (**9a,b**) was dissolved in dry CH_2Cl_2 (50 ml). To the resulting solution, 6-hydroxyhexyl tosylate **10** (1.8 g, 6.7 mmol), triethyl amine (0.68 g, 6.7 mmol) and DMAP (cat. amount) were added in this order. The reaction mixture was stirred at room temperature for 72 h, then the reaction was quenched by addition of water (50 ml). The separated organic phase was extracted twice with a saturated solution of $NaHCO_3$ in H_2O (2 × 20 ml). After evaporation of the solvent under reduced pressure, the oily residue was purified by column chromatography (hexane/ethyl acetate 8/2).

11a was isolated as a white solid (1.2 g, 56%). M.p. = 69 - 71 °C. ^{1}H NMR (300 MHz, $CDCl_3$): δ = 8.01 (d, *J* = 8 Hz, 2H), 7.79 (d, *J* = 8 Hz, 2H), 7.57 - 7.52 (m, 4H), 7.4 - 7.3 (m, 5H), 7.22 (d, *J* = 17 Hz, 1H), 7.12 (d, *J* = 17 Hz, 1H), 4.27 (t, *J* = 6.5 Hz, 2H), 4.03 (t, *J* = 6.5 Hz, 2H), 2.43 (s, 3H), 1.8 - 1.7 (m, 4H), 1.45 - 1.35 (m, 4H); ^{13}C NMR (75 MHz, $CDCl_3$): δ = 166.3, 144.6, 141.7, 136.6, 133.1, 131.1, 129.9, 129.7, 129.1, 128.7, 127.8, 127.5, 126.7, 126.2, 70.3, 64.6, 28.7, 28.5, 25.4, 25.0, 21.6; MS (ESI): *m/z* (%): 501 (50) $[M+Na]^+$, 517 (25) $[M+K]^+$.

11b was isolated as colorless oil (1.42 g, 60%). ^{1}H NMR (300 MHz, $CDCl_3$): δ = 8.01 (d, *J* = 8 Hz, 2H), 7.78 (d, *J* = 8 Hz, 2H), 7.55 (d, *J* = 8 Hz, 2H), 7.47 (d, *J* = 8 Hz, 2H), 7.39 (d, *J* = 8 Hz, 2H), 7.33 (d, *J* = 8 Hz, 2H), 7.20 (d, *J* = 16 Hz, 1H), 7.10 (d, *J* = 16 Hz, 1H), 4.27 (t, *J* = 6.6 Hz, 2H), 4.03 (t, *J* = 6.5 Hz, 2H), 2.44 (s, 3H), 1.75-1.50 (m, 6H) 1.4-1.3 (m, 11H); ^{13}C (75 MHz, $CDCl_3$) δ = 166.4, 151.4, 144.6, 142.0, 133.9, 133.1, 131.0, 129.9, 129.8, 128.8, 127.8, 126.7, 126.5, 126.1, 125.7, 70.3, 64.6, 34.6, 31.2, 28.7, 28.4, 25.4, 25.1, 21.6; MS (ES): *m/z* (%): 557 (40) $[M+Na]^+$, 573 (15) $[M+K]^+$.

General procedure for the synthesis of 12a,b: 4,4′-bipyridine (1.2 g, 7.7 mmol) and the appropriate stilbenic derivative **11a,b** (2.5 mmol) were dissolved in 50 ml of CH_3CN. The resulting solution was refluxed for 72 h, then the solvent was evaporated to dryness under reduced pressure. The desired products were isolated by treating twice the yellowish oily residue with hot ethyl acetate (2 × 25 ml) followed by suction filtration.

12a was isolated as a white solid (0.8 g, 52 %). M.p. = 189.0 - 191.2 °C. ^{1}H NMR (300 MHz, CD_3OD): δ = 9.16 (d, *J* = 6.5 Hz, 2H), 8.90 (d, *J* = 6.5 Hz, 2H), 8.51 (d, *J* = 6.5 Hz, 2H), 8.18 (d, *J* = 8 Hz, 2H), 7.95 (d, *J* = 8.1 Hz, 2H), 7.7 - 7.6 (m, 6H), 7.4 - 7.2 (m, 8H), 4.70 (t, *J* = 7 Hz, 2H), 4.33 (t, *J* = 7 Hz, 2H), 2.34 (s, 3H), 2.10 (t, *J* = 7 Hz, 2H), 1.82 (t, *J* = 7 Hz, 2H), 1.65 - 1.31 (m, 4H); ^{13}C (75 MHz, CD_3OD): δ = 166.6, 152.5, 148.2, 145.1, 144.2, 141.9, 140.1,

136.4, 131.2, 129.6, 128.5, 128.4, 128.0, 127.2, 127.0, 126.4, 126.2, 126.1, 125.4, 123.1, 64.4, 61.5, 31.0, 29.3, 28.1, 25.4, 25.1, 20.7; MS (ESI): *m/z* (%): 463 (100) $[M–TsO^-]^+$.

12b was isolated as a white solid (1.3 g, 77 %). M.p. = 171.8 - 173.8 °C. ^{1}H NMR (300 MHz, $CDCl_3$): δ = 9.29 (d, *J* = 6.5 Hz, 2H), 8.74 (d, *J* = 6.5 Hz, 2H), 8.18 (d, *J* = 6.5 Hz, 2H), 7.94 (d, *J* = 8 Hz, 2H), 7.73 (d, *J* = 8 Hz, 2H), 7.57 (d, *J* = 6 Hz, 2H), 7.51 (d, *J* = 8 Hz, 2H), 7.45 (d, *J* = 8 Hz, 2H), 7.38 (d, *J* = 8 Hz, 2H), 7.17 (d, *J* = 16.5 Hz, 2H), 7.08 (d, *J* = 6 Hz, 2H), 7.04 (d, *J* = 16.5 Hz, 2H), 4.77 (d, *J* = 7 Hz, 2H), 4.20 (d, *J* = 7 Hz, 2H), 2.23 (s, 3H), 1.94 (d, *J* = 7 Hz, 2H), 1.64 (d, *J* = 7 Hz, 2H), 1.31 (bs, 13H); ^{13}C (75 MHz, CD_3OD): δ = 166.6, 154.1, 151.7, 145.9, 142.4, 141.3, 139.7, 134.3, 131.4, 130.2, 129.0, 126.8, 126.5, 126.2, 126.1, 121.9, 64.9, 62.1, 34.9, 31.8, 31.2, 28.7, 26.0, 25.9, 21.3; MS (ESI): *m/z* (%): 519 (100) $[M–TsO^-]^+$.

General procedure for the synthesis of axles 2 and 3: 6-hydroxyhexyl tosylate **10** (0.3 g, 1.1 mmol) and the appropriate salt **12a,b** (0.7 mmol) were dissolved in CH_3CN (50 ml). The resulting reaction mixture was refluxed for 10 days and then cooled to room temperature. The solvent was evaporated to dryness under reduced pressure and the crude yellowish solid residue was triturated twice with hot ethyl acetate (2 × 25 ml). After decantation of the ethyl acetate, the desired axles **2** and **3** were purified by recrystallization from CH_3CN.

2 was isolated as a white solid (0.45 g, 70%). M.p. = 127.0 - 128.2 °C. ^{1}H NMR (300 MHz, CD_3OD): δ = 9.21 - 9.17 (m, 4H), 8.60 (d, *J* = 6.5 Hz, 4H), 7.95 (d, *J* = 8.5 Hz, 2H), 7.67 (d, *J* = 8.5 Hz, 2H), 7.63 (d, *J* = 8.5 Hz, 2H), 7.56 (d, *J* = 7.5 Hz, 2H), 7.39 - 7.27 (m, 5H), 7.19 (d, *J* = 8 Hz, 6H), 4.7 - 4.6 (m, 4H), 4.30 (t, *J* = 6.5 Hz, 2H), 3.54 (t, *J* = 6.5 Hz, 2H), 2.33 (s, 6H), 2.1 (bs, 4H), 1.8 (bs, 2H), 1.6 - 1.3 (m, 10H): ^{13}C (100 MHz, CD_3OD): δ = 172.9, 166.6, 149.7, 145.6, 142.3, 140.3, 138.9, 136.8, 131.3, 129.6, 128.7, 128.6, 128.4, 128.2, 128.0, 126.9, 126.6, 126.2, 125.6, 64.5, 61.8, 56.9, 30.9, 30.8, 27.9, 25.4, 25.2, 24.8, 21.1, 20.0; MS (ESI): *m/z* (%): 281 (50) $[M–2TsO^-]^{2+}$.

3 was isolated as a white solid (0.47 g, 70%). M.p. = 131.3 - 132.8 °C. ^{1}H NMR (300 MHz, CD_3OD): δ = 9.2 (bs, 4H), 8.6 (bs, 4H), 7.93 (d, *J* = 8.3 Hz, 2H), 7.67 (d, *J* = 8.3 Hz, 2H), 7.60 (d, *J* = 8.3 Hz, 2H), 7.49 (d, *J* = 8.3 Hz, 2H), 7.39 (d, *J* = 8.3 Hz, 2H), 7.2 - 7.1 (m, 6H), 4.8 - 4.6 (m, 4H), 4.30 (t, *J* = 6 Hz, 2H), 3.54 (t, *J* = 6 Hz, 2H), 2.33 (s, 6H), 2.1 (bs, 4H), 1.8 (bs, 2H), 1.7 - 1.4 (m, 10H), 1.31 (s, 9H): ^{13}C (75 MHz, CD_3OD): δ = 170.4, 155.2, 153.6, 149.5, 147.0, 146.3, 144.2, 137.9, 134.9, 133.41, 132.37, 130.7, 130.2, 130.0, 129.9, 129.4, 129.2, 68.3,

65.6, 65.1, 37.9, 35.7, 34.9, 34.8, 34.2, 31.9, 29.4, 29.3, 29.1, 28.8, 23.8; MS (ESI): *m/z* (%): 986 (15) $[M+Na]^+$, 791 (30) $[M-TsO^-]^+$, 310 (100) $[M-2TsO^-]^{2+}$.

General procedure for the synthesis of dumbbells 4 and 5: Same procedure employed for the synthesis of **2**-**3** but using 6-(tosyloxy)hexyl 2,2-diphenylacetate **13** (1.1 mmol) as alkylating agent.

4 was isolated as a white solid (0.57 g, 75%): M.p. = 172.5 - 173.5 °C; ^{1}H NMR (300 MHz, DMSO-d_6): δ = 9.24 (d, *J* = 7 Hz, 2H), 9.19 (d, *J* = 7 Hz, 2H), 8.62 (d, *J* = 6 Hz, 4H), 7.98 (d, *J* = 8.5 Hz, 2H), 7.8 - 7.5 (m, *J* = 8.5 Hz, 8H), 7.4 - 7.2 (m, 17H), 5.08 (s, 1H), 4.73 (t, *J* = 7.5 Hz, 2H), 4.63 (t, *J* = 7.5 Hz, 2H), 4.32 (t, *J* = 6.5 Hz, 2H), 4.14 (t, *J* = 6.5 Hz, 2H), 2.34 (s, 6H), 2.2 - 2.1 (m, 2H), 2.1 - 2.0 (m, 2H), 1.9 - 1.8 (m, 2H), 1.7 - 1.5 (m, 6H), 1.3 (bs, 4H); ^{13}C (75 MHz, DMSO - d_6): δ = 168.2, 151.5, 147.3, 144.2, 142.1, 140.7, 138.7, 132.9, 131.2, 130.4, 130.2, 130.0, 129.9, 129.6, 128.6, 128.5, 128.2, 127.8, 127.2, 66.1, 63.5, 64.4, 58.5, 32.6, 32.5, 29.8, 29.5, 27.1, 26.9, 26.8, 26.5, 21.6; MS (ESI): *m/z* (%) 379.1 (100) $[M-2TsO^-]^{2+}$, 929 (15) $[M-TsO^-]^+$.

5 was isolated as a white solid (0.56 g, 70%). M.p. = 176.5 - 177.5 °C; ^{1}H NMR (300 MHz, CD_3OD): δ = 9.22 (d, *J* = 8 Hz, 2H), 9.17 (d, *J* = 8 Hz, 2H), 8.60 (d, *J* = 6.5 Hz, 2H), 7.95 (d, *J* = 8 Hz, 2H), 7.67 (d, *J* = 8 Hz, 4H), 7.62 (d, *J* = 8 Hz, 2H), 7.51 (d, *J* = 8 Hz, 2H), 7.41 (d, *J* = 8 Hz, 2H), 7.3 - 7.1 (m, 16H), 5.05 (s, 1H), 4.73 (t, *J* = 7.5 Hz, 2H), 4.62 (t, *J* = 7.5 Hz, 2H), 4.31 (t, *J* = 6.5 Hz, 2H), 4.13 (t, *J* = 6.5 Hz, 2H), 2.33 (s, 6H), 2.12 - 2.08 (m, 2H), 2.02 - 1.96 (m, 2H), 1.81 (t, *J* = 7 Hz, 2H), 1.7 - 1.5 (m, 6H), 1.32 (s, 9H); ^{13}C (75 MHz, CD_3OD): δ = 171.9, 165.9, 147.3, 142.0, 132.7, 131.2, 130.1, 129.9, 129.8, 128.0, 127.7, 127.2, 127.0, 66.1, 63.4, 58.5, 32.6, 32.5, 31.9, 29.9, 29.5, 27.1, 26.9, 26.8, 26.5, 21.6; MS (ESI): *m/z* (%) 407.4 (100) $[M-2TsO^-]^{2+}$.

General procedure for synthesis of R[1⊃4]$_{up}$ and R[1⊃5]$_{up}$: axle **4** or **5** (0.04 mmol) was suspended in a solution of **1** (0.06 g, 0.04 mmol) in dry toluene (10 ml). The resulting heterogeneous mixture was stirred at RT until the solution turned to a deep-red color (2 h). Diphenylacetyl chloride (0.015 g, 0.06 mmol) and triethylamine (0.006 g, 0.06 mmol) were then added. After 3 days the solvent was completely removed under reduced pressure. The red solid residue was dissolved in CH_2Cl_2 (15 ml) and the solution extracted twice (2 × 15 ml) with an aqueous solution of HCl (10% w/v). The separated organic

phase was extracted twice (2 × 15 ml) with an 0.1 M aqueous solution of NaOTs to regenerate the TsO^- anions. The separated organic phase was then dried with $CaCl_2$ and evaporated to dryness under reduced pressure.

R[**1**⊃**4**]$_{up}$: the red solid residue was triturated with *n*-hexane (3 × 20 ml) to afford 0.06 g of **R**[**1**⊃**4**]$_{up}$ (63%) as a red solid. M.p. = 121.5 - 122.8 °C; ^{1}H NMR (300 MHz, C_6D_6): δ = 9.47 (s, 6H), 8.43 (d, *J* = 8.1 Hz, 2H), 8.3 (bs, 4H), 8.2 - 7.9 (m, 10H), 7.8 (bs, 3H), 7.69 (s, 6H), 7.6 - 7.5 (m, 13H),7.45 (d, *J* = 7.3 Hz, 2H), 7.3 - 7.1 (m, 16H), 7.1 - 6.9 (m, 5H), 6.8 (bs, 7H), 5.22 (s, 1H), 4.65 (d, *J* = 14.5 Hz, 6H), 4.5 - 4.4 (m, 4H), 4.0 (bs, 15H), 3.7 (bs, 8H), 3.6 - 3.4 (m, 14H), 2.2 (bs, 2H), 2.06 (s, 6H) 1.9 (bs, 4H), 1.79 (s, 29H), 1.6 (bs, 2H), 1.40 (s, 9H), 1.4-1.1 (m, 11H), 0.9-0.8 (m, 4H); ^{13}C (100 MHz, C_6D_6): δ = 172.1, 166.0, 153.5, 152.8, 148.1, 148.0, 144.4, 142.9, 141.2, 139.5, 139.0, 137.5, 137.1, 133.8, 132.1, 131.0, 130.0, 129.7, 129.3, 128.9, 128.8, 128.6, 128.4, 126.9, 126.5, 125.7, 124.8, 121.2, 118.1, 116.7, 72.4, 69.9, 66.3, 64.5, 61.0, 60.6, 57.3, 34.5, 31.5, 29.8, 29.2, 28.6, 28.3, 26.9, 25.7, 25.2, 20.8, 15.2; MS (ESI): *m/z* (%): 1112 (100) $[M-2TsO^-]^{2+}$; elemental analysis (%) calculed for $C_{155}H_{176}O_{22}S_2N_8$ (2567.25): C 72.52, H 6.91, S 2.50, N 4.36; found: C 72.89, H 7.03, S 2.37, N 4.39.

R[**1**⊃**5**]$_{up}$: the red solid residue was triturated with *n*-hexane (3 × 20 ml) to afford 0.06 g of **R**[**1**⊃**5**]$_{up}$ (63%). M.p. = 146.5 - 148.0 °C; ^{1}H NMR (300 MHz, C_6D_6): δ = 9.5 (bs, 6H), 8.43 (d, *J* = 8 Hz, 2H), 8.3 (bs, 4H), 8.1 - 7.9 (m, 10H), 7.8 (bs, 3H), 7.69 (s, 6H), 7.6 - 7.4 (m, 13H), 7.3 - 7.1 (m, 13H), 7.04 (bs, 5H), 6.9 (bs, 2H), 6,8 (bs, 5H), 5.22 (s, 1H), 4.65 (d, *J* = 14.5 Hz, 6H), 4.5 - 4.4 (m, 4H), 4.1 - 3.9 (bs, 15H), 3.8 - 3.6 (bs, 8H), 3.6 - 3.4 (m, 14H), 2.2 (bs, 2H), 2.1 (s, 6H) 1.9 (bs, 4H), 1.79 (s, 29H), 1.6 (bs, 2H), 1.40 (s, 9H), 1.4 - 1.1 (m, 11H), 0.9 (bs, 4H); ^{13}C (100 MHz, C_6D_6): δ = 172.1, 166.0, 153.5, 152.8, 151.0, 148.1, 148.0, 144.3, 143.0, 142.0, 141.0, 139.6, 139.3, 139.0, 137.4, 134.4, 133.8, 132.1, 131.0, 130.0, 129.5, 129.2, 129.1, 129.0, 128.9, 128.7, 128.4, 127.0, 126.9, 126.8, 126.5, 125.7, 124.8, 121.2, 119.6, 119.1, 118.1, 116.7, 72.4, 69.9, 66.3, 64.9, 64.5, 61.0, 60.6, 59.7, 57.3, 57.1, 34.5, 34.3, 34.1, 31.5, 31.0, 29.8, 29.3, 29.2, 28.6, 28.2, 27.7, 26.8, 26.0, 25.2, 20.8, 15.2; MS (ES): *m/z* (%): 1140 (100) $[M-2TsO^-]^{2+}$; elemental analysis (%) calculed for $C_{159}H_{188}O_{22}S_2N_8$ (2623.35): C 72.79, H 7.07, S 2.44, N 4.27; found: C 73.51, H 7.30, S 1.69, N 4.27.

Synthesis of R[**1**⊃**4**]$_{down}$: axle **4** (0.01 g, 0.009 mmol) was added to a 0.6 ml solution of wheel **1** (0.013 g, 0.009 mmol) in C_6D_6 placed in a 5 mm NMR tube. The resulting

heterogeneous mixture was heated at 70 °C for 12 h until the solution turned homogeneous and deep-red colored and analysed by ^{1}H and ^{13}C NMR and mass spectroscopy. ^{1}H NMR (300 MHz, C_6D_6): δ = 9.5 (bs, 6H), 8.4 (d, *J* = 8 Hz, 2H), 8.28 (d, *J* = 7 Hz, 4H), 8.2 (bs, 2H), 8.1 (bs, 6H), 7.95 (d, *J* = 6.5 Hz, 2H), 7.8 (bs, 6H), 7.69 (s, 6H), 7.46 (d, *J* = 7 Hz, 4H), 7.45 (d, *J* = 7 Hz, 4H), 7.4 - 7.2 (m, 8H), 7.2 - 7.1 (m, 6H), 7.1 - 7.0 (m, 5H), 6.9 (bs, 4H), 6.78 (t, *J* = 7 Hz, 3H), 5.23 (s, 1H), 4.69 (d, *J* = 14 Hz, 6H), 4.7 (bs, 2H), 4.13 (t, *J* = 7 Hz, 2H), 4.05 (s, 9H), 4.0 (bs, 8H), 3.7 (bs, 8H), 3.6 - 3.5 (m, 12H), 2.2 (bs, 2H), 2.04 (s, 8H), 1.8 (bs, 31H), 1.4 (bs, 4H), 1.24 (t, *J* = 7 Hz, 9H), 1.0 (bs, 2H), 0.9 (bs, 2H); ^{13}C (100 MHz, C_6D_6): δ = 172.0, 165.9, 153.5, 152.8, 148.1, 148.0, 144.3, 143.2, 143.0, 141.1, 139.4, 139.2, 137.5, 136.7, 133.8, 132.1, 131.6, 130.0, 129.3, 129.0, 128.7, 128.6, 127.2, 126.8, 126.5, 125.6, 125.3, 124.8, 121.2, 118.1, 116.7, 72.4, 70.0, 66.3, 64.7, 61.0, 60.4, 59.7, 57.4, 38.2, 34.6, 31.5, 31.3, 29.8, 29.6, 29.2, 28.3, 25.5, 24.9, 20.7, 15.2, 13.9; MS (ESI): *m/z* (%): 1112 (100) $[M-2TsO^{-}]^{2+}$.

UV-Vis spectroscopy and photoisomerization experiments. Absorption spectra were recorded by using a Perkin Elmer λ45 or λ650 spectrophotometer with air-equilibrated CH_2Cl_2 or DMSO solutions at RT (298 K), with concentrations in the 1×10^{-5} - 1×10^{-3} M range. Solutions were examined in 1 cm spectrofluorimetric quartz cells (wavelength experimental error: ±1 nm). Photochemical reactions were performed on stirred air-equilibrated CH_2Cl_2 solutions at RT by using a Hanau Q400 medium pressure Hg lamp (150 W). The selection of the desired irradiation wavelength (λ = 313 or 334 nm) was accomplished by the use of an appropriate interference filter.

References

[1] a) E. R. Kay, D. A. Leigh, F. Zerbetto, *Angew. Chem. Int. Ed.,* **2007**, *46*, 72-191; b) M. N. Chatterjee, E. R. Kay, D. A. Leigh, *J. Am. Chem. Soc*., **2006**, *128*, 4058-4073. c) W. R. Browne, B. L. Feringa, *Nature Nanotech*., **2006**, *1*, 25-35.

[2] N. Koumura, R. W. Zijistra, R. A. Van Delden, N. Harada, B. L. Feringa, *Nature* , **1999**, *401*, 152-155.

[3]a) W. B. Sherman, N. C. Seeman, *Nano Lett.,* **2004**, *4*, 1203-1207; b) F. C. Simmel, *ChemPhysChem*, **2009**, **10**, 2593-2597. c) J. Bath, A. J. Turberfield, *Nature Nanotech*., **2007**, *2*, 275-284; d) Special issue on DNA-based nanoarchitectures and nanomachines, *Org. Biomol. Chem*., **2006**, *4*(18), 3369-3540.

[4] M. von Delius, E. M. Geertsema, D. A. Leigh, *Nature Chem.,* **2010**, *2*, 96-101.

[5] a) P. R. Ashton, I. Baxter, M. C. T. Fyfe, F. M. Raymo, N. Spencer, J. F. Stoddart, A. J. White, D. J. Williams, *J. Am. Chem. Soc.,* **1998**, *120*, 2297-2307; b) A. Affeld, G. M. Hubner, C. Seel, C. A. Schalley, *Eur. J. Org. Chem.,* **2001**, 2877-2890.

[6] Simple molecular mechanics calculations showed that the stilbene-type unit, for both **2** and **3**, although bulkier than the hexanol chain, when present in the *E* geometry is slim enough to pass through the calixarene annulus of **1**. This suggests that in principle, during the threading phase carried out in apolar media, both axles could thread the wheel with (through) both termini, from the upper rim.

[7] a) Q. C. Wang, D. H. Qu, J. Ren, K. C. Chen, H. Tian, *Angew. Chem. Int. Ed.,* **2004**, *43*, 2661-2665; b) V. Serreli, C. –F. Lee, E. R. Kay, D. A. Leigh, *Nature,* **2007**, *445*, 523-527; c) A. Coskun, D. C. Friedman, H. Li, K. Patel, H. A. Khatib, J. F. Stoddart, *J. Am. Chem. Soc.,* **2009**, *131*, 2493-2495.

[8] a) A. Arduini, F. Calzavacca, A. Pochini, A. Secchi, *Chem. Eur. J.*, **2003**, *9*, 793-799; b) A. Arduini, F. Ciesa, M. Fragassi, A: Pochini, A. Secchi, *Angew. Chem. Int. Ed.*, **2005**, *44*, 278-281.

[9] a) A. Credi, S. Dumas, S. Silvi, M. Venturi, A. Arduini, A. Pochini, A. Secchi, *J. Org. Chem.,* **2004**, *69*, 5881-5887; b) A. Arduini, R. Bussolati, A. Credi, G. Faimani, S. Garaudee, A. Pochini, A. Secchi, M. Semeraro, S. Silvi, M. Venturi, *Chem. Eur. J,.* **2009**, *15*, 3230-3242.

[10] a) A. Arduini, R. Bussolati, A. Credi, A. Pochini, A. Secchi, S. Silvi, M. Venturi, *Tetrahedron* **2008**, *64*, 8279-8286. b) A. Arduini, A. Credi, G. Faimani, C. Massera, A. Pochini, A. Secchi, M. Semeraro, S. Silvi, F. Ugozzoli, *Chem. Eur. J,.* **2008**, *14*, 98-106.

[11] X. Cui, Z. Li, C.-Z. Tao, Y. Xu, J. Li, L. Liu, Q.-X. Guo, *Org. Lett*., **2006**, *8*, 2467-2470.

[12] A. Bouzide, G. Sauvè, *Org. Lett.,* **2002**, *4*, 2329-2332.

[13] R.-A. Binstead, *SPECFIT*, *Spectrum Software Associates*, Chapel Hill, 1996.

[14] a) This percentage of photoisomerization has been evaluated from the kinetic investigations performed on **R**[**1**⊃**4**]up and **R**[**1**⊃**5**]up in DMSO; it is also consistent with the results obtained upon photoisomerization of stilbene under comparable experimental conditions (see for example refs. 13b and 13c); b) J. Saltiel, A. Marinari, D. W.-L. Chang, J. C. Mitchener, E. D. Megarity, *J. Am. Chem. Soc.,* **1979**, *101*, 2982-2996; c) *Photochromism: Molecules and Systems*; H. Dürr, H. Bouas-Laurent Eds.; Elsevier B.V.: Amsterdam, The Netherlands, 2003.

CHAPTER 4

Metal-directed assembly of oriented calix[6]arene-based pseudorotaxanes and rotaxanes.

Chapter 4

Metal-directed assembly of oriented calix[6]arene-based pseudorotaxanes and rotaxanes.

4.1 Self-assembly driven by metal coordination

One of the frontier challenges of supramolecular chemistry as well as nanotechnology is the construction of molecular systems or aggregates of smaller components that in virtue of the structural and chemical information that have inserted and suitably organized in space are able to perform a programmed task. Among the strategies extensively exploited for the construction of extended supramolecular architectures metal coordination[1] offers a series of advantages because of its: i) high directionality of the metal-ligand interaction; ii) high binding energy, (60-200 kJ/mol) which are intermediate between the energies of organic covalent bonds (ca. 150-450 kJ/mol) and the weak intermolecular interactions (ca. 2-120 kJ/mol); iii) possibility to obtain neutral or charged complexes; iv) possibility of choice among a large variety of building blocks as ligands. Indeed the large number of coordination geometries experienced by transition metal ions allows the constructions of self-assembled 1D, 2D and 3D architectures endowed with high level of complexity.[2] This strategy represents a complementary route to the "bottom-up" approach to systems having programmable dimensions (from few $Å^3$ to over a nm^3) and functions. Starting from the early pioneering work by Lehn[3] and Sauvage[4] on the feasibility and usefulness of coordination-driven self-assembly in the formation of a large variety of supramolecular systems, the concepts and perspectives of coordination-driven self-assembly have been delineated and summarized in several insightful reviews.[5] The availability of a large variety of building blocks for metal-coordination having different specificity and stability offers unlimited possibilities to create diverse non-covalent ''supra-structures'' endowed with tunable and unique properties potentially useful for applications in various fields. Because of the particular coordination preference of any transition metal ion, the structure of metal templated systems has the potential to be predictable. Indeed a well-

defined coordination geometry is particularly important in the synthesis of structures of regular geometry, such as grids, polygons, supramolecular or coordination polymers.[6] These latter systems are an infinite array of repeating units, which consists of ligands bridging metal ions, and encompasses an extremely broad and wide range of architectures from relatively simple one dimensional chains to large mesoporous frameworks, involving metal cluster and extended organic networks.[7]

In the last decade, in view of their potential application as sensors, drug delivery or gas storage systems and semi-conductors, a large variety *'metal-organic frameworks'* (**MOFs**) has been described (Figure 4.1).[8, 9]

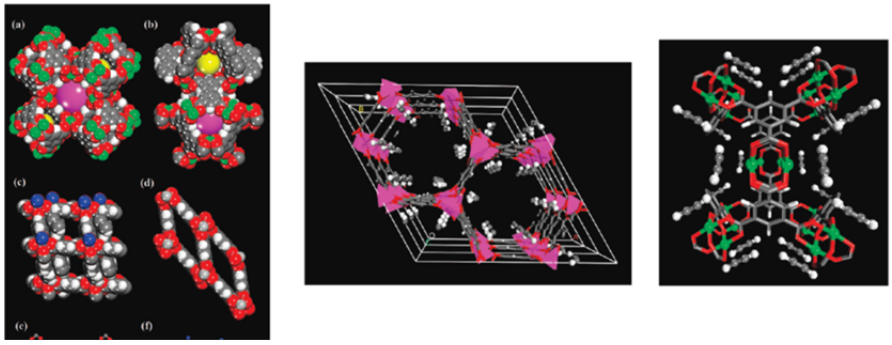

Figure 4.1: examples of metal-organic frameworks (MOFs).

More recently, in view of exploring the possibility to obtain MOFs having properties tunable through external stimuli, rotaxanes have been employed as ligands for the synthesis of 2D and 3D frameworks (Figure 4.2).[10]

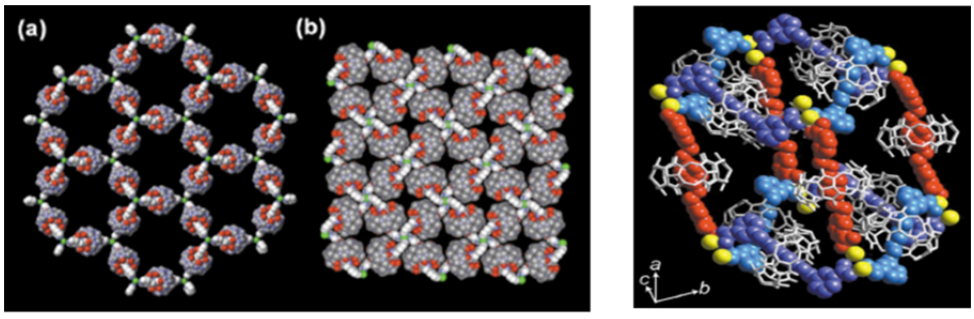

Figure 4.2: examples of metal-organic rotaxane frameworks (MORFs).

One of the more extensively employed building block for the construction of metal coordination driven self-assembled system is the 2,2':6',2''-*terpyridine* (**tpy**). It is a N_3 tridentate heterocyclic ligand that is able to form either homoleptic or heteroleptic octahedral complexes with a large variety of transition metals such as: Zn^{2+}, Co^{2+}, Cu^{2+}, Ni^{2+}, Ru^{2+} (Figure 4.3).

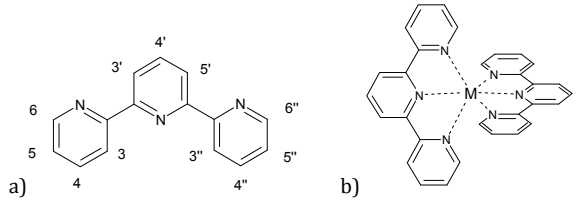

Figure 4.3: a) the 2,2':6',2'' terpyridine ligand and (b) a $[M(tpy)_2]$ complex.

In the literature a large number of functionalized **tpy** is reported.[11] The most exploited are those functionalized at the 4' position. [12]

In particular the **tpy** functionalized in this position is a versatile buildikg block in the field of supramolecular polymer (Figure 4.4).

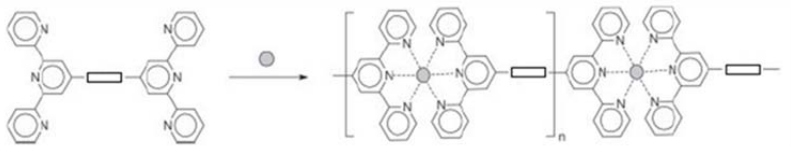

Figure 4.4: Scheme of a terpyridine based supramolecular linear polymer.

In agreement with what previously discussed, there is the possibility to build up new self-assembled systems (coordination polymer, or metal-organic rotaxane frameworks) using calix[6]arene-based rotaxane and a terpiridine bridging ligand as starting material.

With the general aim of exploring the possibility to exploit the unidirectional threading of asymmetrical axles into **1**[13] for the construction of devices and molecular machines endowed with new properties a study has been started in order to verify whether the orientation of the wheel rims towards one particular stopper in oriented pseudorotaxanes and rotaxanes could be employed as further structural element able to subtly modify their properties and/or working mode as molecular machines.

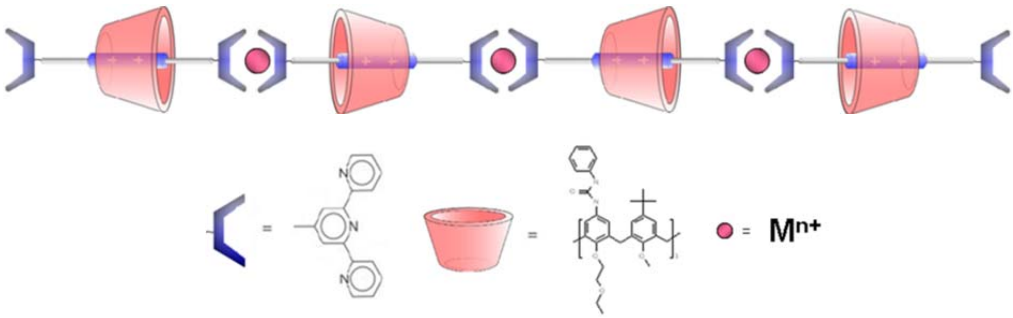

Figure 4.5: schematic representation of a calix[6]arene-based metal organic rotaxane framework.

4.2 Synthesis of the axle and complexation studies.

Axle **T(C6)** where the central 4,4'-bipyridine cationic core of the axle is functionalized with two hexyl chains, one of which bears an -OH group suitable for further functionalization at one terminus and a 2,2':6',2''-**tpy** at the other was synthesized (see Scheme 4.1). This latter unit was selected since it is bulky enough to act as stopper and because of its well-known ability to efficiently bind transition metal cations[14] that, in this axle, could drive the assembly process.

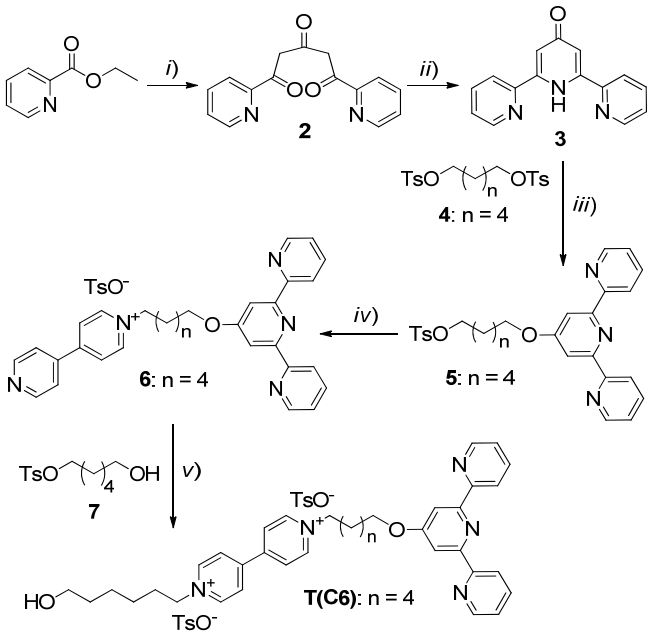

Scheme 4.1: Reagents and conditions: *i*) acetone, NaH, DME, reflux 4h; *ii*) NH_4OAc, EtOH abs., reflux 6h; *iii*) KOH, DMF, rt, 90 min; *iv*) 4,4' bipyridine, CH_3CN, reflux, 48h; *v*) CH_3CN, reflux, 10 d.

For the synthesis of **T(C6)** the sequential approach of Scheme 4.1 was followed.[15] In particular the ethyl picolinate was reacted with acetone in presence of NaH, through a Claisen condensation that yielded **2,** which was converted in the *pyridone* **3** in presence of ammonium acetate. The reaction of di-tosylate **4** with **3** gave the functionalized **tpy 5**. This latter compound was functionalized under SN_2 reaction condition with 4,4' di-pyridine in CH_3CN at reflux for 2 days. The organic salt **6** was subsequently alkylated by reaction with **7** in refluxing CH_3CN for ten days to give the axle **T(C6)** as white powder.

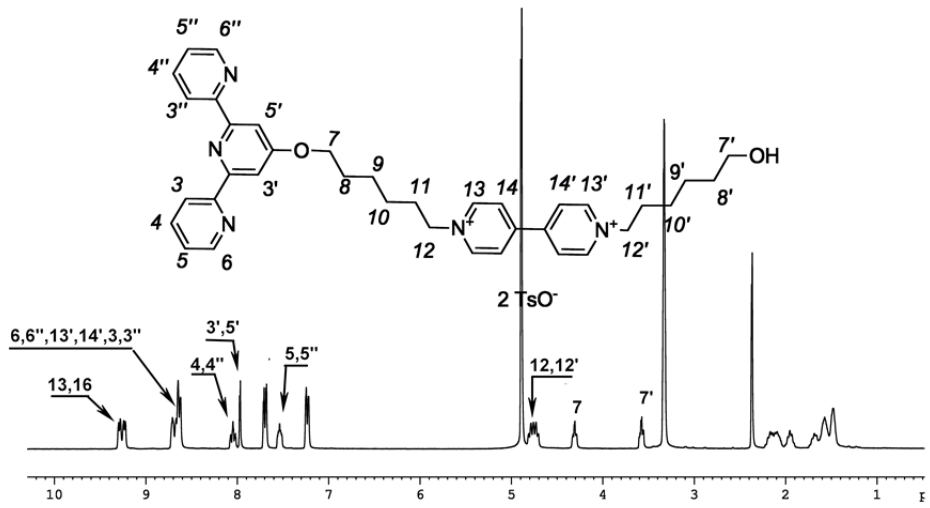

Figure 4.6: **.** ^{1}H NMR (300 MHz) of axle **T(C6)** in CD_3OD.

In the ^{1}H NMR spectrum (Figure 4.6) protons *13, 13'* experience a different chemical shift and resonate at δ = 9.30 and δ = 9.20 ppm respectively because of the asymmetry of the two arms of the axle. The methylene protons *12, 12'* for the same reason resonate as two partially overlapped triplet at δ = 4.71 and δ = 4.79 ppm respectively, while protons *7', 7* resonate as triplet at δ = 3.57 and δ = 4.30 ppm respectively. The signals of the terpyridine moiety were assigned through a 2D COSY and TOCSY spectra (Figure 4.7).

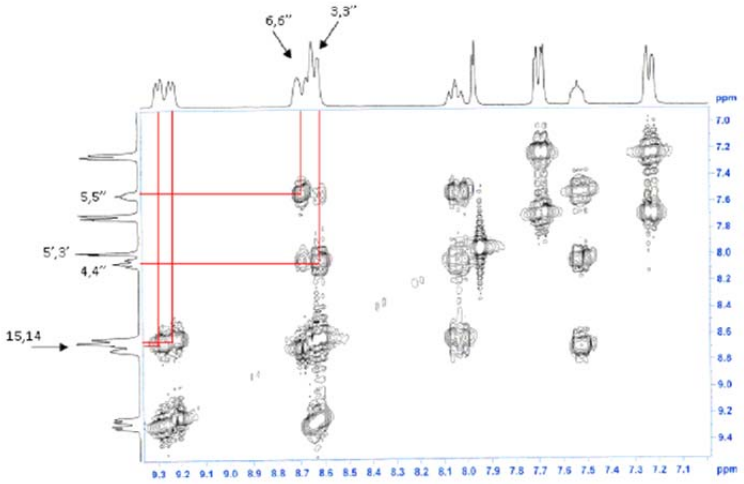

Figure 4.7: 2D ^{1}H-^{1}H COSY spectra (enlargement) of axle **T(C6)** in CD_3OD.

In order to establish whether the binding ability of the terpyridine unit in axle **T(C6)** toward metal cations was affected by the presence of the 4,4'-bipyridinium cationic core, $Zn(TsO)_2$ was used as model. This metal was specifically selected because of its well documented octahedral coordination geometry preference and its ability to form either 1:1 or 2:1 complexes with **tpy** ligands.[7e] Tosylate was choosen as counteranion for homogeneity in a view of the use of **T(C6)** as axle for pseudorotaxane synthesis.

The general procedure followed for the synthesis of the complexes consists in its direct introduction into a NMR tube of the axle and of the metal salt in the appropriate ratio, and then dissolve them with the mixture of deuterated solvents. In agreement with literature data,[16] ^{1}H NMR titration in $CDCl_3/CD_3OD$ = 6/4 showed that **T(C6)** forms either the 1:1 or the 1:2 Zn:**T(C6)** complexes, depending on the ratio between analytes used, and that these complexes are in slow exchange in the NMR timescale (Figures 4.8, 4.9).

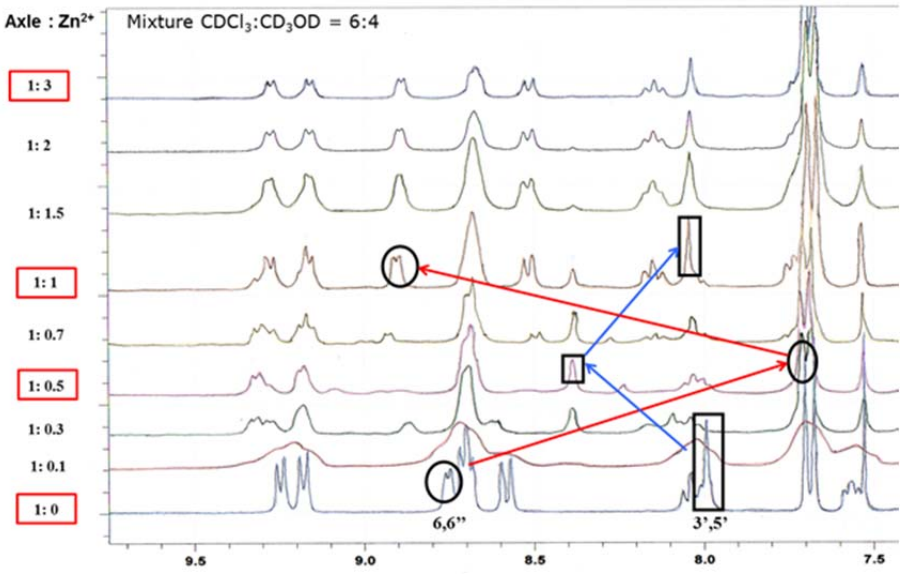

Figure 4.8: . ^{1}H NMR ($CDCl_3/CD_3OD$ = 6/4, 300 MHz, expanded region) titration of **T(C6)** with $Zn(TsO)_2$.

	6, 6'' (ppm)	5, 5'' (ppm)	4, 4'' (ppm)	3, 3'' (ppm)	3', 5' (ppm)
T(C6)	8.75	7.55	8.05	8.55	7.91
T(C6): Zn^{2+}=1:1	8.85	7.75	8.15	8.70	8.05
T(C6): Zn^{2+}=2:1	7.75	7.38	8.00	8.60	8.40

Table 4.1: chemical shift variation of **tpy** protons in the free axle **T(C6)** and in the 1:1 or 2:1 Zn^{2+} complexes.

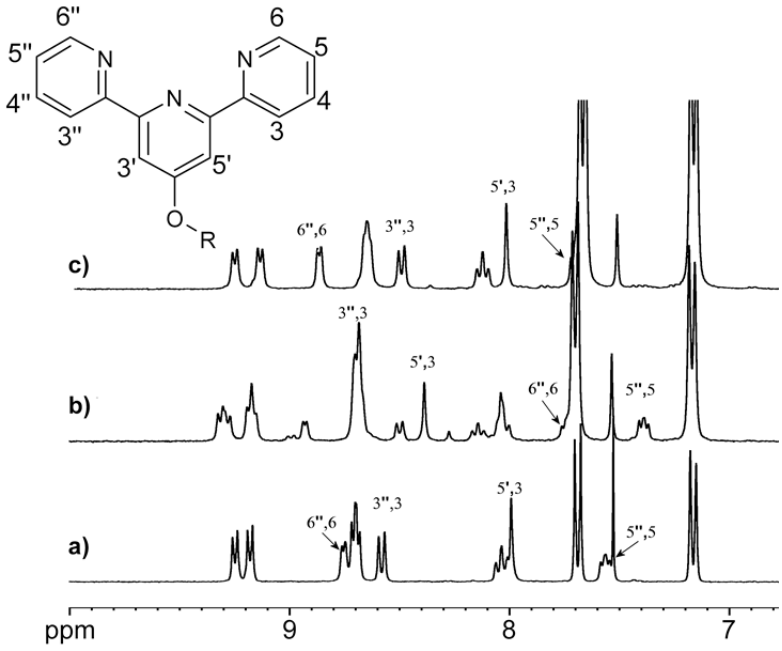

Figure 4.9: . ^1H NMR ($CDCl_3/CD_3OD$ = 6/4, 300 MHz) stack plot (expanded regions) of **T(C6)** with $Zn(TsO)_2$; a) **T(C6)**, b) **T(C6)** + 0.5 eq. $Zn(TsO)_2$, c) **T(C6)** + 2 eq. $Zn(TsO)_2$.

In the 1:1 = **T(C6)**:Zn^{2+} complex all the **tpy** protons resonate at chemical shifts very similar to those they had in the metal-free axle (Table 4.1); only a general slight down-field shift was observed ($\Delta\delta \sim +0.2$ ppm) probably due to the electron-widthdrawing effect of the Zn^{2+} coordination. On the contrary, in the 2:1 = **T(C6)**:Zn^{2+} complex some **tpy** protons experience interesting chemical shift variations. Due to the perpendicular

arrangement of the ligands and of their reciprocal shielding effect, protons *6, 6''* resonate up-field shifted at δ = 7.70 ppm (Figure 4.10). The electron-widthdrawing effect of the Zn coordination in the 2:1 = **T(C6)**:Zn^{2+} complex is evident in the chemical shift experienced by protons *3', 5'* that resonate at δ = 8.38 (Table 4.1).

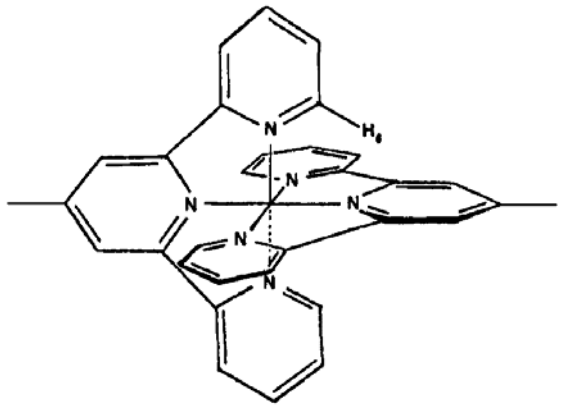

Figure 4.10: Structure of a 2:1 = Terpyridine : Metal complex.

More quantitative data on the binding ability of this ligand were obtained through UV-Vis techniques by titrating $Zn(TsO)_2$ with **T(C6)** in $CHCl_3/CH_3OH$ (6/4) (Figure 4.11). Data treatment showed the formation of firstly the 1:1 complex and then, in presence of an excess of axle, the 2:1 complex. The binding constants ($\log K_{1:1}$ = 6.7 ± 0.3, $\log\beta$ = 12.3 ± 0.3 respectively) were calculated with the Specfit/32 software, selecting different binding models[17] and sampling the spectral data collected in the 290–350 nm wavelength range. The complexation process influences the absorption band. In fact, by adding the axle to the zinc salt solution, two new bands centered at 310 and 322 nm appear. These changes can be assigned to the complexation of the terpyridine unit that fixes the three pyridine units in an all-cis conformation. All the absorptions take place at λ < 350 nm, because the Zn^{2+} has a d^{10} electronic configuration and the close shell does not allow the metal to ligand charge transfer band (MLCT) that characterizes other **tpy** complex.

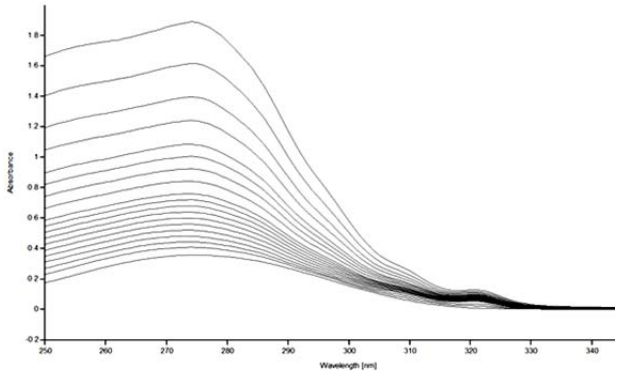

Figure 4.11: UV-Vis titration of $Zn(TsO)_2$ (1 x 10^{-5} M in 0.8 ml CH_3Cl/CH_3OH = 6/4) with **T(C6)** (2 x 10^{-4} M in CH_3Cl/CH_3OH = 6/4) upon addition of 0, 10, 15, 20, 25, 30, 35, 40, 45, 50, 60, 70, 80, 90, 110, 130, 160, 200 µl ($\log K_{1:1}$= 6.7 ± 0.3, $\log\beta$ = 12.3 ± 0.3).

The titration experiments were performed also by reversing the addition order of one species to the other in order to exclude that the binding constant of **T(C6)** toward Zn^{2+} could originate from kinetic reasons. As expected, the addition of **T(C6)** to $Zn(TsO)_2$ solution showed the formation of both the 2:1 and the 1:1 complexes, as previously observed. These data confirmed that the 4, 4' bipyridinium unit does not affect the binding properties of the **tpy** toward the Zn^{2+} cation (Figure 4.12).

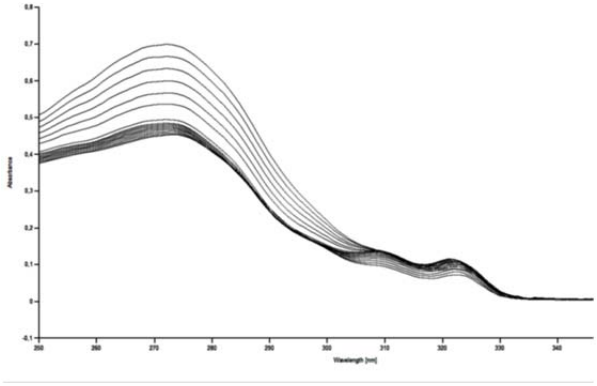

Figure 4.12: UV-Vis titration of **T(C6)** (1 x 10^{-5} M in 0.8 ml CH_3Cl/CH_3OH = 6/4) with $Zn(TsO)_2$ (2 x 10^{-4} M in CH_3Cl/CH_3OH = 6/4) upon addition of 3, 6, 9, 12, 15, 20, 25, 30, 35, 40, 45, 50, 60, 70, 90, 110, 140, 180 µl ($\log K_{1:1}$= 4.8 ± 0.2; $\log\beta$ = 9.7 ± 0.2).

These studies on the model compound allow: *i*) to confirm that the binding ability of the **tpy** moiety in axle **T(C6)** are not affected by the central 4, 4' bipyridinium unit; *ii*) the possibility to monitor the formation of either the 1:1 and the 2:1 Zn^{2+} complexes.

4.3 Syntheses of the pseudorotaxane and rotaxane: NMR and UV-Vis studies

Since the polarity of the solvent plays a crucial role in the strict orientational control of the axle threading into wheel **1**, pseudorotaxane formation was carried out in C_6D_6 instead of the more polar CH_3Cl/CH_3OH solvent mixture.

A slight excess of solid axle **T(C6)** was added to a C_6D_6 solution of **1**. After mixing, the resulting deep red suspension was filtered to remove the excess of un-dissolved salt and submitted to NMR analyses.

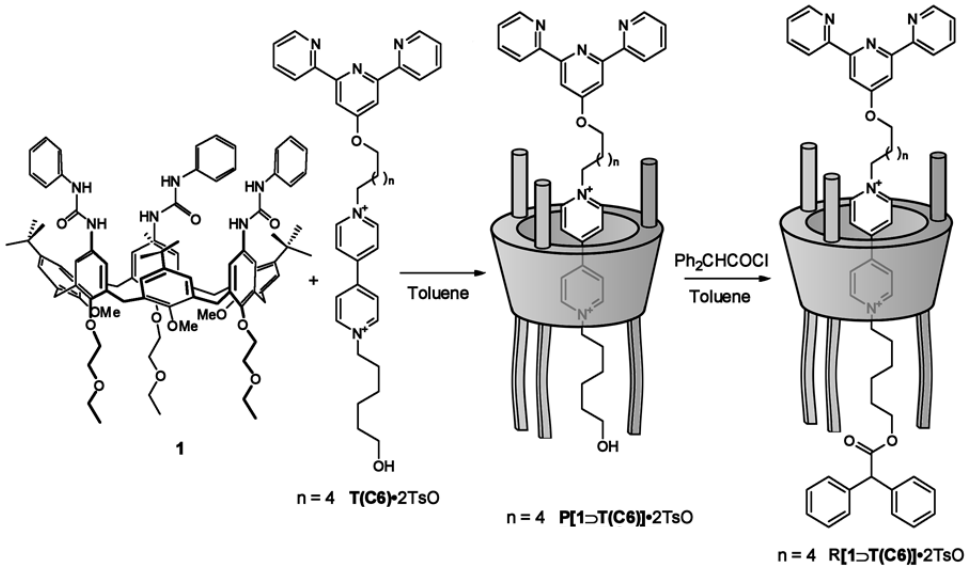

Figure 4.13: Synthesis of oriented pseudorotaxanes **P[1⊃T(C6)],** and rotaxane **R[1⊃T(C6)]**.

The presence of only one set of signals in the ^{1}H NMR spectrum, for **P[1⊃T(C6)]**, showed that only one pseudorotaxane isomer had formed. Structure elucidation of the pseudorotaxane was carried out through NMR techniques (COSY, TOCSY, ROESY, HSQC, HMBC).

In the ^{1}H NMR spectrum (Figure 4.14) signals of the methylene protons of the wheel resonate as two doublets at δ = 4.66 and δ = 3.50 ppm with a geminal coupling constant of 14.7 Hz. The fact that the cationic portion of the axle is confined within the shielding zone of the calix[6]arene cavity is evidenced by the chemical shift of protons *13, 13', 14, 14'* that resonate respectively at δ = 8.05, δ =6.90, δ = 7.99 and δ = 6.85 ppm. Protons *6,6''*, *3',5'* and *3,3''* of the **tpy** unit resonates at δ = 8.93, δ = 8.73 and δ = 8.69 ppm respectively.

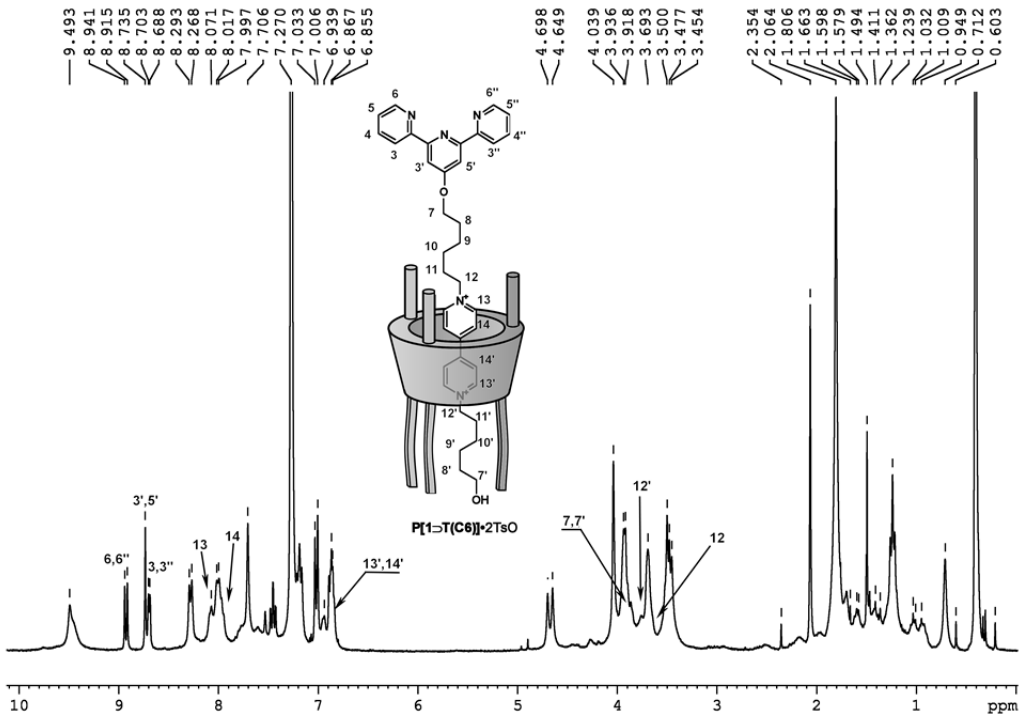

Figure 4.14: ^{1}H NMR (300 MHz) of **P[1⊃T(C6)]** in C_6D_6.

2D TOCSY experiment (Figure 4.15) evidenced the presence of only one set of signals for the two alkyl chains linked to the 4,4′-bipyridinium core in the pseudorotaxane and one of them experience an up-field shift probably due to the shielding effect of the phenylureido moieties present at the upper rim of the wheel. The orientation of the axle within the wheel was established through ROESY experiments; the spatial correlations between the protons of OCH_3 present at the lower rim of the calix[6]arene and protons *8', 9', 10', 11'* of the axle, together with those between protons *11, 10* and *9* and the aromatic protons of phenyureido groups of the wheel, confirm as expected that the axle had threaded the

wheel from the upper rim and that in the pseudorotaxane the **tpy** group is positioned in the proximity of the ureido groups (Figure 4.16).

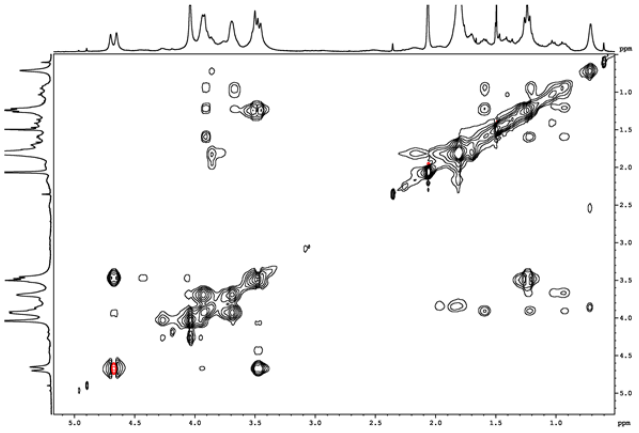

Figure 4.15: ^{1}H-^{1}H 2D TOCSY (300 MHz) of **P[1⊃T(C6)]** in C_6D_6 (mixing time = 0.06 sec).

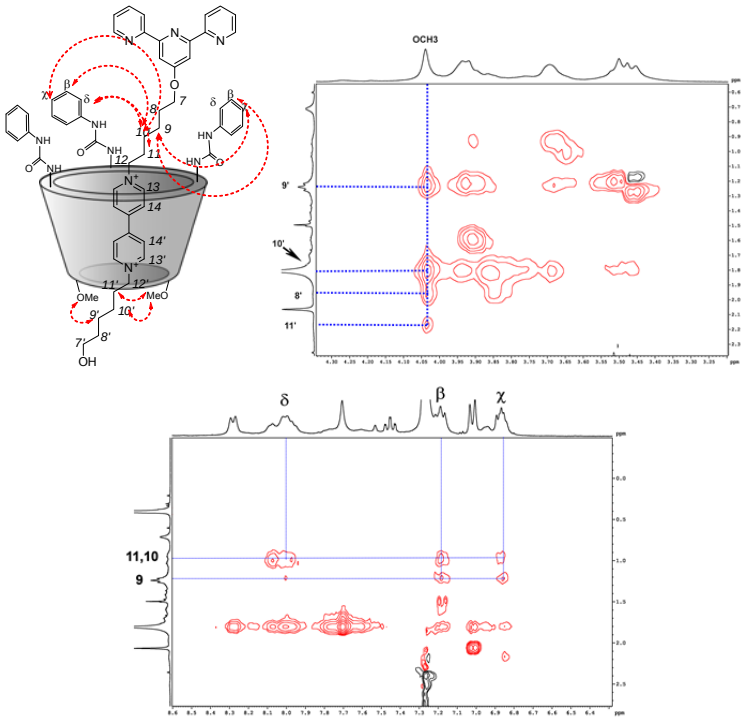

Figure 4.16: ^{1}H-^{1}H 2D ROESY (300 MHz) (enlargements) of **P[1⊃T(C6)]** in C_6D_6 (spinlock = 200ms).

C_6D_6 was used as solvent also to evaluate through NMR experiments the binding features of the **tpy** unit in **P[1⊃T(C6)]** toward Zn^{2+}, since in the $CDCl_3/CD_3OD$ (6/4) mixture **P[1⊃T(C6)]** could not be employed because of extensive dethreading of the axle from the wheel. The spectrum obtained upon addition of an excess of solid $Zn(TsO)_2$ to **P[1⊃T(C6)]** showed the extensive broadening of several signals that hampered the complete assignement of all protons of the pseudorotaxane (Figure 4.17).

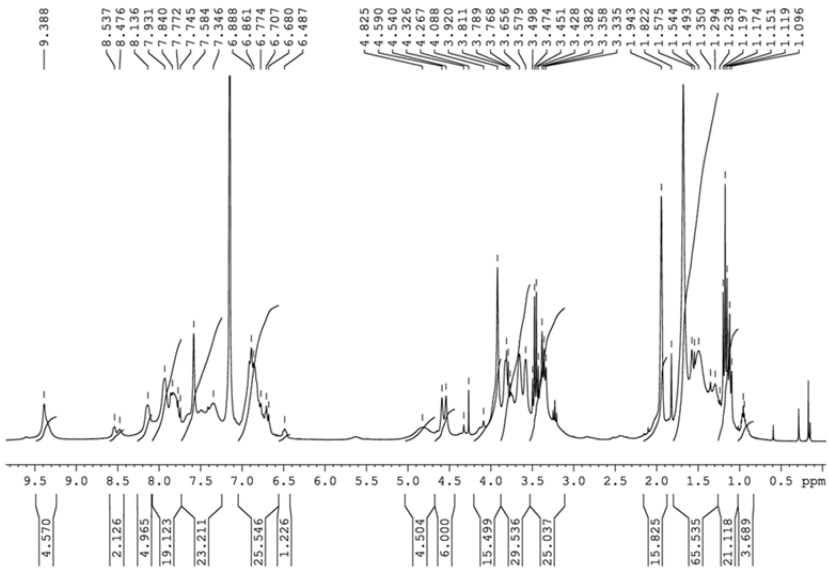

Figure 4.17: ^1H NMR (300 MHz) of **P[1⊃T(C6)]** in presence of a molar excess of $Zn(TsO)_2$ in C_6D_6.

Nevertheless the lack of **tpy** signals in the spectral region between 8.50 and 9.00 ppm, charachterstic for the **P[1⊃T(C6)]**, strongly suggests that these signals resonate to higher fields, overlapped with other aromatic protons. This suggests that the species that had formed was compatible with a unique 2:1 adduct where the two **tpy** units assume an orthogonal orientation around the Zn^{2+} ion.[16c] To further support this hypothesis, NMR-DOSY experiments were carried out to compare the diffusion coefficient of the pseudorotaxane before and after the addiction of the Zn^{2+} salt. For the metal-free **P[1⊃T(C6)]** a value of the diffusion coefficient $D = 2.68 \pm 0.02 \times 10^{-10}$ m^2 s^{-1} was obtained. After addiction of excess of $Zn(TsO)_2$ this value decreases to $D = 2.09 \pm 0.05 \times 10^{-10}$ m^2 s^{-1}. This variation of about the 25% of the initial value is in good agreement with the formation of a dimeric metal-driven assembled system **2P[1⊃T(C6)]:1Zn**.[18]

Then **R[1⊃T(C6)]** was synthesized so as to get more insight into the binding properties of the **tpy** unit in the wheel-**T(C6)** dyad, and to compare them with those already gained for the native **T(C6)**. In fact, **P[1⊃T(C6)]** could not be used because of the extensive dethreading of the axle in the polar $CH_3OH/CHCl_3$ solvents mixture. Rotaxane **R[1⊃T(C6)]** was synthetized (Figure 4.13) reacting the hydroxyl end of the pseudorotaxane **P[1⊃T(C6)]** with diphenylacetyl chloride. This new compound was completely characterized and 1D and 2D NMR experiments confirmed its structure.

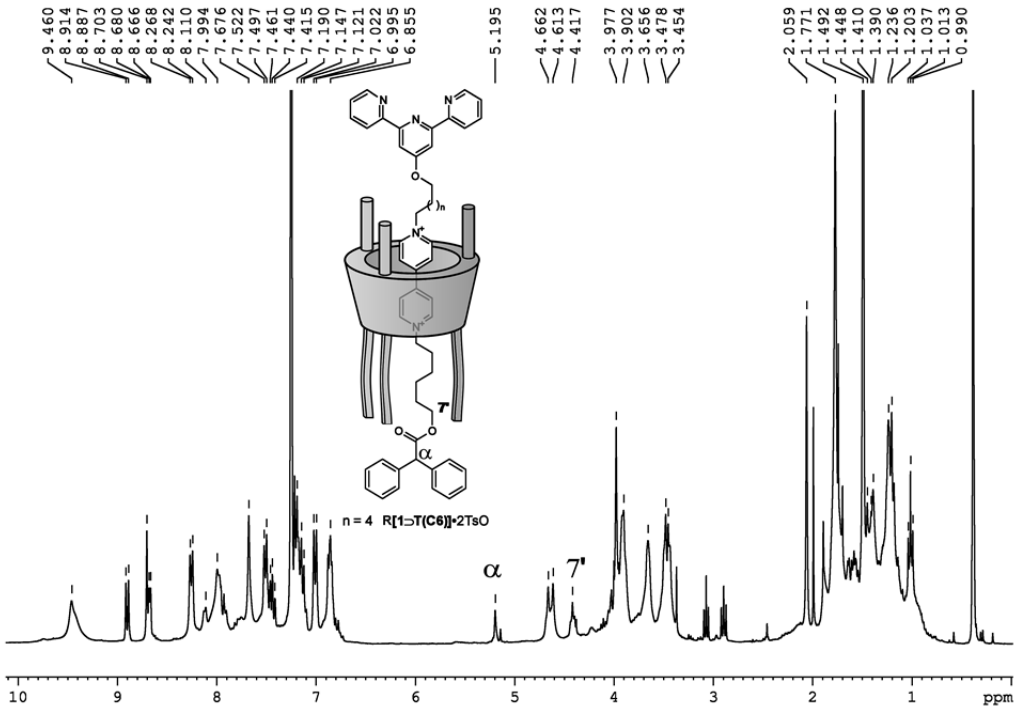

Figure 4.18: ^{1}H NMR (300 MHz) of **R[1⊃T(C6)]** in C_6D_6.

The diagnostic signals of the ^{1}H NMR spectrum are the methyne proton of the diphenylacetyl stopper that resonate at δ = 5.19 ppm and that of protons *7'* that resonate at δ = 4.42 ppm as a triplet (Figure 4.18).

ROESY experiments (Figure 4.19) showed correlations between protons *11, 10, 9* of the axle and the aromatic protons *δ, β, χ* of phenylureido groups of the wheel, thus confirming

that the **tpy** group is still positioned in the proximity of the upper rim of the calix[6]arene, while the diphenylacetil stopper is at the lower rim.

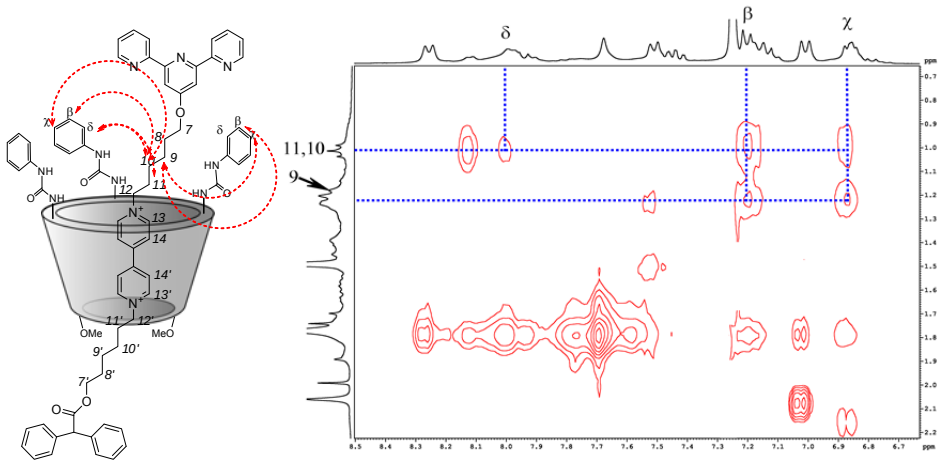

Figure 4.19: ^{1}H-^{1}H 2D ROESY (300 MHz) (enlargement) of **R[1⊃T(C6)]** in C_6D_6 (spinlock = 200ms).

R[1⊃T(C6)] was thus employed as ligand for $Zn(TsO)_2$, and its binding ability was investigated through UV-Vis titrations. Adding an increasing amounts of a **R[1⊃T(C6)]** CH_3Cl/CH_3OH = 6/4 solution to a CH_3Cl/CH_3OH = 6/4 solution of $Zn(TsO)_2$, it emerged that only one complex had formed, with a logβ = 10.7 ± 0.3, consistent with a stoichiometry **R[1⊃T(C6)] : Zn^{2+}** = 2:1 (Figure 4.19).

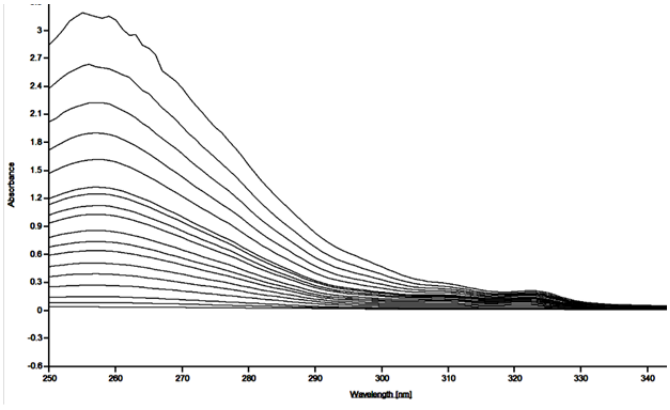

Figure 4.19: UV-Vis titration of $Zn(TsO)_2$ (1 x 10^{-5} M in 0.8 ml CH_3Cl/CH_3OH = 6/4) with **R[1⊃T(C6)]** (1 x 10^{-4} M in CH_3Cl/CH_3OH = 6/4) upon addition of 0, 10, 20, 30, 40, 50, 60, 70, 80, 90, 110, 120, 150, 180, 220, 270, 350 µl (log$K_{1:2}$= 10.7 ± 0.3).

This stoichiometry does not change even in the presence of a large excess of Zn^{2+} or by reversing the addition order of one species to the other (Figure 4.20).

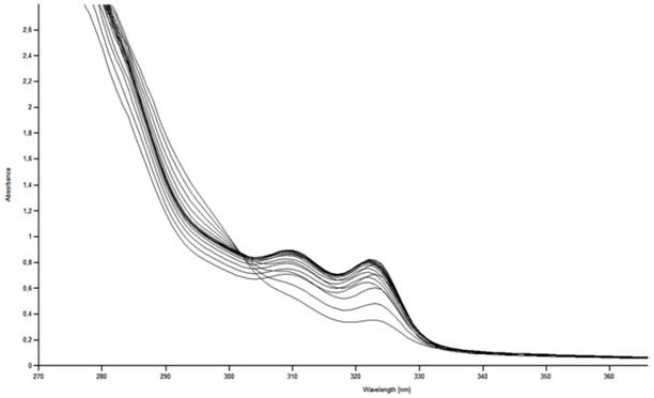

Figure 4.20: UV-Vis titration of **R[1⊃T(C6)]** (1 x 10^{-5} M in 0.8 ml CH_3Cl/CH_3OH = 6/4) with $Zn(TsO)_2$ (2 x 10^{-4} M in CH_3Cl/CH_3OH = 6/4) upon addition of 3, 6, 9, 12, 15, 18, 21, 24, 27, 30, 35, 40, 45, 50, 70, 110, 160, 240 µl ($\log K_{1:2}$= 10.7 ± 0.4).

The fact that either the pseudorotaxane and the rotaxane do form only the 2:1 complex could tentatively ascribed to the interaction between the tosylates anions of the metal salt and the three ureido groups present on the calix[6]arene. In fact in the 2:1 complexes (**2R[1⊃T(C6)]:1Zn** or **2P[1⊃T(C6)]:1Zn)** there is a perfect match between the number of tosylate anions (four from the axles and two from the metal center) and the number of the ureido binding sites (three on each wheel).

In order to evaluate the role played by the tosylates and to further confirm this hypothesis, **R[1⊃T(C6)]** was titrated with the Zn^{2+} salt having the less coordinating BF_4^- as counteranions. As expected, in this case both the **1R[1⊃T(C6)]:1Zn** and the **2R[1⊃T(C6)]:1Zn** complexes form ($\log K_{1:1}$ = 7.3 ± 03, $\log\beta$ = 12.7 ± 0.3, respectively) confirming that anion binding pivots the formation of only the 2:1 complex (Figure 4.21).[19]

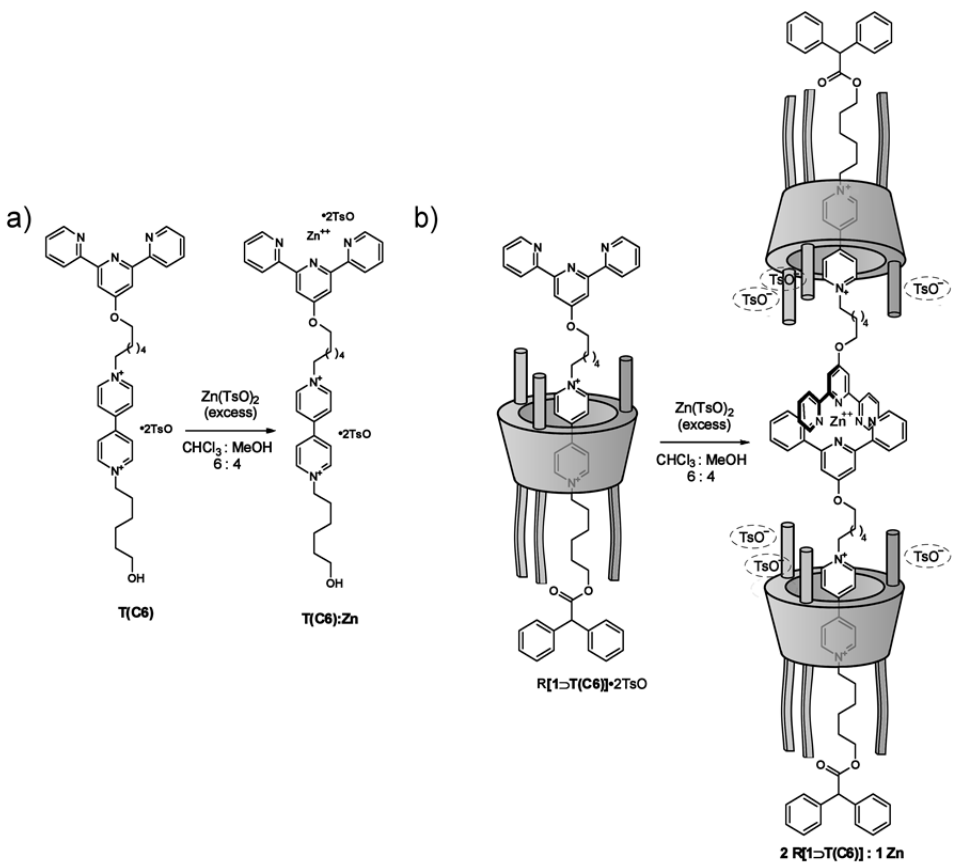

Figure 4.21: Different behaviour of a) axle **T(C6)** and b) **P[1⊃T(C6)]** in the presence of an excess of $Zn(TsO)_2$.

4.4 Electrochemical experiments

A consequent question that emerged was whether the complexation of the Zn^{2+} ion at the terpyridine unit could affect the ability of the whole systems **R[1⊃T(C6)]** or **P[1⊃T(C6)]** to work as molecular machines. To address this issue, the electroactivity of the bipyridinium group in the different systems was examined by cyclic voltammetry (CV). Experiments were carried out in CH_2Cl_2 containing TBAP as supporting electrolyte, before and upon progressive addition of Zn^{2+} (0.5 to 3 molar eq.) to the solution. As expected, all the metal-free systems **T(C6)**, **P[1⊃T(C6)]** and **R[1⊃T(C6)]** showed the same electrochemical behaviour as observed for similar, previously reported, systems (Figure 4.22).[20]

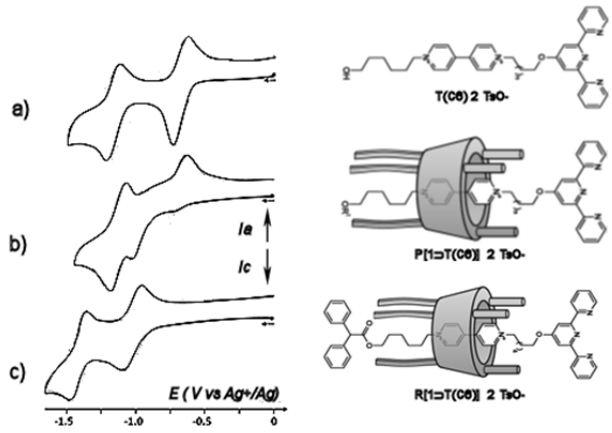

Figure 4.22: Cyclic voltammogramms of a) **T(C6)**, b) **P[1⊃T(C6)]** and c) **R[1⊃T(C6)]** in CH_2Cl_2 + 0.5 M TBAP.[14] Scan rate: 100 mV/s

Namely the free axle **T(C6)** and the rotaxane **R[1⊃T(C6)]** were both characterized by two monoelectronic reversible reduction waves at $E_{1/2}'$ = –0.68 V vs Ag^+/Ag and $E_{1/2}''$ = –1.17 V for the free axle (the symmetric shape of the first reduction wave is ascribed to some adsorption phenomena of the axle onto the electrode material) and $E_{1/2}'$ = –1.02 V and $E_{1/2}''$ = –1.42 V for the rotaxane. As expected, when included in the cavity of the wheel, it is more difficult to reduce the axle and large negative shifts (~ –400 mV) for the reduction waves were thus logically observed. For the same reason, in the case of the pseudorotaxane **P[1⊃T(C6)]**, the first reduction wave was observed at a lower potential

(E_{pc}' = –1.02 V). However, in this latter system the 1e⁻ reduction of the bipyridine unit destabilizes the axle-wheel complex which results in the fast dethreading of the axle from **1**. For this reason, this first reduction wave is irreversible and both the second system ($E_{1/2}'$ = –1.13 V) and first oxidation peak ($E_{pa'}$ = –0.62V) observed during the reverse scan, are close to those observed for the free axle **T(C6)**.

Subsequently the electrochemical behaviour of these species upon addition of increasing amounts of Zn^{2+} (0.5 to 3 molar eq. as TsO^- salt) to a CH_2Cl_2 solution (10^{-4} M) of **T(C6)**, **P[1⊃T(C6)]** and **R[1⊃T(C6)]** was investigated. When the metal ion was added to the solution of axle **T(C6)** no significant modification of the CV curve was observed, indicating that the complexation of the metal ion has no influence on the redox behaviour of the viologen unit. Moreover the reduction potentials of the violgen are not affected by the complexation stoichiometry of the terpiridine unit.

On the contrary, in the case of the **P[1⊃T(C6)]** system, the presence of Zn^{2+} induced a negative decay of the first reduction wave (–20 to –30 mV) already after the first addition of metal salt. Therefore it seems that when Zn^{2+} is bound to the terpyridine unit the dethreading process of the axle is more difficult to realize and it requires more energy. This result, together with the UV-Vis. data suggests that the bipyridinium core communicates through the calixarene component with the terpy-Zn domain.

Quite unexpectedly, in the case of rotaxane **2R[1⊃T(C6)]:1Zn**, after addition of $Zn(TsO)_2$, a positive shift (up to +50 mV) of the two reversible waves was observed. Again, the redox potential of the bipyridinium unit is affected, although in the opposite direction, by the presence of the metal ion bound at the terpyridine unit. This behaviour could be tentatively explained invoking a possible steric effect exerted by the diphenylacetyl stopper, positioned at the lower rim of the calix[6]arene, that, with its presence, imposes a closer proximity of the wheel upper rim to the terpyridine-Zn^{2+} stopper. A π-π stacking interactions between the electron-rich aromatic rings of the phenylureido groups and the electron-poor terpiridine moiety could stabilize the calix[6]arene in this position. In contrast with the **2P[1⊃T(C6)]:1Zn**, where the Brownian motion of the wheel could take place along both arms of the axle, the conformational situation in **2R[1⊃T(C6)]:1Zn** could result in the protrusion of the bipyridine unit from the lower rim of the calix that could thus be more easily reduced (Figure 4.23).[21]

The electrochemical experiments were carried out in the presence a large amount (10^{-2} M) of TetraButylAmmonium Perchlorate (TBAP) used as supporting electrolyte, which minimizes the role of the TsO^- anion in the binding process and no significant changes in the voltammogramms could be observed when $Zn(TsO)_2$ was replaced by the corresponding BF_4^- salt.

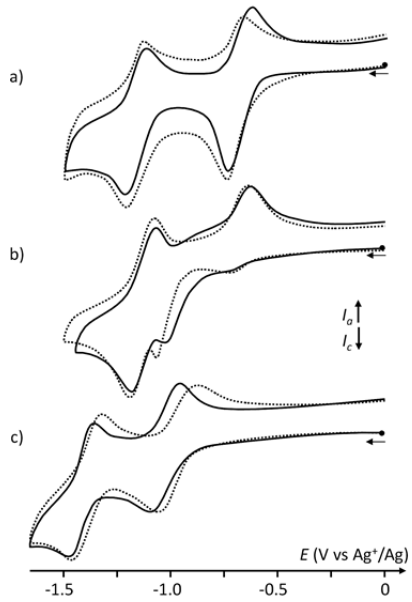

Figure 4.23: Cyclic voltammogramms of a) **T(C6)**, b) **P[1⊃T(C6)]** and c) **R[1⊃T(C6)]** in CH_2Cl_2 + 0.5 M TBAP. Scan rate: 100 mV/s. Full line: no Zn^{2+}, dashed line: 1 eq. of Zn^{2+} added.

In order to verify whether these reduction potential variations of the axle were the consequence of the proximity of the upper rim of the wheel with the terpyridine unit, the axle **T(C12)**, where the span between the terpy unit and the 4,4'-bipy is 12 carbon atoms, was synthesized following the same synthetic scheme 4.2.

The ^1H NMR spectrum of axle **T(C12)** recorded in CD_3OD is almost identical to those obtained for the axle **T(C6)** in the same solvent. The only difference is in the aliphatic part of the spectra where the intense broadened signal, resonating at δ = 1.3 ppm assigned to the central alkyl protons of the twelve carbon atoms chain, is visible.

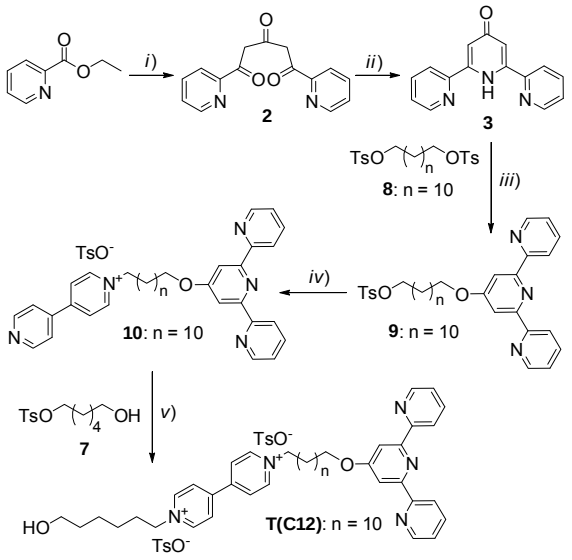

Scheme 4.2: Reagents and conditions: *i*) acetone, NaH, DME, reflux 4h; *ii*) NH_4OAc, EtOH abs., reflux 6h; *iii*) KOH, DMF, rt, 90 min; *iv*) 4,4' bipyridine, CH_3CN, reflux, 48h; *v*) CH_3CN, reflux, 10 d.

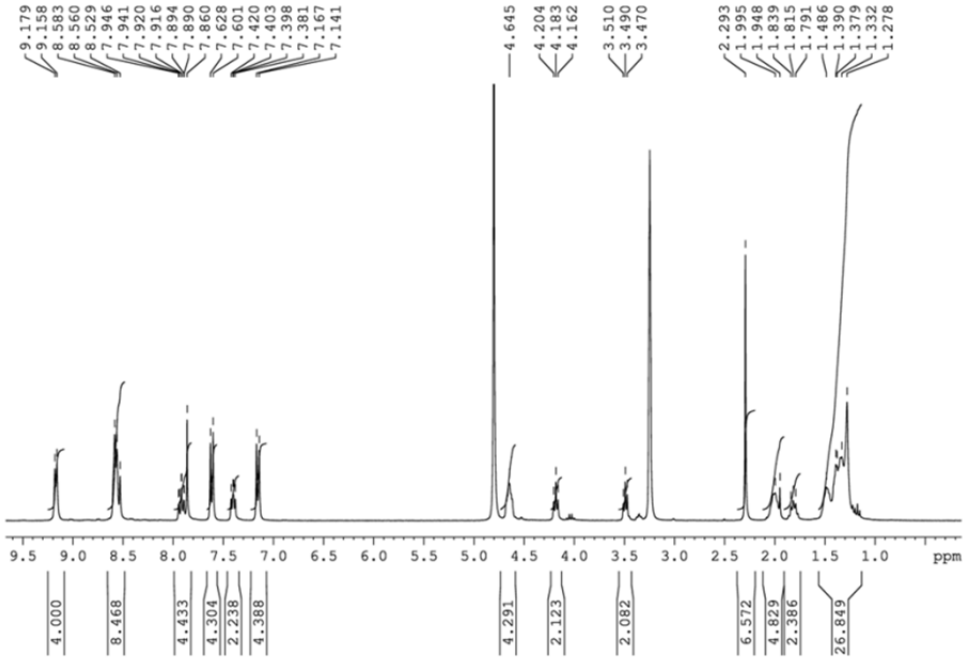

Figure 4.24: ^1H NMR (400 MHz) of axle **T(C12)** in CD_3OD.

A slight excess of solid axle **T(C12)** was then added to a C_6D_6 solution of **1**; after mixing, the resulting deep red suspension was filtered to remove the excess of un-dissolved salt and submitted to NMR analyses. As expected, the spectral (Figure 4.25, 4.26) data showed that the oriented pseudorotaxane **P[1⊃T(C12)]** that bears the terpiridine stopper at the upper rim of the wheel had formed.

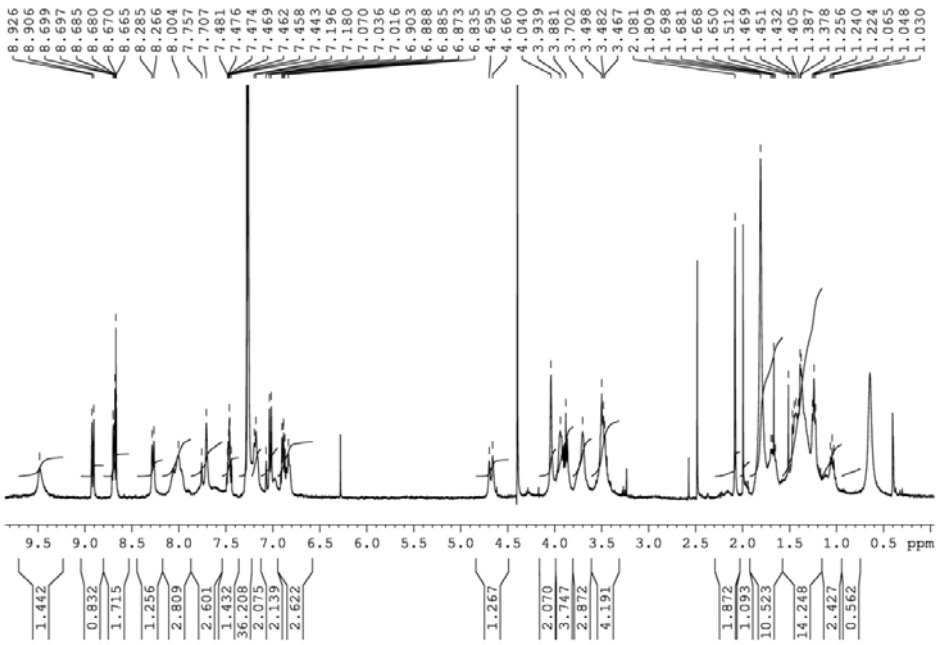

Figure 4.25. ^{1}H NMR (300 MHz) of **P[1⊃T(C12)]** in C_6D_6.

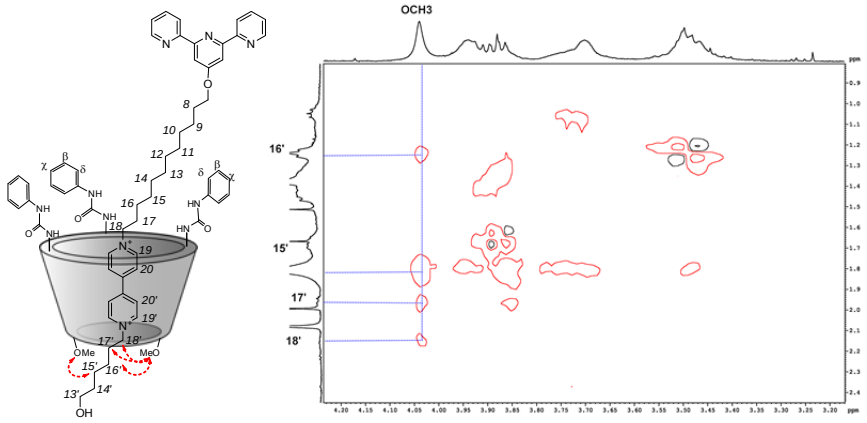

Figure 4.26: ^{1}H-^{1}H 2D ROESY (300 MHz) (enlargement) of **P[1⊃T(C12)]** in C_6D_6.

The CV behaviour of **P[1⊃T(C12)]** was similar to that observed for **P[1⊃T(C6)]**, the first reduction wave was observed at a lower potential (E_{pc}' = –0.99 V) and both the second system ($E_{1/2}'$ = –1.08 V) and first oxidation peak ($E_{pa'}$ = –0.59V) observed during the reverse scan were close to those observed for the free axle **T(C6)** as results of the dethreading of the axle from the wheel.

However, no significant changes in the CV curve were highlighted for **P[1⊃T(C12)]** upon addition of Zn^{2+} ions. This result clearly indicates that, in this system, the distance between the terpyridine-Zn unit and the upper rim of the wheel is too high and does not allow any "communication" among components.

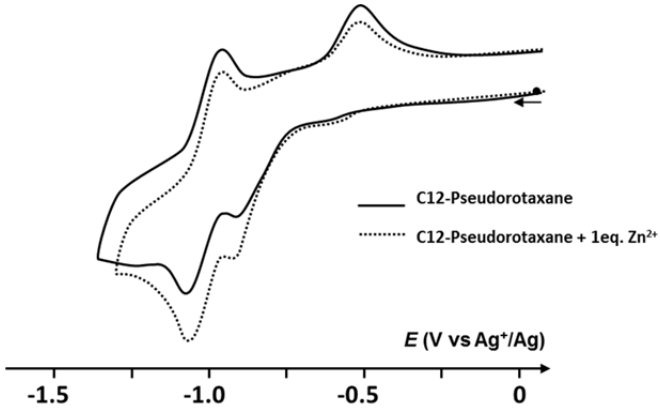

Figure 4.27: Cyclic voltammogramms of **P[1⊃T(C12)]** in CH_2Cl_2 + 0.1 M TBAP. Scan rate: 100 mV/s. Full line: no Zn^{2+}, dashed line: 1 eq. of Zn^{2+} added.

In Table 4.1 all the potential for **T(C6)**, **P[1⊃T(C6)]**, **R[1⊃T(C6)]** and **P[1⊃T(C12)]**, in presence of 0, 0.5, 1, 2, 3 equivalents of Zn^{2+} are reported.

Eq.	**T(C6)**	**P[1⊃T(C6)]**	**R[1⊃T(C6)]**	**P[1⊃T(C12)]**
0	$E_{1/2}'$ = -0.68 $E_{1/2}''$ = -1.17	E_{pc}' = -1.02 E_{pa}' = -0.62 $E_{1/2}''$ =-1.13	$E_{1/2}'$ = -1.02 $E_{1/2}''$ = -1.42	E_{pc}' = -0.99 E_{pa}' = -0.59 $E_{1/2}''$ = -1.08
1	$E_{1/2}'$ = -0.69 $E_{1/2}''$ = -1.17	E_{pc}'= -1.05 E_{pa}'= -0.62 $E_{1/2}''$ = -1.13	$E_{1/2}'$ = -0.97 $E_{1/2}''$ = -1.40	E_{pc}' = -0.99 E_{pa}' = -0.59 $E_{1/2}''$ = -1.08
2	$E_{1/2}'$ =--0.69 $E_{1/2}''$ = -1.16	E_{pc}'= -1.06 E_{pa}'= -0.62 $E_{1/2}''$ = -1.14	$E_{1/2}'$ = -0.98 $E_{1/2}''$ = -1.40	E_{pc}' = -1.00 E_{pa}' = -0.59 $E_{1/2}''$ = -1.08
3	$E_{1/2}'$ = -0.72 $E_{1/2}''$ = -1.17	E_{pc}'= -1.07 E_{pa}'= -0.62 $E_{1/2}''$ = -1.16	$E_{1/2}'$ = -0.97 $E_{1/2}''$ = -1.40	E_{pc}' = -0.99 E_{pa}' = -0.59 $E_{1/2}''$ = -1.08

Table 1. Electrochemical data (V) of **T(C6)**, **P[1⊃T(C6)]**, **R[1⊃T(C6)]**, **P[1⊃T(C12)]** in presence of 0, 1, 2 and 3 molar equivalent of $Zn(TsO)_2$; Scan rate: 100 mV/s, E' and E'' correspond to the first and second electron-transfers of the viologen unit, respectively.

4.5 Conclusions

The data reported confirm the possibility to assemble through metal coordination, oriented calix[6]arene-based pseudorotaxane and rotaxane systems. Moreover the experiments suggest that the presence of the wheel, in rotaxane **R[1⊃T(C6)]**, affects the complexation behaviour of the terpyridine unit, allowing only the 2:1 stoichiometry with Zn^{2+}. This fact could be ascribed to the interactions between the TsO^- anions of the metal and the ureido groups present at the upper rim of the wheel that stabilize the 2:1 complex. In addiction the Zn^{2+} complexation by the terpyridine unit in the pseudorotaxane **P[1⊃T(C6)]** and rotaxane **R[1⊃T(C6)]** systems seems to have effects on the electrochemical behaviour of the viologen unit. In particular the metal coordination causes a negative shift of *ca.* -30 mV of the first reduction wave in the pseudorotaxane, whereas in the case of the rotaxane it causes a positive shift of both the first and second reduction potential of +40 mV. The anionic complexation cannot explain these data because the CV experiments were carried out in presence of a large excess of TBAP as supporting electrolyte that makes the presence of the TsO^- anions of the metal insignificant. So it is only the presence of the Zn ion on the terpiridine ligand that causes these shift, and it is the proximity of this ligand to the calixarene macrocycle that permits this effect. In fact using the pseudorotaxane **P[1⊃T(C12)]** where there is an increased distance between the terpyridine moiety and the upper rim of the wheel, the metal coordination has no effects on the electrochemical behaviour of the viologen unit.

These data suggest that the metal coordination, the distance between binding sites and their orientation induce a reciprocal exchange of chemical information among the different domains in both **P[1⊃T(C6)]** and **R[1⊃T(C6)]**.

Experimental Section

General. Toluene and DMF were dried using standard procedure, all other reagents were of reagent grade quality obtained from commercial suppliers and were used without further purification. ^{1}H and ^{13}C NMR spectra were recorded at 300 or 400 and 75 or 100 MHz, respectively. M.p. are uncorrected. Chemical shifts are expressed in ppm (δ) using the residual solvent signals as an internal reference. MS and HRMS analyses were determined in the ESI mode with a Micromass ZMD and a LTQ ORBITRAP XL Thermo, respectively. Compounds **2**,[15] **3**,[15] **4**,[22] **7**[13b, 13e] and **8**[23] were synthesised according to literature procedures.

UV Titrations. Spectroscopic measurements were carried out using a Perkin-Helmer Lambda Bio 20 spectrophotometer. Small aliquots of a solution (c = 2 × 10^{-4} M in CH_3Cl/CH_3OH = 6/4) of the titrant (**T(C6)** or **R[1⊃T(C6)]**) were added to a solution (c = 1 × 10^{-5} M in CH_3Cl/CH_3OH = 6/4) of the Zn^{2+} salt contained in a quartz cuvette (path length = 1 cm) and maintained at 300 K through an external thermostat. The titrations were also done in the opposite way adding small aliquots of a solution (c = 2 × 10^{-4} M in CH_3Cl/CH_3OH = 6/4) of the titrant Zn^{2+} to a solution (c = 1 × 10^{-5} M in CH_3Cl/CH_3OH = 6/4) of the (**T(C6)** or **R[1⊃T(C6)]**) contained in a quartz cuvette (path length = 1 cm) and maintained at 300 K through an external thermostat The binding constants were calculated with the Specfit/32 software selecting different binding models[17] and sampling the spectral data collected in the 290–350 nm wavelength range.

NMR diffusion experiments. DOSY experiments were carried out in C_6D_6 at 300 K using a stimulated echo sequence with bipolar gradients.[24] The diffusion coefficient *D* of the species diffusing in solution was determined by monitoring the intensity decay of at least six resonances present in the NMR spectrum of the specie as a function of gradient strength applied to the sample. The fitting of the attenuation profiles was carried out using the equation:

$$I = I_0 e^{-D\gamma^2 g^2 \delta^2 [\Delta - (\delta/3) - (\tau/2)]}$$

where I is the intensity of the observed resonance (attenuated), I_0 the intensity of the reference resonance (unattenuated), D the diffusion coefficient, γ the gyromagnetic ratio, g the gradient strength, δ the gradient pulse length, Δ the diffusion time, and τ the dephasing and rephasing correction time. For each sample 16 experiments were carried out, in which the gradient strength g was varied from 5 to 95% of the maximum gradient intensity (5.35 G/mm).

Electrochemical measurements. Electrochemical experiments were conducted in a conventional three-electrode cell under an argon atmosphere at 293 K using a CH Instrument (CHI660B). Measurements were done with solutions of the compounds (~0.5 mM) in CH_2Cl_2 containing tetra-*n*-butylammonium perclorate (TBAP, 0.1 M) as supporting electrolyte. The reference electrode was $Ag/AgNO_3$ (10 mM in CH_3CN containing 0.1 M $TBABF_4$). The working electrode was a carbon disc (3 mm in diameter) polished with 1 µm diamond paste before each record and the counter electrode was a platinum wire.

Syntheses

General procedure for the synthesis of compound (5) and (9): In a 250 ml two necked-round bottom flask, compound **3** (1.0 g, 4 mmol) and KOH (0.7 g, 12 mmol) were dissolved in 50 ml of dry DMF. The resulting solution was stirred at room temperature for 20 minutes, then the appropriate ditosylate **4** or **8** (25.2 mmol), previously dissolved in 30 ml of dry DMF, was added. After stirring for 90 minutes at room temperature , the reaction was quenched by addition of water. The white precipitate formed was recovered by suction filtration and dissolved in 30 ml of ethyl acetate. The organic phase was extracted twice with a 10% solution of HCl (2 x 20 ml). The pH of the joined aqueous extracts was adjusted to 8 and the white precipitated formed was extracted with EtOAc (3 x 15 ml). The organic phase was dried over anhydrous Na_2SO_4 and evaporated to dryness under reduced pressure. The desired terpyridine was obtained pure after recrystallization from CH_3CN as a white solid.

5 (1.0 g, 50% yield), ^{1}H NMR (300 MHz, $CDCl_3$): δ = 8.69 (dd, ^3J = 4.5, ^4J = 0.6, 2H), 8.62 (d, J = 8.1, 2H), 8.00 (s, 2H), 7.9-7.7 (m, 4H), 7.33 (m, 4H), 4.18 (t, J = 6.3, 2H), 4.05 (t, J = 6.3,

2H), 2.43 (s, 3H), 1.8-1.7 (m, 4H), 1.5-1.4 (m, 4H), ^{13}C NMR (100 MHz, $CDCl_3$): δ = 21.5, 25.0, 25.3, 28.7, 29.0, 67.8, 70.4, 107.3, 121.3, 123.7, 129.8, 136.7, 138.0, 144.3, 149.0, 156.2, 157.1, 167.2; MS (ESI): *m/z* (%): 526 (100) $[M+Na^+]^+$; m.p. = 134-135 °C.

9 (1.2 g, 55% yield), ^{1}H NMR (300 MHz, $CDCl_3$): δ = 8.70 (d, *J* = 4.5, 2H), 8.62 (d, *J* = 7.8, 2H), 8.05 (s, 2H), 7.85 (t, *J* = 6.5, 2H), 7.79 (d, *J* = 8.4, 2H), 7.33 (m, 4H), 4.23 (t, *J* = 6.3, 2H), 4.02 (t, *J* = 6.3, 2H), 2.44 (s, 3H), 1.9-1.8 (m, 2H), 1.8 (bs, 2H), 1.7-1.6 (m, 2H), 1.4-1.2 (m, 12H); ^{13}C NMR (100 MHz, $CDCl_3$): δ = 21.1, 24.9, 25.5, 28.4, 28.6, 28.9, 29.0, 29.1, 67.8, 70.4, 106.8, 120.8, 123.6, 129.5, 136.7, 138.0, 144.3, 148.6, 155.5, 156.6, 166.9; MS (ESI): *m/z* (%): 610 (50) $[M+Na^+]^+$; m.p. = 99.5-100.8 °C.

General procedure for the synthesis of compound (6) and (10): In a 100 ml two necks-round bottom flask, the appropriate terpyridine derivative **5** or **9** (1.4 mmol) and 4,4'-bipyridine (0.65 g, 4.2 mmol) were dissolved in CH_3CN (50 ml). The resulting solution was refluxed for 2 days, then the solvent was evaporated under reduced pressure. The sticky residue was triturated with EtOAc (3 x 20 ml) until the tosylate salt precipitated from the trituration solvent as a solid compound. The solid was recovered by suction filtration and recrystallized from CH_3CN to afford product **6** or **10** as a white solid.

6 (0.8g, 85% yield). ^{1}H NMR (300 MHz, CD_3OD): δ = 9.11 (d, *J* = 5.1, 2H), 8.76 (d, *J* = 3.3, 2H), 8.65 (d, *J* = 3.3, 2H), 8.59 (d, *J* = 6.0, 2H), 8.45 (d, *J* = 4.8, 2H), 7.98 (d, *J* = 6.9, 2H), 7.89 (s, 2H), 7.70 (d, *J* = 6.3, 2H), 7.5-7.4 (m, 2H), 7.21 (d, *J* = 6.0, 2H), 4.71 (t, *J* = 5.7, 2H), 4.25 (t, *J* = 4.5, 2H), 2.34 (s, 3H), 2.2-2.0 (m, 4H), 1.7-1.5 (m, 4H); ^{13}C NMR (100 MHz, CD_3OD): δ = 19.1, 25.1, 25.2, 28.2, 30.8, 61.2, 67.8, 106.9, 114.0, 121.5, 122.0, 124.1, 125.5, 125.6, 128.4, 137.3, 140.2, 142.0, 145.1, 148.6, 150.3, 153.0, 155.6, 156.8, 167.2; MS (ESI): *m/z* (%): 488 (100) $[M\text{-}TsO^-]^+$; m.p. = 117-120 °C.

10 (0.9g, 80% yield), ^{1}H NMR (300 MHz, CD_3OD): δ = 9.08 (d, *J* = 7, 2H), 8.80 (d, *J* = 5.0, 2H), 8.65 (d, *J* = 3.3, 2H), 8.59 (d, *J* = 7.8, 2H), 8.47 (d, *J* = 7, 2H), 8.0-7.9 (m, 4H), 7.93 (s, 2H), 7.70 (d, *J* = 6.0, 2H), 7.47 (t, *J* = 6.9, 2H), 7.21 (d, *J* = 6.0, 2H), 4.64 (t, *J* = 5.7, 2H), 4.23 (t, *J* = 4.5, 2H), 2.35 (s, 3H), 2.1-2.0 (m, 4H), 1.9-1.8 (m, 2H), 1.6-1.5 (m, 2H), 1.4-1.3 (m, 14H); ^{13}C NMR (100 MHz, CD_3OD): δ = 19.9, 25.6, 25.8, 28.6, 28.7, 28.9, 29.0, 29.1, 29.2, 31.2, 61.4, 68.1, 107.3, 121.6, 122.1, 124.1, 125.5, 125.7, 128.4, 137.3, 140.2, 142.2, 145.1, 148.6, 150.4, 153.6, 155.8, 156.9, 167.4; MS (ESI): *m/z* (%): 573 (100) $[M\text{-}TsO^-]^+$; m.p. = 91.5-93.5 °C.

General procedure for the synthesis of compound T(C6) and T(C12): In a 100 ml two necks-round bottom flask compound **6** (0.85g, 1.3mmol) or **10** (0.96g, 1.3 mmol) and compound **7** (0.35g, 1.3 mmol) were dissolved in CH_3CN (50ml) and the solution was refluxed for 10 days. Then the solvent was evaporated at reduced pressure and the residue obtained was triturated with EtOAc (3x 20 ml) until **T(C6)** and **T(C12)** precipitated from the trituration solvent as a solid compound. The solid was recovered by suction filtration and purified by recrystallization from CH_3CN to afford product **T(C6)** or **T(C12)** as a white solid.

T(C6) (0.5g, 41% yield). ^{1}H NMR (300 MHz, CD_3OD): δ = 9.30 (d, *J* = 5.1, 4H), 9.20 (d, *J* = 8.2, 2H), 8.70-8.61 (m, 8H), 8.03 (d, *J* = 9.3, 2H), 7.89 (s, 2H), 7.97 (s, 2H), 7.70 (d, *J* = 8.1, 4H), 7.52 (m, 2H), 7.22 (d, *J* = 7.8, 4H), 4.8-4.6 (m, 4H), 4.30 (t, *J* = 4.5, 2H), 3.57 (t, *J* = 6.0, 2H), 2.34 (s, 6H), 2.2-2.1 (m, 4H), 2.0-1.9 (m, 4H), 1.7-1.6 (m, 10H); ^{13}C NMR (100 MHz, D_2O): δ = 166.4, 155.5, 153.4, 148.5, 145.3, 145.0, 142.2, 139.5, 138.4, 129.3, 126.4, 126.2, 125.3, 125.0, 121.0, 107.4, 62.0, 61.9, 61.4, 30.9, 30.5, 30.3, 27.4, 25.0, 24.4, 20.4; MS (ESI): *m/z* (%): 589 (45) $[M\text{-}2TsO^- \text{-}H^+]^+$, 294 (100) $[M\text{-}2TsO^-]^{2+}$; m.p. = 127-129 °C.

T(C12) (0.72g, 55% yield). ^{1}H NMR (400 MHz, CD_3OD): δ = 9.14 (d, *J* = 4.1, 4H), 8.6-8.4 (m, 8H), 7.9-7.8 (m, 4H), 7.67 (d, *J* = 8, 4H), 7.4-7.3 (m, 2H), 7.11 (d, *J* = 8, 4H), 4.7-4.5 (m, 4H), 4.2-4.1 (m, 2H), 3.5-3.4 (m, 2H), 2.26 (s, 6H), 2.1-2.0 (m, 4H), 1.9-1.8 (m, 2H), 1.5-1.2 (m, 22H); ^{13}C NMR: (100 MHz, CD_3OD): δ = 167.4, 156.9, 155.8, 149.6, 145.6, 142.2, 140.3, 137.3, 128.4, 126.9, 125.5, 124.1, 121.6, 107.1, 68.1, 61.9, 61.2, 31.8, 31.1, 31.0, 29.2, 29.1, 29.0, 28.7, 28.6, 25.8, 25.6, 25.5, 25.0, 19.9; MS (ESI): *m/z* (%): 337 (100) $[M\text{-}2TsO^-]^{2+}$; m.p. = 103.5-105.5 °C.

General procedure for the synthesis of compound P[1⊃T(C6)] and P[1⊃T(C12)]: In a 50 ml two necked-round bottom flask, the calix[6]arene wheel **1** (0.146 g, 0.10 mmol) was dissolved in toluene (20 ml) and compound **T(C6)** (0.103 g, 0.11 mmol) or **T(C12)** (0.116g, 0.11mmol) was added. The solution gradually assumed a deep red color and it was stirred at RT for 30 min. The solution was filtered and the solvent was evaporated at reduced pressure. The pseudorotaxane **P[1⊃T(C6)]** or **P[1⊃T(C12)]** was obtained as a red solid.

P[1⊃T(C6)] (0.23 g, 95% yield). ^{1}H NMR (300 MHz, C_6D_6): δ = 9.5 (br s, 6H), 8.93 (d, *J* = 7.8, 2H), 8.73 (s, 2H), 8.69 (d, *J* = 4.5, 2H), 8.28 (d, *J* = 7.5, 4H), 8.1-8.0 (m, 10H), 7.7-7.6 (m,

12H), 7.46 (d, *J* = 7.8, 2H), 7.2-7.1 (m, 6H), 7.00 (d, *J* = 8.1, 4H), 6.9-6.8 (m, 9H), 4.66 (d, *J* = 14.7, 6H), 4.03 (s, 9H), 3.9-3.8 (m, 10H), 3.8-3.6 (m, 10H), 3.5-3.4 (m, 12H), 2.35 (br s, 2H), 2.06 (s, 6H), 1.9-1.6 (m, 32H), 1.5-1.3 (m, 11H), 1.1-0.9 (m, 4H); ^{13}C NMR (100 MHz, C_6D_6): δ = 169.7, 157.6, 156.5, 152.9, 149.1, 138.9, 136.3, 133.8, 126.5, 123.5, 121.3, 121.0, 118.1, 116.7, 107.8, 72.2, 69.9, 67.6, 66.5, 66.3, 59.7, 44.6, 39.2, 31.6, 31.3, 29.8, 29.2, 26.9, 22.8, 20.8, 20.2, 15.1, 13.9; MS (ESI): *m/z* (%): 1027 (45) $[M\text{-}2TsO^-]^{2+}$; Elemental analysis calculated for $C_{141}H_{165}N_{11}O_{20}S_2$: C 70.62, H 6.94, N 6.43, S 2.67, found C 70.40, H 7.15, N 6.34, S 2.85. m.p. = 152.7-154.1°C.

P[1⊃T(C12)] (0.25g, 95% yield). ^{1}H NMR (400 MHz, C_6D_6): δ = 9.5 (br s, 6H), 8.93 (d, *J* = 7.8, 2H), 8.73 (m, 4H), 8.28 (d, *J* = 7.5, 4H), 8.1-7.9 (m, 10H), 7.8-7.6 (m, 12H), 7.5-7.4 (m, 2H), 7.2-7.1 (m, 6H), 7.00 (d, *J* = 8.1, 4H), 6.95 (bs, 2H), 6.90-6.7 (m, 7H), 4.66 (d, *J* = 14.7, 6H), 4.03 (s, 9H), 4.0-3.9 (m, 10H), 3.8-3.6 (m, 10H), 3.5-3.4 (m, 12H), 2.2 (bs, 2H), 2.1 (s, 6H), 1.9-1.6 (m, 33H), 1.5-1.3 (m, 25H), 1.1-1.0 (m, 4H); ^{13}C NMR (100 MHz, C_6D_6): δ = 167.6, 157.3, 156.5, 152.8, 149.0, 148.0, 144.2, 143.1, 136.2, 133.8, 132.2, 129.3, 128.7, 126.5, 124.8, 123.4, 121.1, 118.1, 116.7, 116.1, 107.8, 72.2, 69.9, 67.9, 66.3, 62.2, 61.0, 60.7, 34.6, 33.5, 31.5, 29.7, 29.6, 29.4, 29.2, 28.9, 26.1, 25.9, 20.8, 15.1; HRMS: *m/z* (%): calculated for $[M\text{-}TsO^-]^+$ 2310.25249, found 2310.24756 (100);m.p.= 143.9-146.2 °C.

Synthesis of compound R[1⊃T(C6)]: In a 50 ml two necked-round bottom flask pseudorotaxane **P[1⊃T(C6)]** (0.10 g, 0.04 mmol) was dissolved in toluene (20 ml) and diphenyl-acetylchloride (0.011 g, 0.05 mmol) and NEt_3 (6.0 μg, 0.06 mmol) were added. The solution was stirred at RT for 12h. The solvent was then removed at reduced pressure and the crude solid was purified by flash chromatography (CH_2Cl_2 : CH_3OH = 95 : 5). Product **R[1⊃T(C6)]** was obtained as a red solid (0.05 g, 50% yield). ^{1}H NMR (300 MHz, C_6D_6): δ = 9.5 (br s, 6H), 8.90 (d, *J* = 7.8, 2H), 8.70 (s, 2H), 8.67 (d, *J* = 4.2, 2H), 8.25 (d, *J* = 7.5, 4H), 8.1-7.9 (m, 10H), 7.8-7.6 (m, 6H), 7.50 (d, *J* = 7.2, 2H), 7.5-7.4 (m, 2H), 7.2-7.1 (m, 12H), 7.00 (d, *J* = 7.8, 4H), 6.9-6.7 (m, 9H), 5.20 (s,1H), 4.66 (d, *J* = 14.7, 6H), 4.4-4.3 (m, 2H), 3.99 (s, 9H), 3.9-3.85 (m, 8H), 3.8-3.6 (m, 10H), 3.5-3.4 (m, 12H), 2.1 (br s, 2H), 2.05 (s, 6H), 1.88 (s, 2H), 1.80 (s, 24H), 1.7-1.5 (m, 6H), 1.2-1.1 (m, 11H), 1.1-0.9 (m, 4H); ^{13}C NMR (100 MHz, C_6D_6): δ = 167.5, 157.5, 156.4, 153.0, 149.0, 148.0, 143.1, 142.9, 141.0, 139.5, 139.0, 137.5, 136.1, 133.7, 132.0, 126.4, 125.5, 123.4, 122.0, 121.0, 118.0, 116.7, 114.0, 107.7, 72.5, 69.9, 67.5, 67.0, 66.3, 61.0, 60.9, 59.0, 57.2, 50.0, 38.2, 34.5, 33.3, 32.6,

31.9, 31.5, 31.3, 29.8, 29.7, 29.4, 29.0, 28.9, 28.7, 28.6, 28.5, 28.0, 26.8, 22.7, 20.8, 20.2, 15.2, 14.0; MS (ES): *m/z* (%): 1125 $[M\text{-}2TsO^-]^{2+}$; Elemental analysis calculated for $C_{155}H_{175}N_{11}O_{21}S_2$: C 71.82, H 6.80, N 5.94, S 2.47, found C 72.10, H 6.75, N 6.02, S 2.65; m.p. = 157.7-159.3 °C.

References

[1] a) R. Chakrabarty, P. S. Mukherjee, P. J. Stang *Chem. Rev.* doi:10.1021/cr200077m; b) *Transition Metal in Supramolecular Chemistry*, (Eds.: L. Fabbrizzi, A. Poggi), Kluwer, Dordrecht, **1994**; c) *Transition Metals in Supramolecular Chemistry* (Eds.: J.-P. Sauvage), Wiley, New York, **1999**.

[2] B. H. Northrop, Y.-R. Zheng, K.-W. Chi, P. J. Stang *Acc. Chem. Res.,* **2009**, *42*, 1554-1563.

[3] J.-M. Lehn, *Supramolecular Chemistry: Concepts and Perspectives*, VCH: Weinheim, Germany, **1995.**

[4] J.-P. Sauvage, C. Dietrich-Buchecker, Eds. *Molecular Catenanes,Rotaxanes, and Knots: A Journey Through the World of Molecular Topology*; Wiley-VCH: Weinheim, Germany, **1999**.

[5] a) , M. J. Wiester, P. A.Ulmann, C. A. Mirkin, *Angew.Chem., Int. Ed.* **2011**, *50*, 114; b) B. Breiner, J. K. Clegg, J. R. Nitschke, *Chem. Sci.* **2011**, *2*, 51. c) Z. Laughrey, B. C. Gibb, *Chem. Soc. Rev.* **2011**, *40*, 363. d) R. W. Saalfrank, H. Maid, A. Scheurer, *Angew Chem.,Int. Ed.* **2008**, *47*, 8794. e) M. Ruben, J.-M. Lehn, P. Muller, *Chem. Soc.Rev*. **2006**, *35*, 1056. f) M. Schmittel, V. Kalsani, *Top. Curr. Chem*. **2005**, *245*, 1. g) J.-P. Collin, V. Heitz, J.-P. Sauvage, *Top. Curr. Chem.* **2005**, *262*, 29. h) C.-C. You, R. Dobrawa, C. R. Saha-Moller, F. Wurthner, *Top. Curr. Chem*. **2005**, *258*, 39.

[6] J. W. Steed, D. R. Turner, K. J. Wallace, *Core concepts in Supramolecular Chemistry and NanoChemistry*, Chapter 3, 121-132, John Wiley and Sons, Ltd, Chichester, UK, **2007**.

[7] a) J. W. Steed, D. R. Turner, K. J. Wallace, *Core concepts in Supramolecular Chemistry and NanoChemistry*, Chapter 4.6, 209-227, John Wiley and Sons, Ltd, Chichester, UK, **2007**; b) R.Dobrawa, F. Würthner, *J. Polym. Sci., Part A: Polym. Chem.*,**2005,** *43*, 4981-4995; c) U. S. Schubert, H. Hofmeier, G. R. Newkome, *Modern Terpiridine Chemistry*, **2006**, WILEY-VCH; d) E. C. Constable, *Chem. Soc. Rev.*, **2007,** *36*, 246; e) R. Shunmugam, G. J. Gabriel, K. A. Aamer, G. N. Tew, *Macromol. Rapid Commun.,* **2010**, *31*, 784–793.

[8] a) S. L. James, *Chem. Soc. Rev.,* **2003**, *32*, 276-288; b) R. Robson, *J. Chem. Soc., Dalton Trans.,* **2000**, 3735-3744; c) M. O'Keeffe, M. A. Peskov, S. J. Ramsden, O. M. Yaghi, *Acc. Chem. Res.,* **2008**, *41*, 1782-1789; d) J. L. C. Rowsell, O. M. Yaghi, *Micropor. Mesopor. Mater.,* **2004**, *73*, 3-14; e) S. Kitagawa, R. Kitaura, S.-I. Noro, *Angew. Chem. Int. Ed.,* **2004**, *43*,2334-2375.

[9] see as examples: a) Lin W. , *Topics in Catalysis,* **2010**, *53*, 869-875; b) G. Qian. , *Acc. Chem. Res.*, **2010**, *43*, 1115-1124; c) C. Serre, *Angew. Chem. Int. Ed. ,* **2010**, *49*, 6260-6266; d) L. Zhang, *Adv. Mat.*, **2010**, *22*, 117 –130; e) H. Garcia, *J. Mat. Chem.*, **2010**, *20*, 3141-3156.

[10] a) S. J. Loeb *Chem. Commun.,* **2005**, 1511–1518; b) S. J. Loeb *Chem. Soc. Rev.,* **2007**, *36*, 226–235; c) S. J. Loeb, (J. L. Atwood, J. W. Steed, Eds.), *Organic Nanostructures* **2008**,33-61; d) K. Kim, *Chem. Soc. Rev.,* **2002**, *31*, 96; e) H. Onigo, *J. Am. Chem. Soc.,* **1981**, *103*, 1303.

[11] a) R. P. Thummel, Y. Janhg, *Inorg. Chem.*, **1986**, *25*, 2527-2534; b) H. Hofmeier, U. S. Schubert, *Chem. Soc. Rev.*, **2004**, *33*, 373-399.

[12] R.-A. Fallahpour, *Synthesis*, **2003**, 155-184.

[13] a) A. Arduini, R. Ferdani, A. Pochini, A. Secchi, F. Ugozzoli, *Angew. Chem. Int. Ed.*, **2000**, *39*, 3453-3456; b) A. Arduini, F. Calzavacca, A. Pochini, A. Secchi, *Chem. Eur. J.*, **2003**, *9*, 793-799; c) A. Credi, S. Dumas, S. Silvi, M. Venturi, A. Arduini, A. Pochini, A. Secchi, *J. Org. Chem.*, **2004**, *69*, 5881-5887; d) A. Arduini, F. Ciesa, M. Fragassi, A: Pochini, A. Secchi, *Angew. Chem. Int. Ed.*, **2005**, *44*, 278-281; e) A. Arduini, R. Bussolati, A. Credi, G. Faimani, S. Garaudée, A. Pochini, A. Secchi, M. Semeraro, S. Silvi, M. Venturi, *Chem. Eur. J.*, **2009**, *15*, 3230-3242.

[14] J. P. Sauvage, J. P. Collin, J. P. Chambron, J. Guillerez, C. Coudret, V. Balzani, F. Barigelletti, L. DeCola, L. Flamigni, *Chem. Rev.* **1994**, *94,* 993-1019.

[15] a) E. C. Constable, M. D. Ward, *J. Chem. Soc. Dalton Trans.* **1990**, 1405-1409; b) F. Drahowzal, D. Klamann, *Monatsh. Chem.* **1951**, *82*, 460-469.

[16] a) R. Dobrawa, F. Würthner, *Chem. Commun.* **2002**, 1878-1879; b) R. Dobrawa. M. Lysetska, P. Ballester, M. Grüme, F. Würthner, *Macromol.* **2005**, *38*, 1315-1325; c) V. Stepanenko, M. Stoker, P. Müller, M. Buchner, F. Würthner, *J. Mater. Chem.* **2009**, *19*, 6816-6826.

[17] SPECFIT/32TM Global Analysis System.

[18] C. A. Schalley, *Analytical Methods in Supramolecular Chemistry,* Chapter 6, Wiley-VCH,Weinheim, **2007**.

[19] a) E. Fan, J. A. Van Arman, J. Kincaid, A. D. Hamilton, *J. Am. Chem. Soc.* **1993**, *115*, 369-370; b) P.

Dydio, T. Zielinski, J. Jurczak, *Org. Lett.* **2010**, *16*, 1076-1078; c) M. Menand, I. Jabin, *Chem. Eur. J.* **2010**, *16,* 2159-2169.

[20] A. Credi, S. Dumas, S. Silvi, M. Venturi, A. Arduini, A: Pochini, A: Secchi, *J. Org .Chem.* **2004**, *69*, 5881-5887.

[21] A. Arduini, R. Bussolati, A. Credi, A. Pochini, A. Secchi, S. Silvi, M. Venturi, *Tetrahedron* **2008** *64*, 8279-8286.

[22] A. Bouzide, G. Sauvè, *Org. Lett.* **2002**, *4*, 2329-2332.

[23] E. J. P. Fear, J. Thrower, J. Veitch, *J. Chem. Soc.* **1958**, 1322-1325.

[24] D. Wu, A. Chen, C. S. Johnson, Jr., *J. Magn. Reson* **1995**, *A115*, 123.

CHAPTER 5

Amphiphilic calix[6]arene wheels

Chapter 5

Amphiphilic calix[6]arene wheels

5.1 Introduction

With the general objective to expand and transfer the recognition properties of calixarene-based hosts to the emerging and rapidly expandig fields of drug delivery[1] and bio-nanotechnology[2], amphiphilic calixarene derivatives that are able to self-assemble in water and yield three-dimensional aggregates belonging to the class of vesicles or micelles have been reported in literature during this last decade.[3]

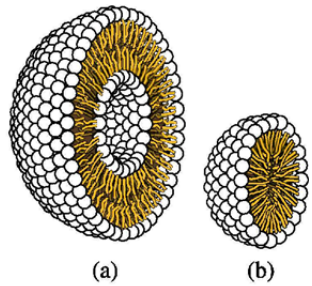

Figure 5.1: Example of structures formed from self-assembly of amphiphilic molecules, (a) a vesicle, (b) a micelle.

These studies suggested to hypothesize that the structural information present in wheel **1** (Figure 5.2) and their orientation in space, which are key control elements during the unidirectional threading processes with suitable axles, could be interpreted also as latent features for the construction, in water, of 3D self-organized systems in which every single component could work as a molecular machine based on pseudorotaxanes.

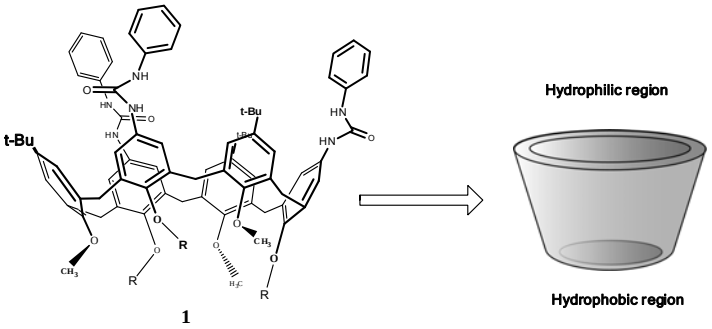

Figure 5.2: the different behaviour of the two rims of the calix[6]arene wheel **1**.

5.2 Design and syntheses of the amphiphilic calix[6]arenes

Since various attempts to verify the previously described hypothesis by employing **1** had failed because of its extremely low solubility in water, two calix[6]arene derivatives, in which the spatial organization of the key structural elements was maintained and the amphiphilic character magnified, were synthetized. In the design phase it was thus decided to increase the hydrophilic domain by inserting six 1,2 di-ethylene-glycol-monomethyl ethers groups at the upper rim and increasing the lipophilic region of the calixarene skeleton by increasing the length of the alkyl chains of the lower rim (Figure 5.3).

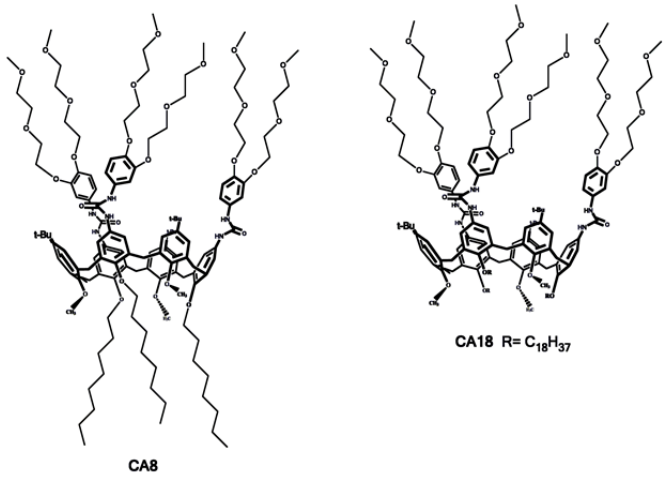

Figure 5.3: the two calix[6]arene-based amphiphilic receptors designed **CA8** and **Ca18**.

For the synthesis of receptors **CA8** and **CA18** the convergent reaction sequence reported in Scheme 5.1 was followed.

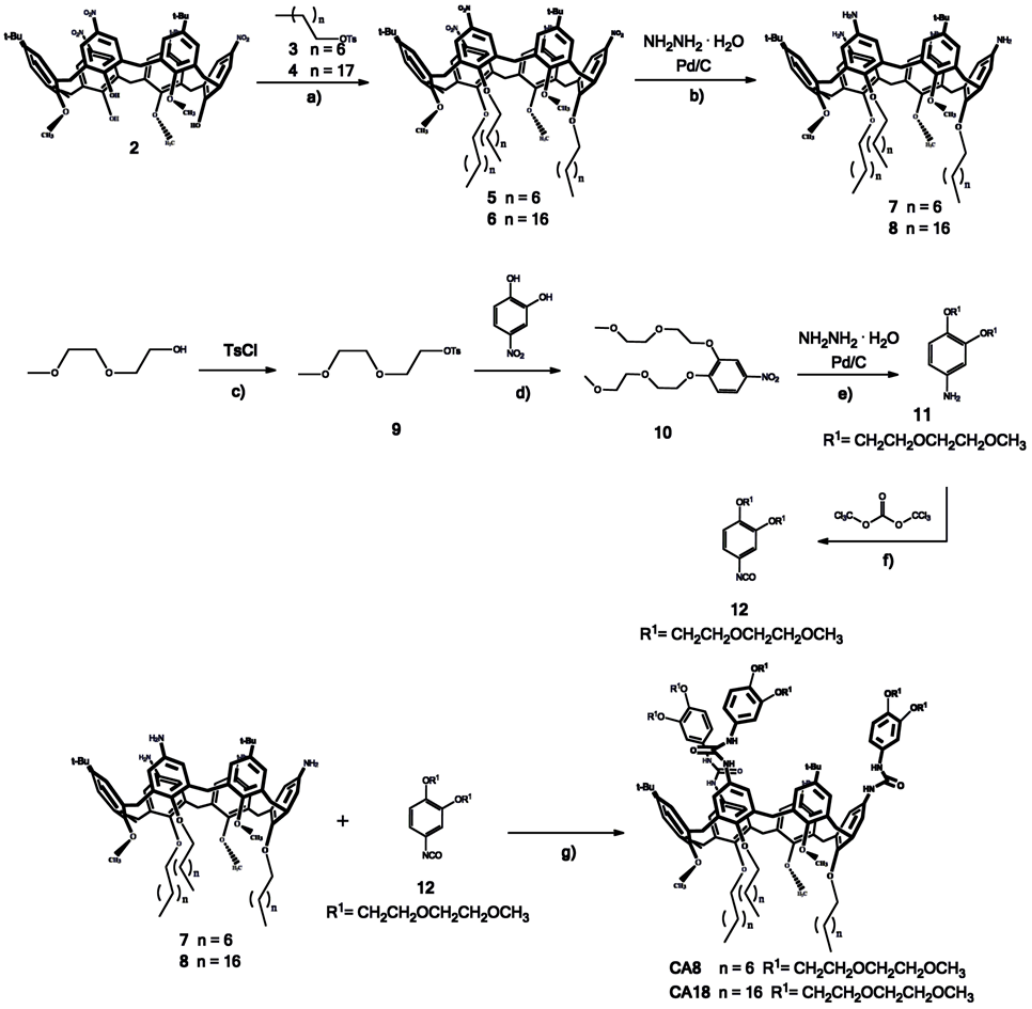

Scheme 5.1: synthetic scheme for calix[6]arene **CA8** and **CA18** synthesis. Reagents and conditions: (a) K_2CO_3,CH_3CN reflux, 48 h; (b)$NH_2NH_2{\cdot}H_2O$, Pd/C, MeOH reflux, 48h; (c) NEt_3, DMAP, dry CH_2Cl_2, 48h; (d) K_2CO_3, CH_3CN reflux, 48 h; (e) $NH_2NH_2{\cdot}H_2O$, Pd/C, MeOH reflux, 48h; (f)dry Toluene reflux, 6 h; (g) dry CH_2Cl_2, 48h.

The 38, 40, 42–trihydroxy-11, 23, 35–tris (1,1 dimethylethyl)-5, 17, 29–trinitro-37, 39, 41 trimethoxy calix[6]arene **2** was functionalized of the phenolic oxygens with **3** or **4** in refluxing CH_3CN, yielding compound **5** or **6** respectively. The tri-ammino compounds **7**

and **8** were obtained by reducing the nitro groups in the presence of $NH_2NH_2 \cdot H_2O$ with Pd/C as catalyst in refluxing MeOH. Meanwhile the synthesis of the hydrophilic groups of the receptor was performed. The -OH terminus of the 2-(2- Ethoxyethoxy)ethanol was reacted with TsCl in dry CH_2Cl_2 to yield the tosylate **9**. This compound was used to functionalize the phenolic oxygens of the 4-nitrocathecol giving **10**. The nitro group was then reduced in presence of $NH_2NH_2 \cdot H_2O$ with Pd/C as catalyst in refluxing MeOH yielding the ammino derivative **11** that was immediately reacted with triphosgene to yield the corresponding isocianate **12**. The amphiphilic receptors **CA8** and **CA18** were synthetized reacting, in dry CH_2Cl_2 compound **12** with **7** or **8** respectively.

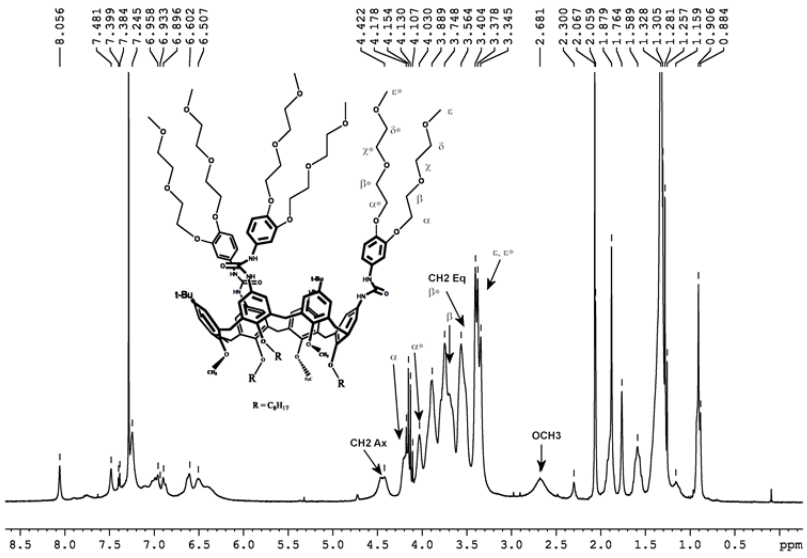

Figure 5.4: ^{1}H NMR (300 MHz) of calix[6]arene **CA8** in $CDCl_3$.

In the ^{1} H NMR spectra of **CA8** (Figure 5.4) and **CA18** taken in $CDCl_3$ (Figure 5.5), the presence of intense signals in the region from 4.2 to 3.2 ppm relative to the di-ethylene-glycol-monomethyl ether chains, together with the signals of the methoxy groups, that resonate at δ = 2.71 ppm, and with the signals of the bridging methylene protons of the calix[6]arene, that resonate as two broad signals at δ = 4.45 and δ = 3.65 ppm, confirm the structure of both compound **CA8** and **CA18**.

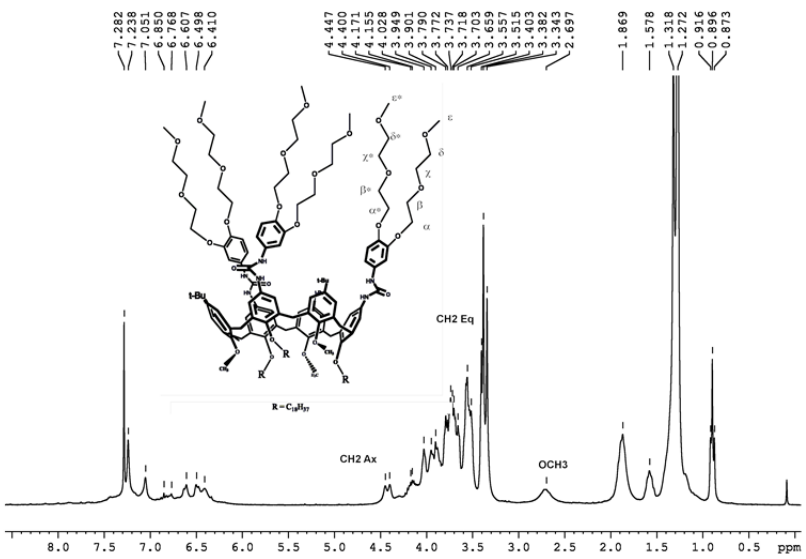

Figure 5.5: ^{1}H NMR (300 MHz) of calix[6]arene **CA18** in $CDCl_3$.

In order to verify the capability of these receptors to function as wheel in the formation of pseudorotaxane with di-alkyl viologen salts, in separate experiments receptor **CA8** or **CA18** and a slight excess of di-octyl viologen ditosylate were equilibrated in C_6D_6 at room temperature (Scheme 5.2). The deep red solution obtained in both cases, after removal of the excess of axle, was characterized through NMR techniques. In the ^{1}H NMR spectra was observed, for both solution, the presence of diagnostic signals indicating that the pseudorotaxane complexes had formed.[4]

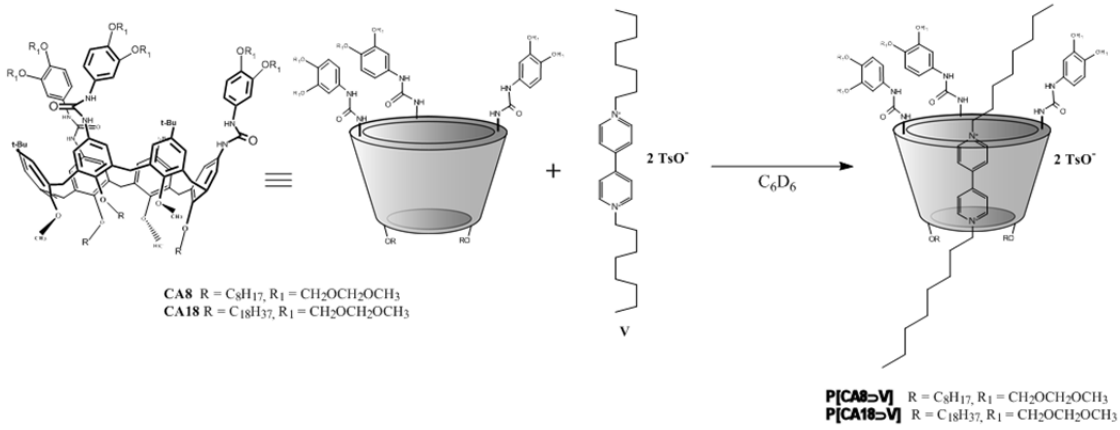

Scheme 5.2: Self-assembly of **P[CA8⊃V]** and **P[CA18⊃V].**

As expected, the threading of the axle into receptors **CA8** or **CA18** results in a substantial rearrangement of the calix[6]arene structure. For example in the ^{1}H NMR spectrum of **P[CA8⊃V]** (Figure 5.6) a downfield shift of about 1.0 ppm of the methoxy groups and the appearance of the AX quartet, at δ = 4.50 and δ = 3.40 ppm, experienced by the six pseudo axial and six pseudo equatorial protons of the bridging methylene protons are clearly evidenced. In addition, the six ureido NHs, because of their involvement in hydrogen bonding with the two tosylate anions are downfield shifted of about 3 ppm and resonate at δ = 9.25 ppm.

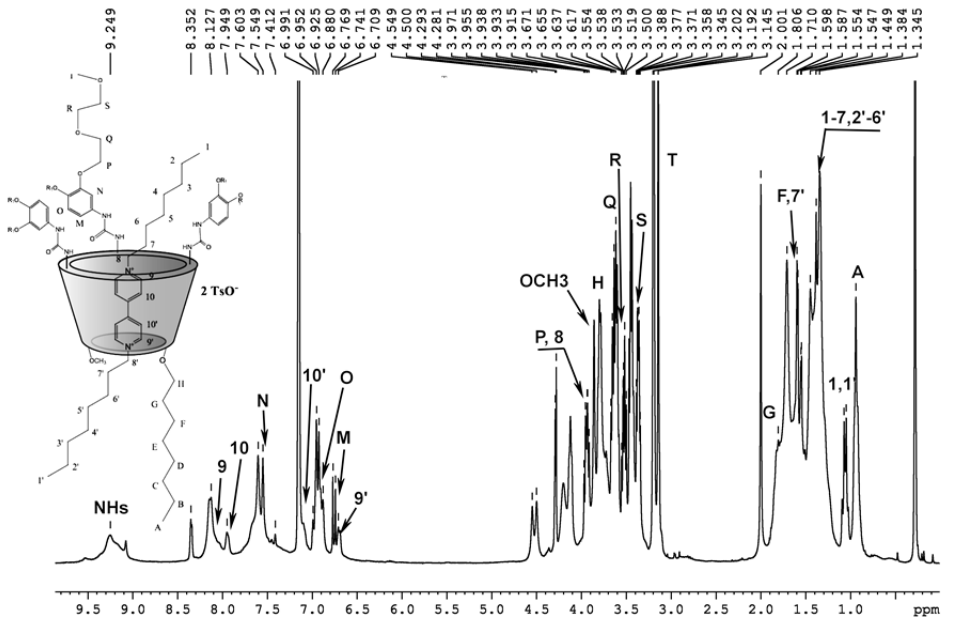

Figure 5.6: ^{1}H NMR (300 MHz) of **P[CA8⊃V]** in C_6D_6.

Through 2D NMR experiments (COSY, TOCSY, ROESY, HSQC, HMBC), the structure of the complex was confirmed. In particular, as for the pseudorotaxane investigated in the previous chapters, the inclusion of the 4,4′-bipyridinium core inside the wheels also affects also the resonances of the protons of the axle. The bipy aromatic protons resonate as four doublets denoted as *9*, *10*, *10′* and *9* centered, in both pseudorotaxanes, at δ = 8.13, 7.94, 7.10 and 6.71 ppm, respectively (Figure 5.7). The presence of four signals indicates that the axle has effectively threaded the wheels, since the protons of its aromatic di-

cationic core experience an asymmetrical magnetic environment due to their inclusion into the non-symmetric cavities of the calix[6]arene.

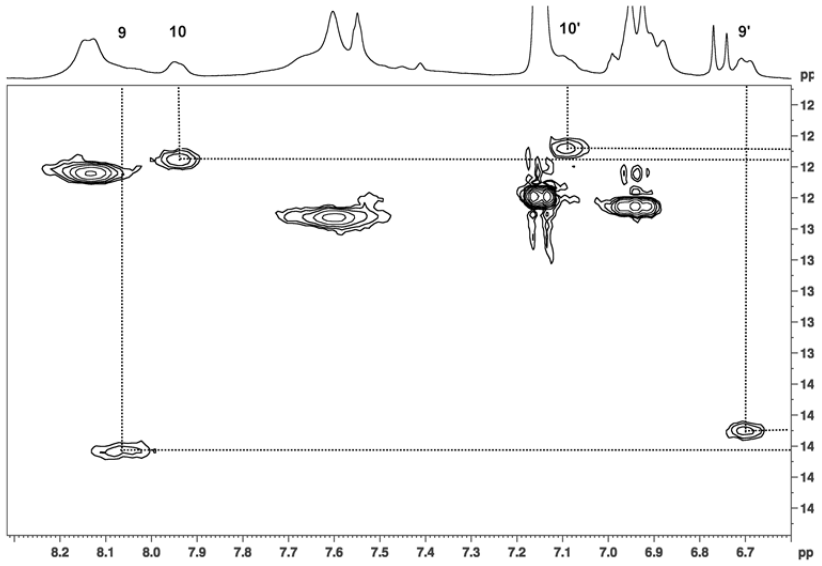

Figure 5.7: ^{1}H-^{13}C 2D HSQC (300 MHz) (enlargements) of **P[CA8⊃V]** in C_6D_6.

5.2 Self-assembly studies in water

The capability of compound **CA8**, **CA18** and their complexes with the di-octyl viologen tosylate to self-assemble in water to generate 3D architectures were studied using two techiques: the Trasmission Electron Microscopy (TEM) and the Dynamic Light Scattering (DLS).

In a transmission electron microscope (TEM)[5] (Figure 5.8) the electrons from a source such as an electron gun enter the sample, are scattered as they pass through it, then they are focused by an objective lens, subsequently are amplified by a magnifying (projector) lens, and finally they produce the desired image. The wavelength of the electrons in the incident beam is given by Eq. 1:

$$\lambda = \frac{0.0388}{\sqrt{V}}\text{nm} \quad (1)$$

where the energy acquired by the electrons is E = eV and V is the accelerating voltage expressed in kilovolts. Images are formed because different atoms interact with and absorb electrons to a different extent. Electrons interact much more strongly with matter than X rays or neutrons do with comparable energies or wavelengths

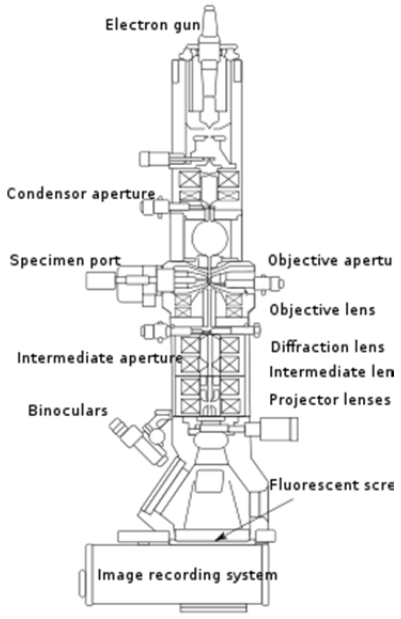

Figure 5.8: Layout of optical components in a basic TEM

The scattering process experienced by electrons during their passage through the specimen determine the kind of information obtained. The higher the operating voltage of a TEM instruments, the greater its lateral spatial resolution is. High voltage TEM instruments (400 kV) have point-to-point resolution better than 0.2 nm, but an electrons beam characterized by high voltage can destroy the sample, in particular if it is of organic matter. For analyses on receptors **CA8** and **CA18** an 85kV electrons beam was used.

The samples analyzed with this technique were four different aqueous solutions containing: *i*) **CA8** ($8 \cdot 10^{-6}$ M), *ii*) **CA18** ($8 \cdot 10^{-6}$ M), *iii*) **CA8** + di-octylviologen ditosylate ($8 \cdot 10^{-6}$ M), *iv*) **CA18** + di-octylviologen ditosylate ($8 \cdot 10^{-6}$ M).

The solubility of these samples in water is very low and the aqueous solution requests a preliminary filtration on Millipore HVLP (0.45 μm) to separate the undissolved solid particles. What appears from the TEM images is the presence, in all samples, of small aggregates characterized by a spherical shape whose size is about 100 nm. However, also the presence of larger aggregates, not characterized by regular in shape, was evidenced, and some of which appear to be formed by several small clusters joined together (Figure 5.9).

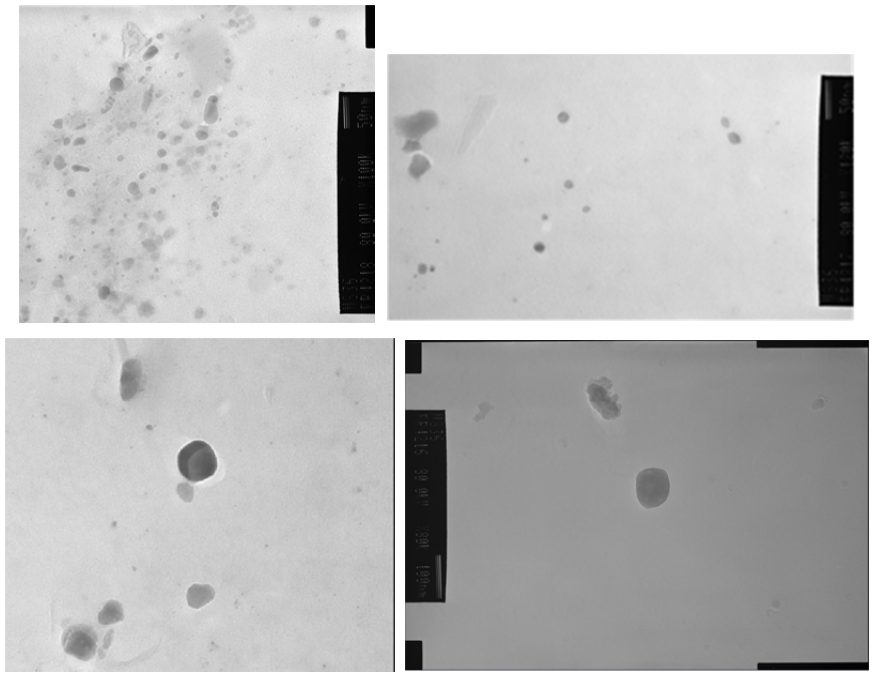

Figure 5.9: TEM images of **CA8** self-assembled structure in water.

These TEM analyses did not show particular differences in the dimensions and morphology of the aggregates into the aqueous solutions in presence or not of the organic guest. An increase in the dimensions of the aggregates was expected in the passage from the free receptors to the complexes with the viologen salts, because of the different conformation that the calix[6]arene assumes in these two situations. It has a trigonal prismatic conformation when it is free, while it assumes a truncated cone conformation complexing viologen salts. Probably during the evaporation of the solvent on the TEM grid the sample is subjected to a variation with respect to the behavior it has in the solution. For this reason these systems have been studied with the DLS technique that permitted to evaluate the dimension of the aggregates directly in solution.

DLS represents a powerful technique to determine the size distribution profile of small particles in solution.[6] When light hits small particles or aggregates, the light scatters in all directions (Rayleigh scattering) as long as the particles are small compared to the wavelength (<250 nm). If the light source is a laser, and thus is monochromatic and coherent, then it observes a time-dependent fluctuation in the scattering intensity. These fluctuations are due to the fact that small molecules in solution are undergoing Brownian motion. Therefore the distance between either constructive or destructive interference by the surrounding particles and within this intensity fluctuation information is contained about the time scale of movement of the scatterers. The dynamic information of the particles is then derived from an autocorrelation of the intensity trace recorded during the experiment.

The samples analyzed with this technique were four different aqueous solutions containing: *i*) **CA8** ($8 \cdot 10^{-6}$ M), *ii*) **CA18** ($7.4 \cdot 10^{-6}$ M), *iii*) **CA8** + di-octylviologen ditosylate ($8 \cdot 10^{-6}$ M), *iv*) **CA18** + di-octylviologen ditosylate ($1.8 \cdot 10^{-6}$ M).

For the calculation of the autocorrelation functions, two software were used, NNLS and Contin, whose results were in agreement for all experiments done.

The analyses on the sample containing receptor **CA8** revealed the presence of a predominant distribution of aggregates whose average dimension was 122 ± 32 nm (Figure 5.10). The dimensions measured for this self-assembled structures in solution were in substantial agreement with those obtained by TEM analyses. In this sample another distribution of entities with average dimension of about 1,5 nm was present. This second distribution could be referred to the presence in solution of not assembled receptors.

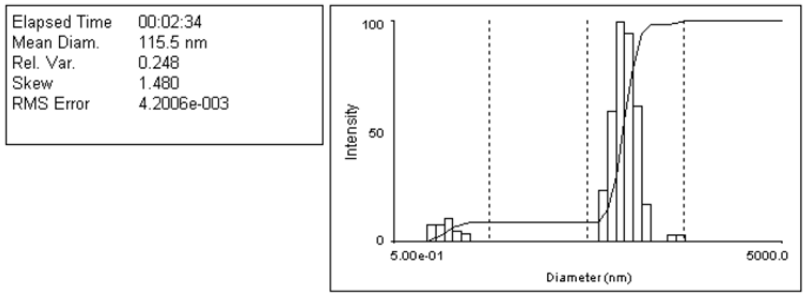

d	G(d)	C(d)	d	G(d)	C(d)	d	G(d)	C(d)
1.00	0	0	9.36	0	9	87.66	59	30
1.23	8	2	11.47	0	9	107.42	100	55
1.50	8	4	14.06	0	9	131.64	95	79
1.84	11	7	17.23	0	9	161.33	62	94
2.26	5	8	21.12	0	9	197.71	17	99
2.76	4	9	25.88	0	9	242.29	0	99
3.39	0	9	31.71	0	9	296.92	0	99
4.15	0	9	38.86	0	9	363.87	3	99
5.09	0	9	47.63	0	9	445.92	3	100
6.23	0	9	58.37	0	9	546.46	0	100
7.64	0	9	71.53	24	15	669.68	0	100

Figure 5.10: DLS analysis output of sample containing receptor **CA8**.

The analyses on the sample containing receptor **CA8** + di-octylviologen ditosylate revealed the presence of two predominant distribution of aggregates. The smaller is centered around 100 nm, and could be assigned to the presence of the same self-assembled system present in the former sample. The principal distribution of aggregates, instead, is centered at 420 nm (Figure 5.11). Even in this sample it was possible to revealed the presence of a small distribution at 1.5 nm probably referred to the presence of the free receptor **CA8** in solution.

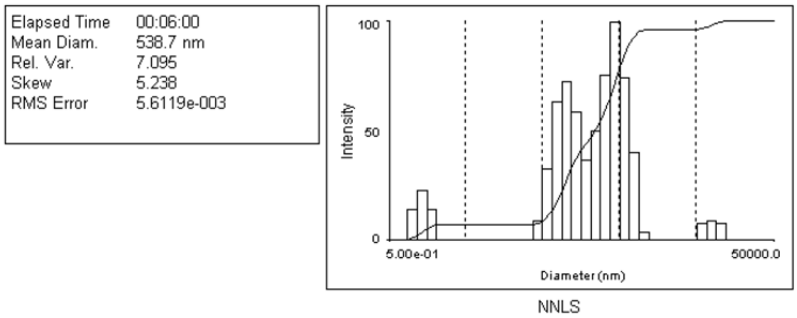

d	G(d)	C(d)	d	G(d)	C(d)	d	G(d)	C(d)
1.00	14	2	23.71	0	7	562.34	75	90
1.33	23	5	31.62	0	7	749.89	40	96
1.78	14	7	42.17	9	9	1000.00	4	96
2.37	0	7	56.23	33	13	1333.52	0	96
3.16	0	7	74.99	64	23	1778.28	0	96
4.22	0	7	100.00	73	33	2371.37	0	96
5.62	0	7	133.35	59	41	3162.28	0	96
7.50	0	7	177.83	37	47	4216.97	0	96
10.00	0	7	237.14	50	54	5623.41	8	98
13.34	0	7	316.23	76	65	7498.94	9	99
17.78	0	7	421.70	100	79	10000.00	8	100

Figure 5.11: DLS analysis output of sample containing receptor **CA8** + di-octylviologen ditosylate salt.

From these preliminary analyses it seemed that receptor **CA8** is able to self-assemble, in aqueous solution, generating 3D structures that could be tentatively identified as vesicles or micelles (Figura 5.12). Moreover it seemed that the complexation of the viologen salt from the calix[6]arene derivative could have the effect to increase the dimension of these self-assembled structures. The hypothesis proposed was that the changing in the conformational structure of calix[6]arene **CA8**, passing from the guest-free conformation to the complexed one, affected the 3D self-assembly mode of the molecules causing a variation in the dimensions of the aggregates.

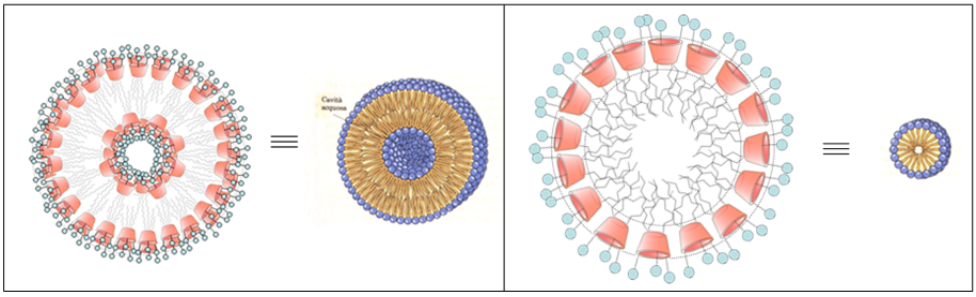

Figure 5.12: schematic representation of a vesicle-like structure (left) or a micelle-like structure (right) constituted by receptor **CA8**.

The DLS analyses performed on the aqueous solution containing the receptor **CA18** (Figure 5.13) revealed the presence of entities with an average dimension of 215 ± 56 nm. A second distribution centered at 1.4 nm was also present, probably referred to the non-aggregated receptor. In this case this distribution is significantly larger than for receptor

CA8 indicating, probably, that the receptor **CA18** forms self-assembled structures in aqueous solution more hardly.

Elapsed Time	00:06:00
Mean Diam.	124.4 nm
Rel. Var.	0.834
Skew	0.137
RMS Error	5.3052e-003

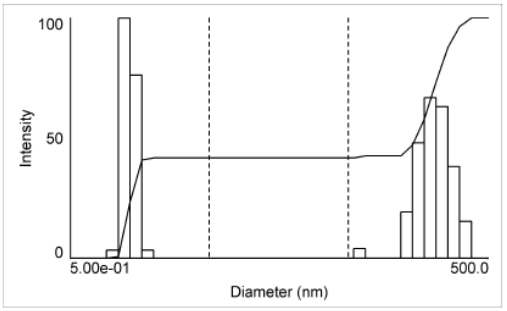

NNLS

d	G(d)	C(d)	d	G(d)	C(d)	d	G(d)	C(d)
1.00	3	1	8.53	0	42	72.73	0	43
1.22	100	24	10.36	0	42	88.38	0	43
1.48	76	41	12.59	0	42	107.40	0	43
1.79	3	42	15.30	0	42	130.50	19	47
2.18	0	42	18.59	0	42	158.58	48	58
2.65	0	42	22.59	0	42	192.69	67	73
3.22	0	42	27.45	0	42	234.15	63	88
3.91	0	42	33.36	0	42	284.52	38	96
4.75	0	42	40.54	0	42	345.73	15	100
5.78	0	42	49.26	0	42	420.11	0	100
7.02	0	42	59.86	4	43	510.49	0	100

Figure 5.13: DLS analysis output of the sample containing receptor **CA18**.

The analyses on the sample containing receptor **CA18** + di-octylviologen ditosylate revealed that the addition of the organic salt did not modify the dimension of the aggregates present in solution (Figure 5.14).

Elapsed Time	00:12:01
Mean Diam.	99.0 nm
Rel. Var.	1.109
Skew	0.307
RMS Error	3.3164e-003

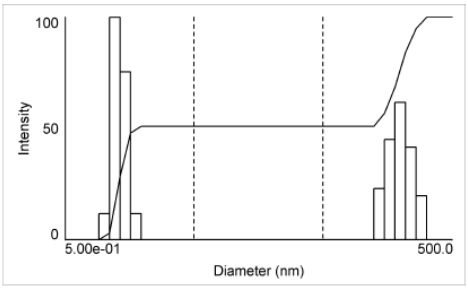

NNLS

d	G(d)	C(d)	d	G(d)	C(d)	d	G(d)	C(d)
1.00	12	3	7.98	0	51	63.66	0	51
1.21	100	29	9.64	0	51	76.89	0	51
1.46	76	48	11.64	0	51	92.87	0	51
1.76	12	51	14.06	0	51	112.16	0	51
2.13	0	51	16.98	0	51	135.47	23	57
2.57	0	51	20.51	0	51	163.62	45	68
3.10	0	51	24.77	0	51	197.62	62	84
3.75	0	51	29.92	0	51	238.69	42	95
4.53	0	51	36.13	0	51	288.29	20	100
5.47	0	51	43.64	0	51	348.20	0	100
6.61	0	51	52.71	0	51	420.55	0	100

Figure 5.14: DLS analysis output of sample containing receptor **CA18** + di-octylviologen ditosylate salt.

In order to demonstrate that the capability of these receptors to form aggregate structures in aqueous solution originates from the presence, at the upper rim of the cavity, of the six polar chains, similar DLS analysis were carried out on the calix[6]arene derivative **C8** (Figure 5.15).[8] This receptor bears three apolar octyl chains at the lower rim, but lacks of the di-ethylene-glycol-monomethyl ether chains at the upper.

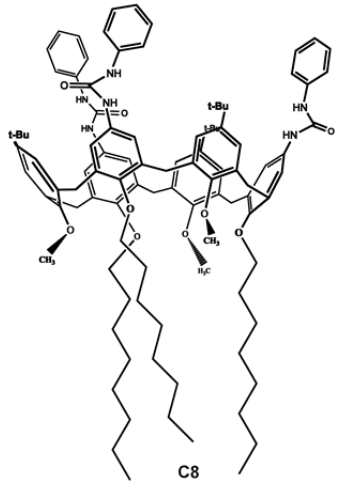

Figure 5.15: the calix[6]arene derivative **C8**.

The DLS analyses of the $7{,}7 \cdot 10^{-6}$ M aqueous solution of **C8** revealed the total lack of self-assembled 3D structure, and the only distribution present is centered at an average dimension of 1.2 nm *ca.* that was attributed, as in the previous cases, to the free molecule in solution.

Elapsed Time	00:24:03
Mean Diam.	1.7 nm
Rel. Var.	1.310
Skew	4.545
RMS Error	8.0453e-004

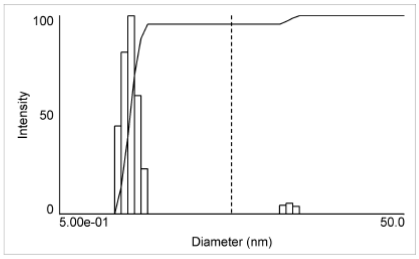

NNLS

d	G(d)	C(d)	d	G(d)	C(d)	d	G(d)	C(d)
1.00	0	0	2.64	0	96	6.97	0	96
1.09	44	14	2.88	0	96	7.61	0	96
1.19	82	39	3.15	0	96	8.32	0	96
1.30	100	70	3.44	0	96	9.08	0	96
1.42	60	89	3.76	0	96	9.92	4	97
1.55	23	96	4.10	0	96	10.84	5	99
1.70	0	96	4.48	0	96	11.84	4	100
1.85	0	96	4.90	0	96	12.93	0	100
2.03	0	96	5.35	0	96	14.12	0	100
2.21	0	96	5.84	0	96	15.42	0	100
2.42	0	96	6.38	0	96	16.85	0	100

Figure 5.16: DLS analysis output of sample containing receptor **CA8.**

Conclusions and Perspectives

These preliminary data confirm the potential to build up micelles-like or vesicles-like 3D self-assembled structures of about 120 and 215 nm in aqueous solution, by employing the amphiphilic nature of the calix[6]arene receptors derivatives **CA8** and **CA18** respectively. Moreover the ability of receptor **CA8** to work as wheel in the formation of pseudorotaxane complexes with di-alkyl viologen salts has an effect in tuning the dimensions of these aggregates, increasing their dimension from 120 to 420 nm. The possibility to build up micelles-like or vesicles-like structures in water, in which every single component of the aggregate could carry out an output responding to an external energy input, could have an important role in the development of new smart systems in the field of drug delivery. An hypothetic model could be constituted by a micelle or vesiscle formed by oriented pseudorotaxanes that is able to complex a guest in its inner compartment, and to release it as a consequence of the dethreading of the axle from the wheel as response to an external energy input (Scheme 5.3).

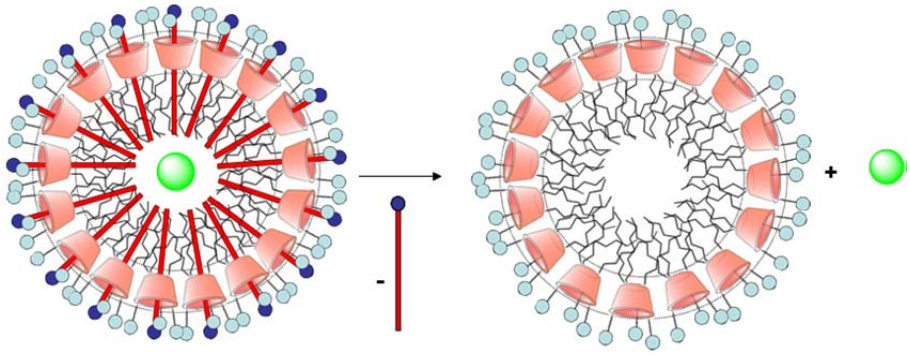

Scheme 5.3: model of a pseudorotaxane-based micelle-like structure that can release the guest complexed in the internal compartment as consequence of the dethreading of the axle from the wheel.

Experimental section

Materials and synthetic methods. Toluene and dichloromethane were dried using standard procedure, all other reagents were of reagent grade quality obtained from commercial suppliers and were used without further purification. NMR spectra were recorded at 400 and 300 MHz for ^{1}H and 100 and 75 MHz for ^{13}C. Melting points are uncorrected. Chemical shifts are expressed in ppm (δ) using the residual solvent signal as internal reference. Mass spectra were recorded in ESI mode. TEM analyses were conducted with a JEOL-JEM FX-2000 instruments at 85 keV, DLS analyses were carried out with a BIC (Brookhaven Instruments Corp) Dynamic Light Scattering Software Ver. 3.34. Calix[6]arene (**2**), (**5**), (**7**)[7], **C8**[8], 2-(2-methoxyethoxy)ethyl 4-methylbenzenesulfonate (**9**)[9], tosylates (**3**)[10] and (**4**)[11], were synthesized according to literature procedures.

Syntheses

1,2-bis(2-(2-methoxyethoxy)ethoxy)-4-nitrobenzene (10): 2-(2-methoxyethoxy)ethyl 4-methylbenzenesulfonate (**9**) (7.7 g, 28.0 mmol) the 4-nitrobenzene-1,2-diol (2.0 g, 12.8 mmol) and the K_2CO_3 (5.3 g, 38.4 mmol) were dissolved in 100 ml of CH_3CN. The resulting solution was refluxed for 48 h, then the solvent was evaporated to dryness under reduced pressure. A water solution of HCl 10% was added to neutralize the excess of K_2CO_3 (50 ml) and extracted with EtOAc (3 x 20 ml). The organic phase was separated, dried with Na_2SO_4 and evaporated under reduced pressure. The oily residue was purified by column chromatography (hexane/ethyl acetate 2/8). **10** was isolated as a yellow oil (4,1 g, 90% yield). ^{1}H NMR (400 MHz, CD_3OD): δ = 7.80 (d, J = 3.2 Hz, 1H), 7.86 (dd, J_{orto} = 8.4 Hz, J_{meta} = 4.0 Hz, 1H), 7.09 (d, J = 12 Hz, 1H), 4.24 (m, 4H), 3.88 (m, 4H), 3.72 (m, 4H), 3.57 (m, 4H), 3.36 (s, 6H); ^{13}C NMR (100 MHz, CD_3OD): δ = 154.5, 148.4, 141.3, 117.6, 111.6, 108.6, 71.6, 70.2, 69.1, 68.9, 57.8; MS (ESI): *m/z* (%): 382 (100) $[M+Na^+]^+$.

3,4-bis(2-(2-methoxyethoxy)ethoxy)aniline (11): compound **10** (3.5g, 9.7 mmol) was suspended in MeOH (150 ml), and a catalytic amount of Pd/C was added under nitrogen atmosphere. The mixture was refluxed for 10 minutes then $NH_2NH_2 \cdot H_2O$ (4.8 g, 970

mmol) was added to the solution that was refluxed for 24 h. Subsequently the solution was filtered on celite under N_2 atmosphere. The solvent was evaporated at reduced pressure. Product **11** was not purified and the crude solid (1.6 g, yield 60%) was submitted immediately to the next synthetic step.

4-isocyanato-1,2-bis(2-(2-methoxyethoxy)ethoxy)benzene (12): triphosgene (0.58 g, 1.9 mmol) was dissolved in dry toluene (100 ml) under nitrogen atmosphere. A dry toluene solution (20 ml) of compound **11** (0.5 g, 1.5 mmol), was dropped to the former solution in an hour. The reaction mixture was then refluxed for 5 h and subsequently the solvent was evaporated at reduce pressure. **12** was obtained as a colourless oil (0.28 g, yield 53%).). ^{1}H NMR (300 MHz, $CDCl_3$): δ = 6.85 (d, *J* = 8.4 Hz, 1H), 6.68 (d, *J* = 2.1 Hz, 1H), 6.64 (d, *J* = 2.4 Hz, 1H), 4.17 (m, 4H), 3.85 (m, 4H), 3.74 (m, 4H), 3.60 (m, 4H), 3.41 (s, 6H); ^{13}C NMR (100 MHz, CD_3OD): δ = 150.2, 142.5, 127.7, 125.8, 119.1, 116.1, 111.8, 71.6, 70.1, 70.0, 69.6, 59.3; MS (ESI): *m/z* (%): 378 (100) $[M+Na^+]^+$, 410 (50) $[M+CH_3OH+Na^+]^+$.

Compound 6: the calix[6]arene derivative **2** (0.5 g, 0.5 mmol) the octadecyl 4-methylbenzenesulfonate **4** (1.3 g, 3.0 mmol) and the K_2CO_3 (0.5 g, 2.2 mmol) were dissolved in 100 ml of CH_3CN. The resulting solution was refluxed for 5 days, then the solvent was evaporated to dryness under reduced pressure. A water solution of HCl 10% was added to neutralize the excess of K_2CO_3 (50 ml) and extracted with EtOAc (3 x 20 ml). The organic phase was separated, dried with Na_2SO_4 and evaporated under reduced pressure. The oily residue was purified by column chromatography (hexane/ethyl acetate 9/1). **6** was isolated as a yellow oil (0.21 g, 25% yield).). ^{1}H NMR (300 MHz, $CDCl_3$): δ = 7.71 (bs, 6H), 7.21 (s, 6H), 4.46 (bs, 6H), 4.10 (bs, 6H), 2.28 (s, 9H), 1.3 (bs, 99H), 0.89 (t, *J* = 8.0 Hz, 9H); ^{13}C NMR (100 MHz, $CDCl_3$): δ = 161.5, 149.7, 143.6, 142.5, 129.4, 126.8, 123.8, 69.3, 34.8, 31.3, 29.6, 29.3, 29.2 25.9, 22.7, 14.1 MS (ESI): *m/z* (%): 1762 (30) $[M+Na^+]^+$.

Compound 8: compound **6** (0.42 g, 0.24 mmol) was suspended in MeOH (50 ml), and a catalytic amount of Pd/C was added under nitrogen atmosphere. The mixture was refluxed for 10 minutes then $NH_2NH_2 \cdot H_2O$ (1.2 g, 24 mmol) was added to the solution that was refluxed for 24 h. Subsequently the solution was filtered on celite under N_2 atmosphere. The solvent was evaporated at reduced pressure. Product **8** was not purified

and the crude solid (0.38 g, yield 95%) was submitted immediately to the next synthetic step.

Compound CA18: compound **8** (0.4 g, 0.2 mmol) and compound **12** (0.32 g, 0.9 mmol) were dissolved in dry CH_2Cl_2 under nitrogen atmosphere. The solution was stirred for 48 h. Then the solvent was evaporated at reduced pressure. The oily residue was purified by column chromatography (ethyl acetate/methanol 8.5/1.5). **CA18** was isolated as a yellow oil (0.21 g, 25% yield). M.p.: 77-78 °C; ^{1}H NMR (300 MHz, $CDCl_3$): δ = 6.64 (bs, 6H), 6.50 (bs, 6H), 4.42 (bs, 6H), 4.03 (bs, 6H), 3.95 (bs, 6H), 3.91 (bs, 6H), 3.79 (bs, 6H), 3.75 (bs, 6H), 3.70 (bs, 12H), 3.56 (bs, 18H), 3.35 (bs, 18H), 2.69 (bs, 9H), 1.89 (bs, 6H), 1.58 (bs, 6H), 1.30 (bs, 111H), 0.90 (bt, 9H); ^{13}C NMR (100 MHz, $CDCl_3$): δ =149.1, 146.5, 135.6, 133.1, 127.7, 115.5, 107.8, 71.9, 71.9, 70.7, 70.6, 69.8, 69.6, 69.4, 59.0, 58.9, 34.0, 31.9, 31.5, 30.5, 29.7, 29.3, 26.3, 22.6, 14.1.; HRMS: *m/z* (%): calculated: 2713.8634, found 2715.8656 (100) $[M+H^+]^+$;

Compound CA8: compound **7** (0.4 g, 0.3 mmol) and compound **12** (0.4 g, 1.2 mmol) were dissolved in dry CH_2Cl_2 under nitrogen atmosphere. The solution was stirred for 48 h. Then the solvent was evaporated at reduced pressure. The oily residue was purified by column chromatography (ethyl acetate/methanol 8.5/1.5). **CA8** was isolated as a yellow oil (0.21 g, 40% yield). M.p.: 77-78 °C; ^{1}H NMR (300 MHz, $CDCl_3$): δ = 6.85 (bs, 6H), 6.55 (bs, 6H), 4.45 (bs, 6H), 4.20 (bs, 6H), 4.10 (bs, 6H), 3.95 (bs, 6H), 3.85 (bs, 6H), 3.80 (bs, 6H), 3.75 (bs, 12H), 3.56 (bs, 12H), 3.48 (bs, 6H) 3.35 (bs, 18H), 2.69 (bs, 9H), 1.95 (bs, 6H), 1.58 (bs, 6H), 1.30 (bs, 51H), 0.90 (bt, 9H); ^{13}C NMR (100 MHz, $CDCl_3$): δ = 152.9, 151.0, 149.7, 143.6, 143.3, 142.2, 128.7, 128.1, 126.8, 126.4, 118.6, 113.8, 111.9, 105.4, 71.6, 70.1, 70.0, 69.6, 69.3, 59.3, 34.8, 31.9, 31.3, 30.2, 29.6, 29.3, 25.9, 22.7, 14.1; HRMS: *m/z* (%): calculated: 2293.3834, found 2295.3943 (100) $[M+H^+]^+$;

References

[1] a) A. Chonn, P. R. Cullis, *Adv. Drug Delivery Rev*., **1998**, *30*, 73–83; b) A. Samad, Y. Sultana M. Aqil, *Curr. Drug Delivery*, **2007**, *4*, 297; c) A. N. Lukyanov V. P. Torchilin, *Adv. Drug Delivery Rev*., **2004**, *56*, 1273–1289; d) G. S. Kwon T. Okano, *Adv. Drug Delivery Rev*., **1996**, *21*, 107–116; e) V. P. Torchilin, *Adv. Drug Delivery Rev*., **2006**, *58*, 1532–1555; f) J. E. Kipp, *Int. J. Pharm*., **2004**, *284*, 109–122; g) R. B. Gupta, U. B. Kompella, *Nanoparticle Technology for Drug Delivery*, h) Taylor and Francis, New York, **2006**; i) *Drug delivery: principles and applications*, ed. B. Wang, T. Siahaan, R. Soltero, John Wiley and sons, New York, **2005**; l) Y. Kakizawa, K. Kataoka, *Adv. Drug Delivery Rev*., **2002**, *54*, 203–222.

[2] a) D. S. Goodsell, *Bionanotechnology: lessons from nature*, Wiley-Liss, Hoboken, **2004**; b) E. Gazit, *Plenty of Room for Biology at the Bottom: An Introduction to Bionanotechnology*, Imperial College Press, London, **2007**; c) M. Ferrari, *Nat. Rev. Cancer*, **2005**, *5*, 161–171; d) J. H. Park, S. Lee, J.-H. Kim, K. Park, K. Kim, I. C. Kwon, *Prog. Polym. Sci*., **2008**, *33*, 113–137; e) R. Haag and F. Kratz, *Angew. Chem., Int. Ed*., **2006**, *45*, 1198–1215; f) S. Cavalli, F. Albericio, A. Kros, *Chem. Soc. Rev*., **2010**, *39*, 241–263; g) C. R. Yamnitz, G. W. Gokel, *Peptibiotics*, **2009**, 657–674; h) R. M. Capito, A. Mata, S. I. Stupp, *Nanotechnology*, **2009**, *5*, 385–412; i) E. Bilensoy, J. Biomed., *Nanotechnol*., **2008**, *4*, 293–303; l) R. H. de Rossi, O. F. Silva, R. V. Vico, C. J. Gonzalez, *Pure Appl. Chem*., **2009**, *81*, 755–765; m) F. Sallas R. Darcy, *Eur. J. Org. Chem*., **2008**, 957–969; n) G. W. Gokel, W. M. Leevy, M. E. Weber, *Chem. Rev*., **2004**,*104*, 2723–2750.

[3] see as examples: a) Y. Tanaka, M. Miyachi, Y. Kobuke, *Angew. Chem. Int. Ed.,* **1999**, *38,* 504-506; b) J. J. Michels, J. Huskens, J. F. J. Engbersen, D. N. Reinhoudt, *Langmuir*, **2000**, *16*, 4864-4870; c) M. Lee,S.-J. Lee, L.-H. Jiang*, J. Am. Chem. Soc.,* **2004**, *126*, 12724-12725; d) N. Basilio, L. Garcìa-Rìo, M. Martìn-Pastor, *J. Phys. Chem. B* **2010,** *114,* 4816–4820; e) K. Helttunena, P. Shahgaldian, *New J. Chem.,* **2010**, *34***,** 2704–2714; f) Q. L., G. Chen, B. Guan, M. Jiang, *J. Mater. Chem.,* **2011**, *21*, 13262-13267; g) R. V. Rodik, A. S. Klymchenko, N. Jain, S. I. Miroshnichenko, L. Richert, V. I. Kalchenko, Y. Mély, *Chem. Eur. J,.* **2011**, *17*, 5526 – 5538.

[4] a) A. Arduini, F. Calzavacca, A. Pochini, A. Secchi, *Chem. Eur. J.*, **2003**, *9*, 793-799; b) A. Arduini, F. Ciesa, M. Fragassi, A: Pochini, A. Secchi, *Angew. Chem. Int. Ed.*, **2005**, *44*, 278-281.

[5] D. B. Williams, C. B. Carter, *Transmission Electron Microscopy: A Textbook for Materials Science*, Plenum Press, **1996**.

[6] B. Chu, *Laser Light Scattering: Basic Principle and Practice*, 2nd Ed., Dover Publication, **2007**.

[7] A. Arduini, L. Domiano, L.Oglio, A. Pochini, A. Secchi, R. Ungaro, *J .O. C.,* **1997**, *62*, 7866.

[8] J. J. Gonzalez, R. Ferdani, E. Albertini, J. M. Blasco, A. Arduini, A. Pochini, P. Prados, J. de Mendoza, *Chem. Eur. J.,* **2000**, *6*, 73.

[9] E. M. Kim, C. K. Jeung, E. Y. Choi, C. Gao, J. W. Kim, J. H. Lee, O. P. Kwon, *Polymer*, **2011**, 4451-4455.

[10] G. W. Kabalka, M. Varma, S. Varma, *J. O. C.*, **1986**, *51*, 2387.

[11] A. Boccia, V. Lanzillotta, R. Zanoni, L.Pescatori, A. Arduini, A. Secchi, *Phys. Chem. Chem. Phys.,* **2011**, *13*, 4444-4451.

The Author

Rocco Bussolati was born in Parma (Italy) on the 22th of December 1983. In 2002 he obtained his high school leaving qualifications at Liceo Scientifico "Paciolo-D'Annunzio" in Fidenza (PR). In April 2008 he graduated in Chemistry, at the Department of Organic and Industrial Chemistry of the University of Parma, under the supervision of Prof. Arturo Arduini and Prof. Andrea Pochini with a thesis entitled " Study of the factors that govern the orientation of calix[6]arene-based pseudorotaxane". In January 2009 he started a Ph.D. research project at the Department of Organic and Industrial Chemistry of the University of Parma, under the supervision of Prof. Arturo Arduini. During this period he joined as a Ph.D. visiting student for three months (March – May 2011) the group of Prof. Guy Royal at the Département de Chimie Moléculaire, Laboratoire de Chimie Inorganique Redox of the University "Joseph Fourier" in Grenoble (France). The results of the research conducted during the period 2009-2011 are described in this thesis.

Publications

- "Rotaxanes with a calix[6]arene wheel and axles of different length. Synthesis, characterization, and photophysical and electrochemical properties". Arduini Arturo, **Bussolati Rocco**, Credi Alberto, Pochini Andrea, Secchi Andrea, Silvi Serena, Venturi Margherita; *Tetrahedron*, **2008**, 64(36), 8279-8286.

- "Towards controlling the threading direction of a calix[6]arene wheel by using non-symmetric axles". Arduini Arturo, **Bussolati Rocco**, Credi Alberto, Faimani Giovanni, Garaudee Sandrine, Pochini Andrea, Secchi Andrea, Semeraro Monica, Silvi Serena, Venturi Margherita;. *Chemistry - A European Journal,* **2009**, 15(13), 3230-3242.

- "Comunication between components in metal-directed assemblies of oriented calix[6]arene-based pseudorotaxanes and rotaxanes". Arduini Arturo, **Bussolati Rocco**, Masseroni Daniele, Royal Guy, Secchi Andrea; *European Journal of Organic Chemistry,* **2011**, DOI: 10.1002/ejoc.201101597.